รายงานวิจัยฉบับสมบูรณ์

โครงการการศึกษาการขนส่งสารผ่านซิเลีย: การศึกษาโครงสร้างโดยรวมของ ciliary pore complex และ ciliary barrier ของ *Tetrahymena thermophila*

โดย ผศ. ดร. ป๋วย อุ่นใจ

เมษายน 2563

สัญญาเลขที่ RSA5980078

รายงานวิจัยฉบับสมบูรณ์

โครงการการศึกษาการขนส่งสารผ่านซิเลีย: การศึกษาโครงสร้างโดยรวมของ ciliary pore complex และ ciliary barrier ของ *Tetrahymena thermophila*

ผศ.ดร. ป๋วย อุ่นใจ
ภาควิชาชีววิทยา คณะวิทยาศาสตร์
มหาวิทยาลัยมหิดล

สนับสนุนโดยสำนักงานกองทุนสนับสนุนการวิจัย
และมหาวิทยาลัยมหิดล

Acknowledgement

This research has been a long and painstaking journey. I would like to thank all my graduate and undergraduate students who joined my lab and helped me to get through this research particularly Kanpong Boonthaworn, Ponlawoot Raksat, Ekasit Sonpho, Tanatchakorn Asawasriworanan, Pandaree Kornyanee and Padhomchai Pumthongtae.

I am in depth to Prof. Sakol Panyim, Prof. Jisnuson Svasti, Prof. Watanalai Panbangred and Prof. Skorn Mongkolsuk for always helping me with valuable advice. I am grateful to Prof. Yongyuth Yuthavong, Prof. Jim Ketudat Cairnes and Prof. Pimchai Chaiyen for constant encouragement.

I would also like to thank all my dear friends who have always helped me throughout the course of this research, Asst. Prof. Surang Chankamhaengdecha, Prof. Tavan Janvilisri, Asst Prof. Phurt Hanvoravongchai, Asst. Prof. Thanyada Rungrotmongkol, Asst Prof. Natharin Ngamwongsatit, Assoc. Prof. Arthit Chairoungdua, Assoc. Prof. Tuangporn Suttipongchai, Asst. Prof. Seangduen Moonsom, Asst. Prof. Patompon Wongtrakoongate and Assoc. Prof. Varodom Charoensawan.

I am also very thankful to all the supporting staff at Thailand Science Research and Innovation (TSRI) and Faculty of science, Mahidol University who have helped support me wonderfully especially K. Saengpetch Issarapanichkit, K. Paemala Udtanut and K. Kanchanit Woranaipinich.

Finally, I would also like to express my deepest gratitude to TSRI for financial support.

Puey Ounjai

บทคัดย่อ

รหัสโครงการ : RSA5980078

ชื่อโครงการ : การศึกษาการขนส่งสารผ่านซิเลีย: การศึกษาโครงสร้างโดยรวมของ ciliary pore complex และ ciliary barrier ของ *Tetrahymena thermophila*

ชื่อนักวิจัย : ผศ. ดร. ป๋วย อุ่นใจ ภาควิชาชีววิทยา คณะวิทยาศาสตร์ มหาวิทยาลัยมหิดล

E-mail Address : puey.oun@mahidol.edu

(ระยะเวลาโครงการ)

การสื่อสารระดับเซลล์เป็นปัจจัยสำคัญที่ควบคุมชะตาชีวิตของเซลล์ การกระจายสัญญาณและการรับสัญญาณของเซลล์ยูคาริโอตจะเกี่ยวข้องกับออร์แกเนลล์ที่เรียกว่าซิเลีย ทว่ากลไกการควบคุมการสร้างซิเลียนั้นยังไม่เป็นที่ทราบแน่ชัด ในงานวิจัยนี้จึงใช้เทคนิคทางชีวฟิสิกส์เพื่อศึกษาพลศาสตร์ของกระบวนการการสร้างซิเลียในเซลล์ยูคาริโอต โดยใช้โปรโตซัว *T. thermophila* และสาหร่ายสีเขียว *Chlamydomonas reinhardtii* เป็นโมเดลในการศึกษา เราได้ค้นพบว่ากลไกการสร้างซิเลียนั้นจะประกอบไปด้วยสองระยะ นั่นคือจะมีการยืดยาวของโครงสร้างแอคโซนีม (axoneme) และการพัฒนาไปเป็นโครงสร้างสมบูรณ์ที่จะเกิดที่บริเวณส่วนปลายสุดของซิเลีย โครงสร้างสามมิติของปลายซิเลียช่วยให้เราเข้าใจกระบวนการเปิดและปิดการทำงานของจักรกลขนส่งภายในซิเลีย (Intraflagellar transport (IFT) machinery) ที่ทำหน้าที่ควบคุมการขนส่งโปรตีนเข้าและออกจากซิเลีย นอกจากนี้ เพื่อเป็นการต่อยอดองค์ความรู้ให้สามารถเข้าใจบทบาทของสิ่งแวดล้อมจุลภาคที่มีผลต่อการควบคุมชะตาชีวิตของเซลล์ได้ เราจึงได้พัฒนาวิธีการแยกสกัดสารเคลือบเซลล์ที่สมบูรณ์จากสิ่งมีชีวิตที่สามารถซ่อมแซมส่วนที่เสียหายไปได้อย่างรวดเร็วนั่นคือหนอนตัวแบน โครงร่างสารเคลือบเซลล์ที่แยกได้ไม่มีเซลล์และจุลินทรีย์ปนเปื้อน การทดลองฉีดเซลล์ต้นกำเนิดของหนอนตัวแบนกลับเข้าไปในโครงร่างเคลือบเซลล์พบว่ามันสามารถช่วยพยุงชีวิตของเซลล์ต้นกำเนิดได้ การศึกษาทางโปรติโอมและการน๊อคดาวน์ยีนช่วยบ่งชี้ถึงโปรตีนในสารเคลือบเซลล์ที่มีบทบาทสำคัญทั้งในการซ่อมแซมอวัยวะและการสร้างอวัยวะใหม่ งานวิจัยนี้จะช่วยวางรากฐานเพื่อความเข้าใจกระบวนการควบคุมชะตาชีวิตของเซลล์ต้นกำเนิดได้

คำหลัก: การสร้างซิเลีย ซิเลีย สิ่งแวดล้อมจุลภาค สารเคลือบเซลล์

Abstract

Project Code : RSA5980078

Project Title : Characterization of ciliary transport: assessment of overall structure of ciliary pore complex and ciliary barrier of T.thermophila

Investigator : Puey Ounjai, Department of Biology, Faculty of Science, Mahidol University

E-mail Address : puey.oun@mahidol.edu

Project Period :

Cellular communication is an important factor that control cell fate. The reception and distribution of signal in eukaryotic cell often involved a unique organelle called cilium. However, the control mechanism for cilia formation is still unclear. In this research, we thus exploited biochemical and biophysical approaches to characterize the dynamic nature of ciliogenesis in eukaryotic organism including T. thermophila and C. reinhardtii. We proposed a two-step model of ciliogenesis. (I) the growth of the axonemal structure and the maturation of the distal tip complex. The three dimensional structure of the ciliary distal tip provided unique insights on the site of protein complex that regulate the activity of IFT machinery, the transport complex responsible for protein trafficking in and out of ciliary compartment. Furthermore, in order to advance our understanding regarding the impact of microenvironment in the fate determination of stem cell, we established a protocol to isolate the intact extracellular matrix from highly regenerative animal, freshwater flatworm. Recellularization revealed that the ECM structure could support the survival of microinjected stem cells. Proteomic characterization and RNAi screening identified a few proteins of ECM that are important not only in tissue homeostasis but also organ regeneration. This work lays foundation for a better understanding of the mechanism of fate determination of stem cells.

Keywords: ciliogenesis, cilia, microenvironment, extracellular matrix

Executive summary

Cilium is a cellular projection protruding out from the cell membrane of almost all animal cell types. Not only it is implicated in the cellular motility but also in the sensing of external environmental cues. Due to its essential role in cellular communication, cilium is extremely important for proper organ development and the maintenance of organ functionality. Defects in cilium function can cause myriad of severe non-communicable diseases so-called ciliopathies which include early onset retina degeneration, polycystic kidney disease, etc.

There are two major kinds of cilia, motile and non-motile. The structure of motile cilia is based on the "9+2" arrangement of 9 microtubule doublets and (usually) 2 microtubule singlets. The sliding of microtubule doublets against each other driven by the dynein motors provide motility of the organelle. Primary cilia, on the other hand, are non-motile and are proposed to be implicated in sensing of chemical cues and act as cellular antenna. In any case, the motile cilia have also been shown to be involved in various chemical and mechanical signaling processes.

In order to advance understanding of ciliary permeation and scrutinize the mechanism of ciliogenesis, our aim was to elucidate the structure of the ciliary pore complex using cryogenic electron microscopy. Unfortunately, due to unexpected shortage of the microscope time, we have to take the indirect routes to characterize the dynamic of ciliary formation.

Project 1: Characterization of ciliary growth dynamics and 3D structure of ciliary distal tip complex

To characterize the growth dynamics of the ciliary structure, the deciliation protocols suitable for extraction of cilia from different organisms were developed and the recovery of ciliary length were determined. Using negative stain electron microscopy, the shape of complex distal tip of different ciliary structure were visualized. We developed an algorithm to classify and identify different stages of the ciliary tip maturation based on the tip structure. To our surprise, at least 2 steps in the ciliogenesis was identified (I) the regrowth of ciliary axoneme to a proper length and (II) the maturation of ciliary distal tip.

Cryo-electron tomographic reconstruction revealed the first overall 3D architecture of ciliary distal tip. Based on the reconstruction, we suggested that the proposed locations of the remodeling complex for intraflagellar transport (IFT) complex need to be revised. Further attempt has been conducted to established a method to deciliate and purify the ciliary structure from animal model, planarian. We found that treatment with low percentage of ethanol could relatively well deciliate the animal without killing them. Such approach could be further developed as a method for characterization of ciliogenesis in animal.

Project 2: Isolation and characterization of microenvironmental factors from planarians

In order to further characterize the effect of external factors in determining cell fate, we further developed a method to isolate and characterize the extracellular matrix (ECM) in animal with high regenerative potency, freshwater planarians. An ECM-body can be successfully isolated. The

cell-free scaffold appears translucent yet it contains all the internal features, resembling the structure of intact planarian. Furthermore, microinjection suggested that ECM-body can be utilized as biomimetic scaffold for cell culture as it may support survival of injected neoblasts.

Objectives (revised)

1) To characterize the dynamic or ciliary regrowth using electron microscopy and computer vision.
2) Determination of the three-dimensional structure of the ciliary distal tip.
3) Establishment of a method for characterizing microenvironmental effect in animal model with high regenerative ability.

Methodology

Project 1: Characterization of ciliary growth dynamics and 3D structure of ciliary distal tip complex

Cell Culture & Animal Culture:

T. thermophila strain B8026 and SB711 were grown in either PPYS or modified Neff's media. To prepare cells for cilia isolation, stock culture cells were inoculated in SSP media and allowed to grow for 24 h at 30°C, with shaking. The volume of SSP media was then increased eight-fold and cells were cultured for another 24 h under these conditions. Cells were then spun down at 700xg and then transferred to an equal volume of starvation media (10 mM Tris-HCl, pH = 7.5) and cultured for 18 to 20 h before deciliation.

C. reinhardtii algae, strain CC-137+ were cultured in TAP media at room temperature. A light/dark cycle of 18 h/6 h was used. Cells were grown to approximately 1×10^6 cells/ml, and approximately 150 ml of cells were used for each deciliation.

***T. thermophila* Cilia Isolation:**

To ensure that cilia from the same sample were at the same stage of growth, an initial deciliation was performed. It was determined through pilot studies that cells deciliate most completely using a modified version of the dibucaine method (Thompson et al., 1974). Briefly, cells were spun down at 600xg for 7 minutes and re-suspended in half of their growth volume of starvation media, and dibucaine-HCl was added to a concentration of 300 μM for a 5-minute incubation. Then, fresh starvation media was added to double the volume immediately before pelleting cells at 1200xg for 5 minutes. The deciliated cells were suspended in the original volume of fresh starvation media for the regrowth period. After allowing the cilia to regrow for a specified time between 35 minutes and 6 h, the second deciliation was performed. The second deciliation was identical to the first deciliation, except the dibucaine concentration was 450 μM. After the 5-minute dibucaine-HCl incubation, glutaraldehyde was added to 0.025% and EGTA was added to 0.5 mM for a 30 s incubation. Then, an equal volume of 4% sucrose in ice-cold starvation media was added to dilute the dibucaine, and all subsequent steps were performed at 4°C. The sample was centrifuged at 1550xg for 7 minutes to pellet cell bodies. The supernatant was recovered and

centrifuged at 1550xg for 7 minutes again. The supernatant was recovered and centrifuged at 17,000xg for 40 minutes to pellet cilia. The final pellet containing isolated cilia was suspended in a minimal volume of starvation media for plunge-freezing.

Chlamydomonas reinhardtii Flagella Isolation:

Due to the fact that *C. reinhardtii* could not survive the dibucaine deciliation method, so the pH-shock method was employed for the first deciliation (Craige et al., 2013). Briefly, cells were centrifuged at 600 g for 5 minutes and re-suspended in one-tenth their growth volume in fresh TAP media, and acetic acid was used to rapidly drop the pH from neutral to 4.5 for 60 s. Then, the media's pH was rapidly neutralized with aqueous KOH. Fresh TAP media was added to double the volume, and cells were pelleted before resuspension in fresh TAP media. After allowing the cilia to regrow for a specified time between 35 minutes and 3 h, the second deciliation was performed using the dibucaine method, with the following modifications. The cells were concentrated to one-eighth the original volume in modified HMES buffer (10 mM HEPES, 5 mM $MgSO_4$, 0.5 mM EGTA, and 2% sucrose, pH = 7.4), plus 0.025% glutaraldehyde, and 625 μM dibucaine was used for deciliation. The cilia were isolated in the same manner as the Tetrahymena, except the final centrifugation was at 31,000xg for 30 minutes.

Negative Staining Electron Microscopy:

Preparation of isolated cilia for negative staining TEM observation was carried out using 400-mesh copper grids with a thick, continuous carbon coating that had been glow-discharged for 60 s immediately before sample deposition. A 3.0 μl aliquot of specimen was applied to the grid for 90 s. The specimen was blotted, and 1% uranyl acetate was applied to the grid for 90 s. The grid was then blotted and allowed to dry for at least 1 h before transferring into a JEOL-JEM1400 electron microscope operating at 100 keV. For each of the areas of interest, the z-height was adjusted to eucentric position before taking images to ensure magnification accuracy. Micrographs were taken at 8000X magnification and were analyzed using ImageJ.

Analysis of ciliary tip region diameter:

The analysis of the tip region of isolated cilia in negatively stained micrographs was performed using a set of custom-written Java programs. A detailed description is provided in the supplementary material. Briefly, micrographs were contrast-inverted and then bandpass-filtered to enhance the cilium's edge contrast. Then, a polyline was drawn along the central axis of each cilium, starting from the absolute tip, and a width-determination program generated a diameter profile. An interpolating polynomial curve of degree six was fit to the diameter profile, and the location where the slope decreased below 0.0532 (equivalent to a 1.5º incline on each side) is used to define the position separating the mature full diameter region with the cilium tip region of an increasing dimeter (shown as the arrows in Figure 2). Then potential lengths were reported.

From these potential lengths, the cilium's tip region length was measured by determining which potential length agreed with the original micrograph. Parameters for the best-fit curves were determined using the nonlinear least-squares Marquardt-Levenberg algorithm implemented in Gnuplot. With the above strategy, a set of Java programs were written as a plug-in package for ImageJ (Schneider et al., 2012) and used for this analysis.

Characterization of developing cilia and ciliary tip regions:

In order to characterize ciliary development using the length of the entire cilium and the length of the tip region, average lengths of these features were plotted as functions of time. The ciliary tip region measurements appeared to exhibit the following characteristics: the ciliary tip region started at length zero, and it then sequentially reached a local maximum, an inflection point, and asymptotically approached a final length. Based on these conditions, a curve of best fit was determined using a quotient of two trinomials of the form (ax^3+bx^2+cx)/(dx^3+ex^2+fx+g). From these curves, the local maxima and horizontal asymptotes were determined. In order to characterize the length of the entire cilium as a function of time, we fit our data to the solution to the differential equation described in (Marshall and Rosenbaum, 2001).

Cryo-EM sample preparation:

Preparation of isolated cilia for cryo-EM observation was carried out using 300-mesh copper grids with a thin, continuous carbon coating that had been glow-discharged for 30 s immediately before sample preparation. A 2.5 µl aliquot of 0.1% poly-L-lysine (w/v in water) was applied to the grid for 1 minute. The grid was blotted, and subsequently washed twice in water. Then, water was applied to the grid a third time, and the grid was loaded into the Gatan CryoPlunger3. The grid was blotted, and a 2.5 µl aliquot of cilia specimen that had been mixed 3:1 with 15 nm gold particles was applied to it for 20 s. Then, single-side blotting was used to blot the grid for 6.0 s before plunging into liquid ethane at -174°C. The frozen grids were stored in liquid nitrogen until loaded into a JEOL-JEM3200FSC/PP electron microscope. Data were acquired using either a CCD camera or a Gatan K2 Summit direct-electron detector.

Cryo-ET data collection and processing:

All electron tomographic tilt series data sets were collected using SerialEM (Mastronarde, 2005) with a tilt increment of 2 or 3 degrees. The JEM-3200FSC was operated at 300 keV with zero-loss energy filtering, slit width 24 eV. The pixel size on the specimen was 0.36 nm and the total electron dose was about 70 e-/A2. Images were recorded at a target underfocus between 4 and 8 µm on a K2 Summit direct-electron-detection camera (Gatan, Pleasanton, CA) with 5 to 8 frames per second during an exposure time of 1 to 1.5 sec. Frame alignment was carried out with the "Unblur & Summovie" package (Brilot et al., 2012; Campbell et al., 2012; Grant and

Grigorieff, 2015). Tomographic reconstruction was carried out using Etomo/IMOD (Kremer et al., 1996)

Scanning electron microscopy:

Tetrahymena samples collected from different time points of regrowth after deciliation were fixed by 1% glutaraldehyde and placed in pre-processed aluminum carriers from the M. Wohlwend GmbH, Engineering office. Before adding *Tetrahymena* cells, the carriers were carbon coated and glow discharged (two minutes) followed by treatment of poly-L-lysine coating to increase cell attachment. The *Tetrahymena* cells in the carriers were subjected to a six-step gradient dehydration of ethyl alcohol (10%, 20%, 40%, 70%, 90%, and 100%) followed by critical-point drying using Samdri-795 with a 15 minutes purging process. Afterwards, the samples in the carrier were fixed on conductive stubs with silver glue and gold-coated for 45 seconds using a CRESSINGTON Sputter Coater. SEM images were captured at 2kx, 5kx, and 10kx magnifications using Secondary Electrons Secondary Ions detector of a ZEISS NEON 40EsB High Resolution Dual Beam Scanning Electron Microscope.

Project 2: Isolation and characterization of microenvironmental factors from planarians

Animal culture:

D. japonica and local Thai planarians were maintained in an autoclaved spring water tank at room temperature (24 °C) and were fed with chicken liver twice a week. Autoclaved spring water was changed a couple hour after feeding to prevent water spoiling. *S. mediterranea* was maintained in 1X Montjuic salt solution, as described previously for a classical static culture procedure (Newmark and Sánchez Alvarado 2000).

Planarian ECM isolation:

Seven-days starved animals, 0.3-1.0 cm in size, were collected from the tank. This protocol was designed for 20 planarians. Planarians were terminated and stabilized by gently dropping them one at a time into the stabilization solution. The plate containing planarians in stabilization solution was incubated at 4 °C for 1 hr without shaking. After stabilization, the solution was replaced with 40 ml of decellularization solution I for 18 hr at 4 °C. To ensure complete decellularization, the solution was replaced with 40 ml decellularization solution II for 2 hr at 4 °C.

Scanning electron microscopy:

Planarian ECM sample were fixed with 2.5% glutaraldehyde in 0.1 M sodium cacodylate pH 7.2 at 4 °C and washed with 0.1 M sodium cacodylate buffer pH 7.2 at 4 °C. Next, ECM were fixed with 1% osmium tetroxide in 0.1 M sodium cacodylate buffer for 1 hr at 4 °C. The samples were next washed with 0.1 M sodium cacodylate buffer pH 7.0 at 4 °C. Worms were dehydrated by

soaking in a series of concentrations of ethyl alcohol at 30%, 50%, 70% 80%, 90% and 95% for 15 min each, at 4 °C. Finally, absolute ethyl alcohol was used to replace the last 95% ethyl alcohol solution at 4 °C. A residual ethyl alcohol was removed using critical point drying (CPD). The samples were mounted on stubs with double-coated conductive carbon tape. Specimen was coated with Pt-Pd for 4 min using ion sputter before observing under JSM-6510 Series Scanning Electron Microscope (JEOL, Japan). The sample were visualized using Hitachi SU8000.

Nuclear visualization:

Isolated extracellular matrices as well as intact animals are transferred into 24-well plate. A coverslip was added at the bottom of each well. Worms were treated with 5% N-Acetylcysteine for 10 min at RT to terminate them and, wash away excess mucus. The samples were fixed in 0.8% formaldehyde (Sigma-Aldrich, MO) for 1 hr at 4 °C. The samples were rinsed twice with PBST, which is PBS supplemented with 0.3% Triton X-100 (Sigma-Aldrich, MO). Samples were then incubated for 2 hr in a permeabilizing solution composed of 1X PBS and 0.5% Triton X-100 at 4 °C and then rinsed thrice with PBST prior to be stained with 1:400 DAPI solution (Invitrogen, Carlsbad, CA). The samples were then incubated in PBST in darkness for 1 hr at room temperature. Stained specimen was then washed 5 times in PBST, for 5 min each. The samples were then incubated in 80% glycerol for 30 min at 4 °C. Finally, samples were transferred and mounted using 80% glycerol on a clean glass slide. DAPI-stained samples were visualized using an Olympus BX53 fluorescent microscope (Olympus, Singapore). For the samples stained with Hoechst 33342, the samples were fixed with 4% paraformaldehyde, 5% methanol, PBS for 20 min, followed by double washing in PBST, for 10 min each. Subsequently, the solution was replaced with 1:2000 Hoechst 33342 in 1×PBS and incubated for 10 min. The samples were observed under Fluoview FV3000 confocal laser scanning microscope (Olympus, Singapore).

Neoblast isolation and microinjection:

Planarians were cut into 3-4 fragments using a clean scalpel. The fragments were then soaked in Holtfreter's solution diluted in distilled water. The fragments were further subjected to physical mincing and treatment with 0.25% trypsin for several minutes at 20°C. Cells were dissociated by gentle pipetting up and down several times. The dissociated cells were filtered through a 35 μm pore size cell strainer and 20 μm nylon net filter to remove tissue fragments. Single-cells suspension was stained with Dye Cycle (Invitrogen, Carlsbad, CA) for 30 min at room temperature. Flow cytometric analysis was performed using a BD FACS Melody Cell Sorter (Becton-Dickinson, Franklin Lakes, NJ). X-ray-sensitive neoblast cell or X1 fraction were isolated and utilized in a microinjection. X1 cells (1×10^5) could be temporarily maintained in 24-well plates in 1 ml culture medium on a rotary shaker at 20 °C in CO2 incubator. The cells were collected by centrifugation at 300xg for 7 min. Aggregated cells (10 μl) were drawn into a capillary glass of the injector. ECM was placed firmly on a black sterile filter paper for the injection. The cells

were then injected into posterior and anterior parts of a pharynx. After the injection, ECM was transferred gently into a LCDM and expanded-potential stem cells medium cocktail (EPSCM, Yang et al. 2017) and cultivated at 24 °C in a CO2 incubator.

Proteomics analysis:

Isolated ECM-body was subjected to digestion including alkylate reduction and the treatment with PNGaseF Lys-C/Trypsin. Mass spectrometer was performed by Q-Exactive Plus (QE+). Peptide and protein identification was analysed using ProLuCID DTASelect software pagkage.

RNAi food preparation

The workflow for RNAi screening was illustrated in Figure 3.4. One planarian was expected to ingest 1 μl of food in one feeding. In the experiment, 130 μl of food was produced to sustain three feeding cycles. Firstly, bacteria expressing the plasmid containaing the region for dsRNA synthesized under T7 promoter was incubated overnight at 37 °C in 5 ml of 2xYT with kanamycin and tetracycline. For large-scale RNAi food preparation, the 2xYT bacterial culture was scaled up to 30 ml. After overnight incubation, 30 ml of fresh 2xYT with kanamycin and tetracycline was prepared in 50 ml conical tubes. Bacteria solution was aliquoted in 3-4 ml and seeded into 30 ml of fresh 2xYT with Kan and Tet. The 50 ml tube was incubated at 37 °C for 1 hr or until OD600 value of medium reached 0.5-0.8. Isopropyl β-D-1-thiogalactopyranoside (IPTG) at the final concentration of 1 mM was added into the tube to activate dsRNA synthesis for 2 hr. After 2 hr of incubation with IPTG, the tube was centrifuged at 4,000 xg for 6 min to bring down the bacterial pellet. The residual 2xYT medium was removed and aspirated to prevent food rejection by the planarians. Next, liver mixture was prepared by dissolving 2 volume of liver puree into 1 volume of planarian water. Food colouring was added to a puree (1 μl of food coloring per 30 μl of mixture). The coloured liver puree was added to the bacteria pellet. It was critical to mix the liver puree and bacterial pellet thoroughly since it could affect RNAi knockdown efficiency. RNAi food was aliquoted into microtubes and kept in -80 °C prior to feeding.

Homeostasis and regeneration assays

In order to assess a phenotype of RNAi planarians, two approaches were used: homeostasis and tissue regeneration assays. Briefly, a homeostasis assay aimed to investigate whether the gene targeted by RNAi was involved in tissue homeostasis without any injury or amputation. Moreover, it was used for studying tissue turn-over in planarian resulting from neoblast cellular activities, such as proliferation or apoptosis. For the homeostasis assay, the worm was observed for couple days after the last feeding of RNAi. Any signs of dysregulated body plane or of lysis were considered as a defect phenotype. Defects also included the topology of the epithelial surface on the dorsal side. Appearance of lump(s), disintegration, color changing, or morphology distortions

were also considered a defect phenotype. Ultimately, worms that showed no sign of responses to any poking or disturbance would be considered as dead.

A regeneration assay aimed to investigate whether the RNAi-targeted gene was involved in the tissue regeneration process, including wound healing, or in the cellular activities of neoblasts, such as proliferation, migration, differentiation, or apoptosis. Planarians were observed for 1, 3, 5, 7, 9, 11, and 14 day after sagittal amputation. Any signs of incomplete or lack of a newly regenerated tissue (blastema) were considered a defect phenotype. Moreover, absence of eye spot and/or pharynx were included as well. Besides, lump, disintegration, color changing, or morphology distortion were also considered defects. Eventually, worms that showed no sign of responses to any poking or disturbance would be considered dead. A number of defective planarians based on the homeostasis and regeneration assays were recorded and the graph of survival rates was constructed. There were at least three biological replicate analyses for each RNAi-targeted gene in the survival determination experiment.

Irradiation of the animal

Two to four millimeters sized planarians were starved for 7 days prior being subjected to gamma ray irradiation in GammaCell 40 Exactor irradiator for 1,250 for sub-lethal exposure or 6,000 rad for lethal exposure.

Whole-mount *in situ* hybridization (WISH):

Planarians were treated with 5% N-acetyl cysteine (NAC) in 1X PBS solution for 5 min at RT. NAC is a mucolytic reagent that both terminate a worm and remove mucus from the worm surface. NAC was replaced with a fixative solution (4% formaldehyde in 1xPBST, 0.5% Triton X) for 1 hr at RT. The fixative was removed, and worms were rinsed twice with PBST (0.5% Triton X) for 10 min each. PBST was replaced with a 50% methanol solution for 10 min at RT. Next, 50% methanol was removed, and the worms were rinsed twice with 100% methanol for 10 min each at RT. Samples were stored in 100% methanol at -20 °C prior to use. On the next day, 100% methanol was replaced with 50% methanol for 5 min at RT. 50% methanol was replaced with PBST (0.5% Triton X) for 10 min at RT. PBST was replaced with bleach solution under a light directly for 90 min at RT. Worms then were rinsed twice with PBST (0.5% Triton X). PBST was replaced with Proteinase K solution (2 μg/ml) for 10 min at RT. Proteinase K solution was replaced with 4% fixative solution for 10 min at RT. Fixative solution was removed and the samples were rinsed with PBSTx (0.5% Triton X) twice for 10 min each at RT. The samples were incubated in 1:1 PBSTx : Prehyb solution for 2 hr at 54 °C. Prehybe solution was replaced with riboprobe mix for 16 hr at 54 °C (1 ml of hyb solution / 1μl of riboprobe). Samples were then washed intensively several times with hyb solution (0.5% Triton X) three times for 20 min at 54°C. Samples were then washed with 1:1 wash solution (0.5% Triton X) : 2x SSC (0.1% Triton X) three times for 20 min at 54°C and with 2x SSC (0.1% Triton X) three times for 20 min at 54 °C.

Samples were washed with 0.2x SSC (0.1% Triton X) three times for 20 min at 54 °C. Lastly, samples were washed with MABT buffer three times for 20 min each at 54 °C. Then, samples were blocked with 5% horse serum plus 0.5% Roche western blocking reagent in MABT for 2 hr at RT with rocking. The samples were incubated with the appropriate antibody overnight at 4 °C (Anti-DIG-AP 1:3000 in 5% horse / 0.5% Roche western blocking reagent in MABT). Samples were washed 6 times in MABT for 2 hr at RT. The samples were incubated in AP buffer for 1-2 min following with incubation in EQ buffer for 10 min and DEV buffer + NBT/BCIP until the signal appeared. The reaction was stopped by rinsing with 1X PBS twice. Samples were fixed with 4% fixative solution in PBST (0.3% Triton X). The background was cleared by incubating in 100% ethanol. Samples were replaced with 50% ethanol in 1x PBST for 5 min. The solution was replaced with 1X PBS until the worm sank. Lastly, the sample was mounted in 80% glycerol for visualization.

Results

Project 1: Characterization of ciliary growth dynamics and 3D structure of ciliary distal tip complex

Tips of growing cilia display a morphological progression during development

To investigate ciliary development, *Tetrahymena* were deciliated using the dibucaine-HCl method, and cells recovering their cilia at different time points were examined using scanning electron microscopy. We found that cilia exhibit diverse tip region morphologies throughout their development.

Tetrahymena cilia exhibit several distinct morphological features as they develop. During the initial phase of ciliary regrowth, cilia are typically less than two microns in length, and they have a hemi-capsule morphology as they emerge from the ciliary pocket (Fig. 1a-c and 1g-i). In agreement with previous studies(Rannestad, 1974), somatic cilia regrow uniformly along rows following a complete deciliation event. There is also a period of rapid growth between 10 and 135 minutes. As early as 20 minutes after deciliation, the distal ciliary region begins to extend a pointed tip (Fig. 1c and 1i). This ciliary tip region extension coincides with elongation of the whole cilium (Fig. 1d-e and Fig.1j-k). At later time points, ciliary tip regions exhibit shorter lengths (Fig. 1f and Fig.1l). Proximal to this tip region, the cilia appear to be of constant diameter. Taken together, these observations suggest that the tip region undergoes a consistent remodeling process as the cilium develops. However, resolution limits and variations in three-dimensional orientations of the ciliary tips make it difficult to characterize this dynamic morphology systematically using scanning electron micrographs. In order to view developing ciliary ultrastructure in detail, we expanded these studies using negative-staining transmission electron microscopy.

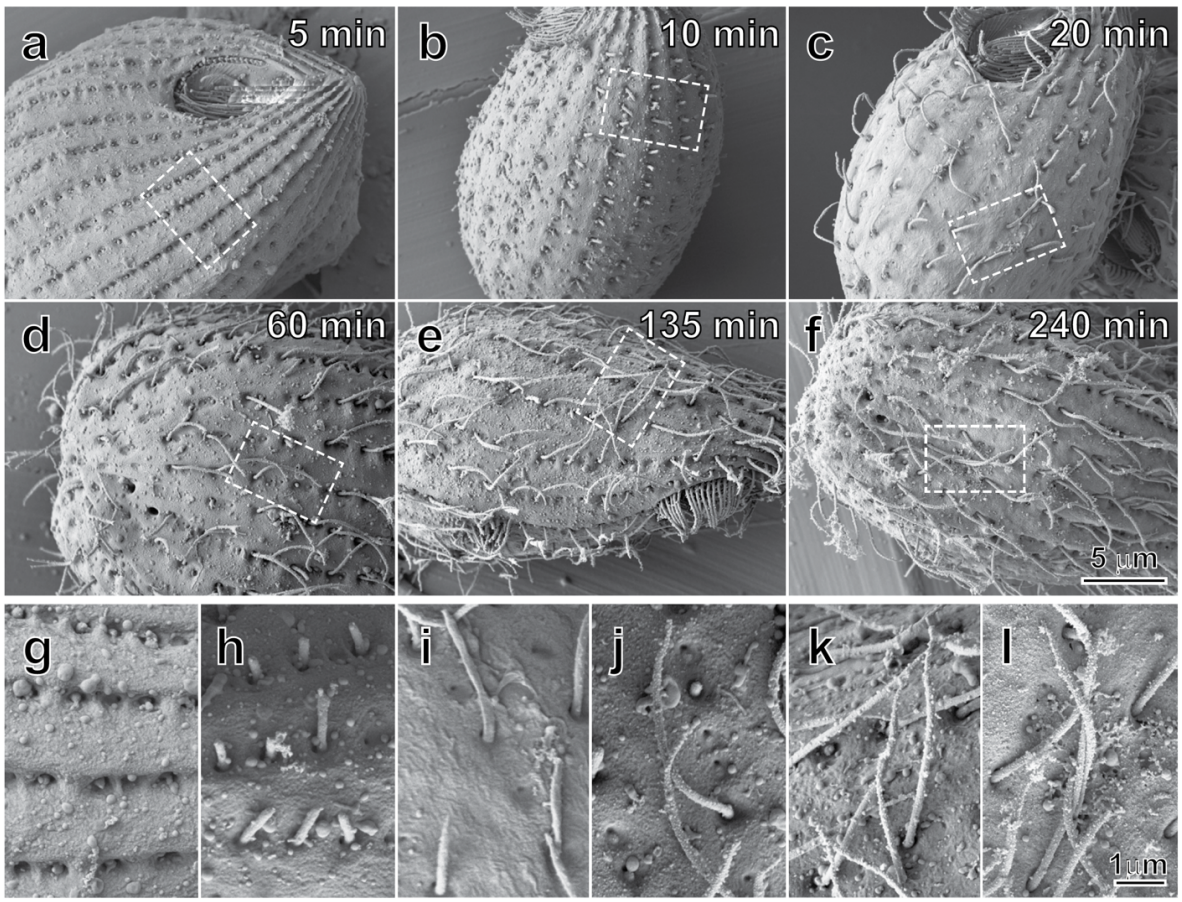

Fig 1 Structural dynamic of cilia development after deciliation from 5 to 240 min (A-F). The expand views of cilia from (A-F) are shown in (G-I) respectively.

The ciliary tip diameter profile progressively transitions during cilium development

To validate and further characterize this time-dependent morphological transition, we used negative-staining EM on re-growing cilia isolated from *Tetrahymena* (Fig 2). The micrographs provided sufficient morphological detail for a quantitative description of ciliary ultrastructural features. Typical morphological features of the growing cilium include a thin diameter at the distal end, followed by a region of increasing diameter, until the cilium reaches full-width (Fig. 2a -2g). It appears that the ciliary region intermediate to the absolute tip and the point of full width is a developing zone lacking the full complement of axonemal components. Portions distal to the mature regions are considered part of the ciliary tip region.

In order to define the transition point between the developing zone and the mature regions objectively, we designed a systematic method and composed a set of customized Java programs as a plug-in package for ImageJ (Schneider et al., 2012), as briefly described in the method section. An explanation of the theory and implementation of this method is summarized in the supplemental text. Using this method, the length of the developing region can be defined objectively, and the progress of the tip region's development can be described based on the length of the developing regions at the tip. Fig 2 shows representative isolated cilia (Fig. 2a-2g), along with their processed images (Fig 2a'-2g'), diameter profiles (Fig. 2h-2n), and derivative plots (Fig. 2o-2u). The arrows in panels indicate the end of the ciliary tip region, as defined above. This quantitative measure clearly shows that the length of the ciliary tip region changes over the 8 h regrowth period. In the beginning of cilia growth, the length of the ciliary tip region elongates and reaches its maximum length after around 135 minutes of regrowth (Fig. 2d). After this maximum length is reached, the ciliary tip region slowly decreases in length until the cilia exhibit short-tipped morphologies (Fig. 2f and 2g). This development process takes place over the course of several hours, with the stable, short-tipped morphologies being present around 5 hours after the initial deciliation.

From these profiles, differences in diameter trends become clearer. In general, cilia with the longest tips (such as those shown at 60, 135, and 180 minutes) had very thin extensions (Fig. 2c-2e); oftentimes cilia with tip regions around two microns had diameters as thin as 75 nm. In ciliary tip regions with these very narrow extensions, a bulging of the very distal portion was occasionally visible, apparently due to the FTC. Meanwhile, cilia with shorter tip regions (such as those shown at 35 and 300 minutes) typically displayed wider, though still thinner than full-width, tip regions. In agreement with typical ciliary diameters, all cilia had full diameters between 200 nm and 300 nm, suggesting that negative staining produced minimal artifacts affecting ciliary diameter. In all of the isolated cilia, the FTC was clearly seen, indicating that the flagellar tip complex assembles at the distal ciliary tip region within 20 minutes of ciliary re-growth, and that the FTC persists throughout the cilium's lifetime. Lastly, many ciliary diameter profiles exhibited a stepped appearance. This could potentially be due to uneven termination of axonemal MTDs in the tip region.

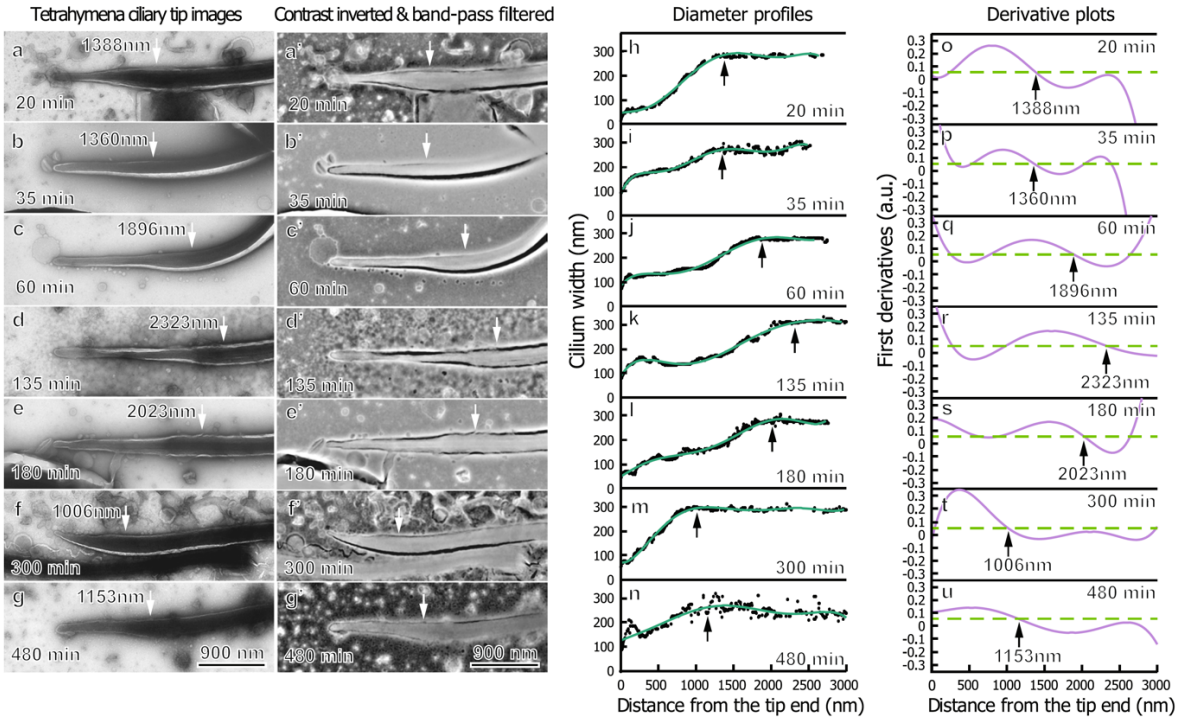

Fig 2 Different morphological ultrastructure of the distal ciliary tips. The arrows in both images indicate the beginning of the tip region. The algorithm can be used quite successfully in identify the stage of growth of cilia distal tip regions.

In order to determine whether these observed morphological characteristics are conserved among protists, isolation and width profile determination experiments were replicated using re-growing cilia from *C. reinhardtii*. Overall, Chlamydomonas exhibited a similar trend of the ciliary tip region growing in length before decreasing in length. However, *Chlamydomonas* cilia did not typically exhibit diameters below 100 nm, and the tip regions were typically less than 20% of the total ciliary length. Therefore, *Chlamydomonas* cilia exhibit a similar, though less dramatic, tip region growth trend.

Development of the ciliary tip region continues after the cilium reaches full length

Previous investigations into ciliogenesis primarily studied length of the entire cilium during the elongation phase and/or cell motility(Hadley and Williams, 1981; Jarvik and Rosenbaum, 1980; McVittie, 1972; Rannestad, 1974; Rosenbaum et al., 1969). In order to consider tip region development in the context of the growing cilium's length, we determined both the average ciliary tip length and the average length of the entire cilium at different times of regrowth.

The method described above was used to measure the average length of the ciliary tip region from at least 27 cilia isolated at different time points for each cell type. As shown in Fig. 3, the ciliary tip regions of both *Tetrahymena* and *Chlamydomonas* initially extend outwards reaching a maximum length of over 2 microns at 135 minutes for *Tetrahymena* (Fig. 3a) and a maximum length of 1.3 microns at 150 minutes for *Chlamydomonas* (Fig. 3c). After the tip region reaches its maximum length, it decreases in length until it asymptotically approaches 1070 nm in *Tetrahymena* and 680 nm in *Chlamydomonas*. Based on the rate of change, in both species, it takes approximately six hours to reach full, mature tip length. The results of these flagellar regeneration kinetics experiments on the full length of both Tetrahymena and Chlamydomonas cilia closely follow previously reported trends (Hadley and Williams, 1981; Rosenbaum et al., 1969). We find that in both species, an initial, rapid growth rate is followed by a plateau phase, in which cilium length remains constant. Furthermore, the full-length of cilia isolated from both *Tetrahymena* and *Chlamydomonas* followed previously modelled regeneration kinetics (Marshall and Rosenbaum, 2001). *Tetrahymena* cilia reach a full length of 6.5 microns, while *Chlamydomonas* cilia reach a full length of 10.7 microns.

Upon comparison of the ciliary tip region and whole cilium length profiles, it becomes clear that tip region development and maturation continue long after the cilium has reached full length. Although the whole cilium grows to full length slightly after one hour after deciliation, it takes approximately six hours for the ciliary tip region to establish a stable length. The time scale of this process is much longer than polymerization rates of tubulin on MTDs (Binder et al., 1975).

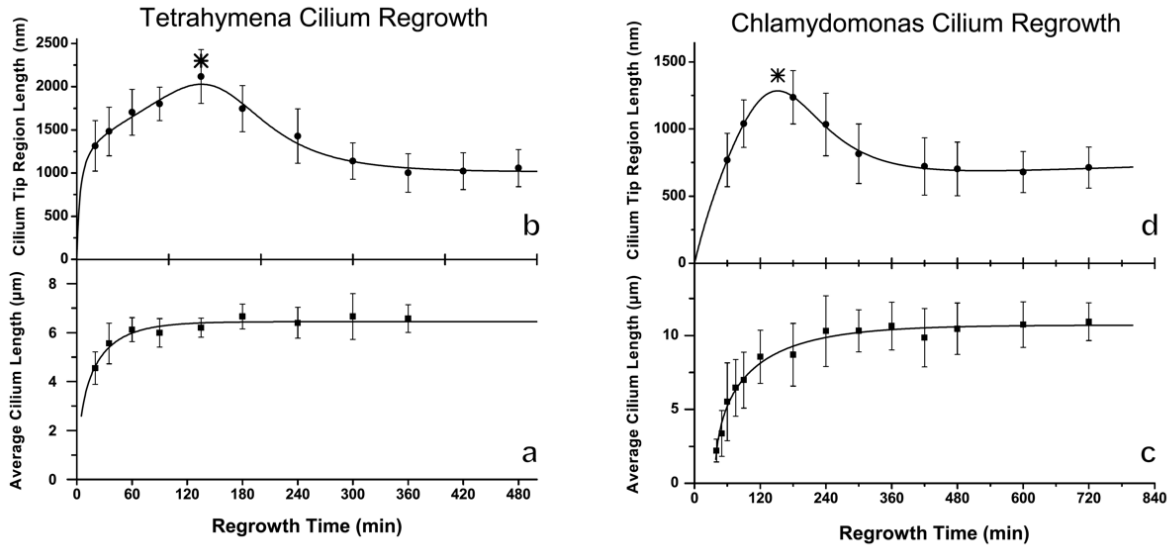

Fig 3 Reciliation rate and cilia maturation of *Tetrahymena* and *Chlamydomonas*.

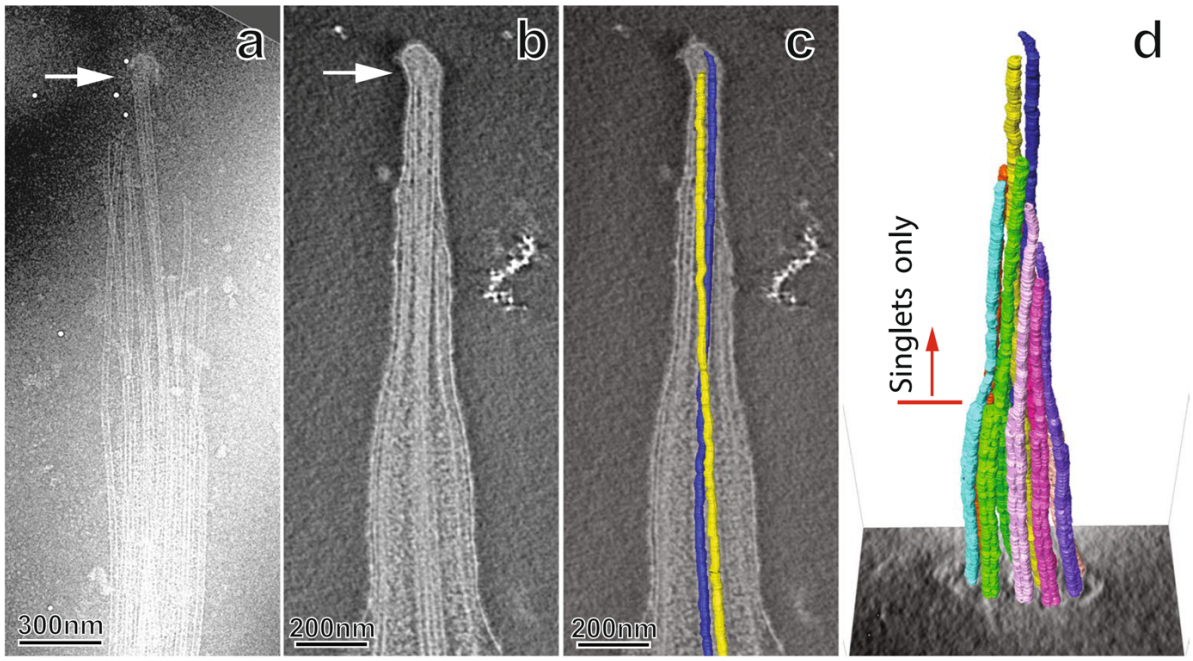

Fig 4 Different morphological ultrastructure of the distal ciliary tips. The arrows in both images indicate the beginning of the tip region. The algorithm can be used quite successfully in identify the stage of growth of cilia distal tip regions.

Structural features of the growing cilium tip

Conventional EM has revealed the tip structure of mature *Tetrahymena* cilia (Dentler, 1980; Dentler and Rosenbaum, 1977; Gaertig et al., 2013), in which the longest portion is the central pair microtubule singlets capped by a ball-shaped FTC resembling a post-light, and the central pair complex is surrounded by 9 microtubule doublets forming a cylindrical configuration. At the distal ends of the microtubule doublets, the complete A-tubule extends farther and is stabilized by a globular protein complex that links to the ciliary membrane by fibrous proteins known as distal filaments. We performed an electron tomographic study on the cilium tips of re-growing cilia to better understand the tip structure in the regrowth phase.

Our EM study demonstrates that the overall structure of the growing tip is largely similar to the architecture of the mature cilium tip; however, the more proximal portion of the ciliary tip region differs from the mature cilium. The growing axoneme's most distal components are two microtubule singlets of the central pair complex and a FTC that caps the central pair microtubule singlets together. Previous studies have used splayed cilia as indications of axonemal composition in the tip region(Sale and Satir, 1976), and during specimen preparation, isolated cilia occasionally displayed membrane damage localized to the tip region. This resulted in a splaying of the tip region's contents, while the remainder of the cilium remained intact. These frayed tip regions allowed for easier visualization of the ciliary tip region's components. Fig. 4a shows that the zone approximately 50 to 400 nm proximal to the FTC is occupied by the central pair microtubules and extended A-tubules. Notably, the A-tubules extended into the ciliary tip region appear undecorated, whereas axonemal spacer proteins (radial spokes and outer dynein arms) are usually visible under cryo-EM (Kishchenko et al., 2015; Lin et al., 2012; Oda et al., 2014; Pigino et al., 2011). This observation, along with the absence of B-tubules suggests that the developing ciliary tip region lacks a full complement of axonemal proteins. While splayed ciliary tip regions provide clear visualization of the ciliary tip region's contents, it is possible that these features could be artifacts caused by membrane disruption.

A more detailed, native state of the developing ciliary tip region was achieved via cryo-ET. Tomograms of developing cilia allow us to verify that like in the matu(Kishchenko et al., 2015)re cilium, the FTC is positioned in the most distal region of the cilia, as shown in the cross-section of a cryo-tomogram of a 3h-regrowth cilium tip (Fig. 4b). At the tip of the growing cilium, the FTC-capped central pair is surrounded by a set of long microtubule singlets, not the standard nine doublet microtubules. These singlets are extensions of the MTD's A-tubule. These microtubule singlets are visible in the tomogram (Fig. 4b), and they are clearly shown in the frayed tip (Fig. 4a). In the tomogram of Fig. 4b, the B-tubules are over one micron away from the FTC. Lastly, we observed that the central pair often has a left-handed twist approximately 0.5 microns from the distal tip region (marked by red lines in Fig 4b).

Project 2: Isolation and characterization of microenvironmental factors from planarians

Deciliation of planarian cilia

In order to develop a new animal model for studying ciliogenesis, we pursued our experiment on freshwater planarians. All the standard deciliation protocol including dibucaine and pH shock were utilized in order to induce cellular autotomy in planarians. It was clear that neither of the protocol could yield effective deciliation of the flatworm (B-D). Treatment with low percentages of ethanol, however, not only allow a more uniform distribution of deciliated regions. Density analysis clearly showed the marked decrease in the number of cilia after the treatment. Notably, almost all of the worms treated with low concentration of alcohol appeared to be survived and could regrow the cilia back.

Isolation of planarian ECM

The isolation of planarian *D. japonica* ECM was done using the protocol summarized in Fig 6A. It was clear that the isolation of ECM from planarian release the translucent scaffold resembling the shape of the worm (Fig 6B-D). The organ organization inside the worm remained largely intact (Fig 6C-D). Nuclease treatment of the ECM-body could provide an extra step to remove a potential small nucleic acid fragments that could remain trapped inside the ECM. The decontamination of ECM was done with extensive washing in sterile culture media. Upon incubation of sterile ECM in media for 4 days, the media was still clear with no apparent change in color (Fig 6F) . PCR based Mycoplasma detection was performed and confirmed that there was no mycoplasma presented in the isolated ECM-body (Fig 6G). Nuclear staining revealed that no residual cell was remained inside the scaffold (Fig 6E). We further microinjected X1-sorted neoblasts into the scaffold The force introduced by microinjection of X1-sorted neoblast into the scaffold could cause some distortion and/or swelling in the ECM body (Fig 6 H). The nuclear staining results of the recelluarlzed ECM further consolidated that the ECM could potentially be helpful house the microinjected cells could remain inside the scaffold for at least 4 days as shown in Fig 6I-K.

RNAi Screening

73 genes were selected from the proteomic inventory of decellularizing planarians for RNAi screening. To silence the gene, feeding silencing method was used. The worms were fed every three days for a total of ten times. Upon the completion of RNAi feeding, planarians were proceeded cut in homeostasis or regeneration assay.

Based on RNAi screening in homeostasis assay, it was clear that knock down of tolloid-like protein 1(*tll*) and kyphoscoliosis peptidase (*ky*) result in aberrant homeostasis (Figure 8). The *tll*-knockdown worms showed the presence of three streaks lined from an anterior to posterior axis. Body of the worms was clearly curling along the dark streaks particularly at the posterior part.

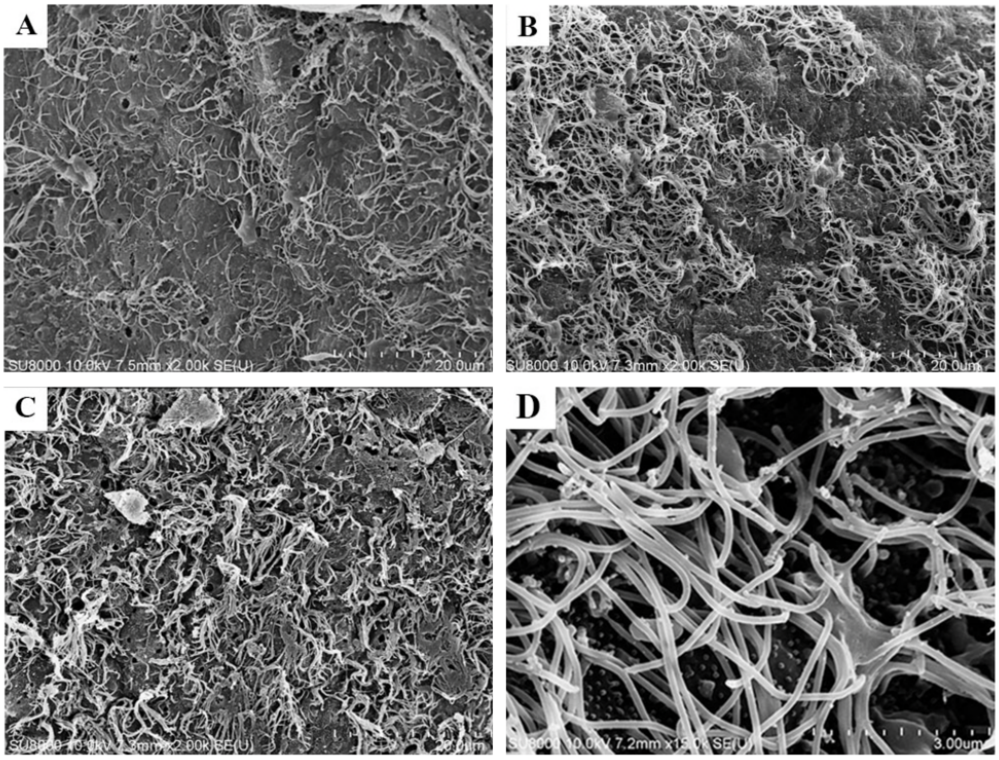

Figure 5 effect of different deciliation protocol for isolation of planarian cilia. (a) Marked decrease in the ciliary structures was observed on the planarian ventral surface after treated with 3% ethanol. (b) The dibucaine method could cause induced some partial deciliation on the surface. (c) The ventral surface from pH-shock condition shows the abnormal cilia architecture. (D) expand view showing the density of cilia before the treatment.

This lead to tube-like appearance at the tail region. Moreover, the posterior surface of the worm appeared to be relatively rough as indicated with red arrow. Body lesion(s) was clearly present on the dorsal surface of the *ky*-knockdown worms as indicated with yellow arrow. Significant reduction in the body size and motility of planarians was also observed. Notably, 47.22% of *ky*-knockdown worms lysed after the completion of RNAi feeding of the program.

Further RNAi screening for pinpointing the gene candidates involved in regeneration demonstrated that tolloid-like protein 1 (*tll*), kyphoscoliosis peptidase (*ky*) and basement membrane heparan sulfate proteoglycan (*hspg)* (Fig 8). All the animal used as negative control showed a normal regenerative tissue, indicating with the presence of eye posts on the newly regenerated tissue with less pigment so-called blastema.

All of the regenerating *tll*-knockdown worms failed to regenerate blastema, indicated by lacking of a new, unpigmented tissue at the wounded edge. In addition, the eye spot of regenerating worms also failed to regenerate as well. Moreover, the planarians bent to form curvy structure while tail of regenerating planarian was ventrally curled up to form tube like structure similar to phenotype observed in *tll*-knockdown worms in the homeostasis assay. The dorsal surface of planarian also appeared to be rough. Although *ky*-knockdown worms were able to form new blastemal tissue, the eye spot was failed to form. The *hspg*-knockdown worms showed bulging structure at the pharyngeal position. The blastema of regenerating *hspg*-knockdown worm were well-developed with a normal eye spot.

Determination of RNAi knockdown efficiency

In order to evaluate the efficiency of RNAi based knockdown, quantitative polymerase chain reaction (qPCR) was conducted. Marked decrease in the RNA level were detected in all the knockdown experiments (Fig 10).

Determination of neoblast-specific gene expression

The locations of the expression of the selected candidate genes were investigated. The first question we would love to address was whether our gene candidates could be expressed in an adult pluripotent stem cell. It has been shown that radiation could be exploited to eradicate all stem cells from planarians body (Reddien et al. 2005). Therefore, we combined the radiation and *in situ* hybridization to identify the locations of gene expression. In *in situ* hybridization experiment, *piwi-1* as was used as a control as this gene was proposed to be the marker for stem cells. The signal from *in situ* hybridization of *piwi-1* would disappear after a few days post radiation. In our case, if the gene candidates express in neoblast, the radiation eradicate or reduce the intensity of *piwi-1* in the *in situ* hybridization experiment (Figure 11). The *hspg* was found to be expressed all over the body of planarians in unirradiated animals, especially at the pharynx. The overall signal of the *hspg* expression appeared to be unchanged after a lethal radiation. The expression of *tll* was also found to be well distributed in every parts of the worm body and remained the

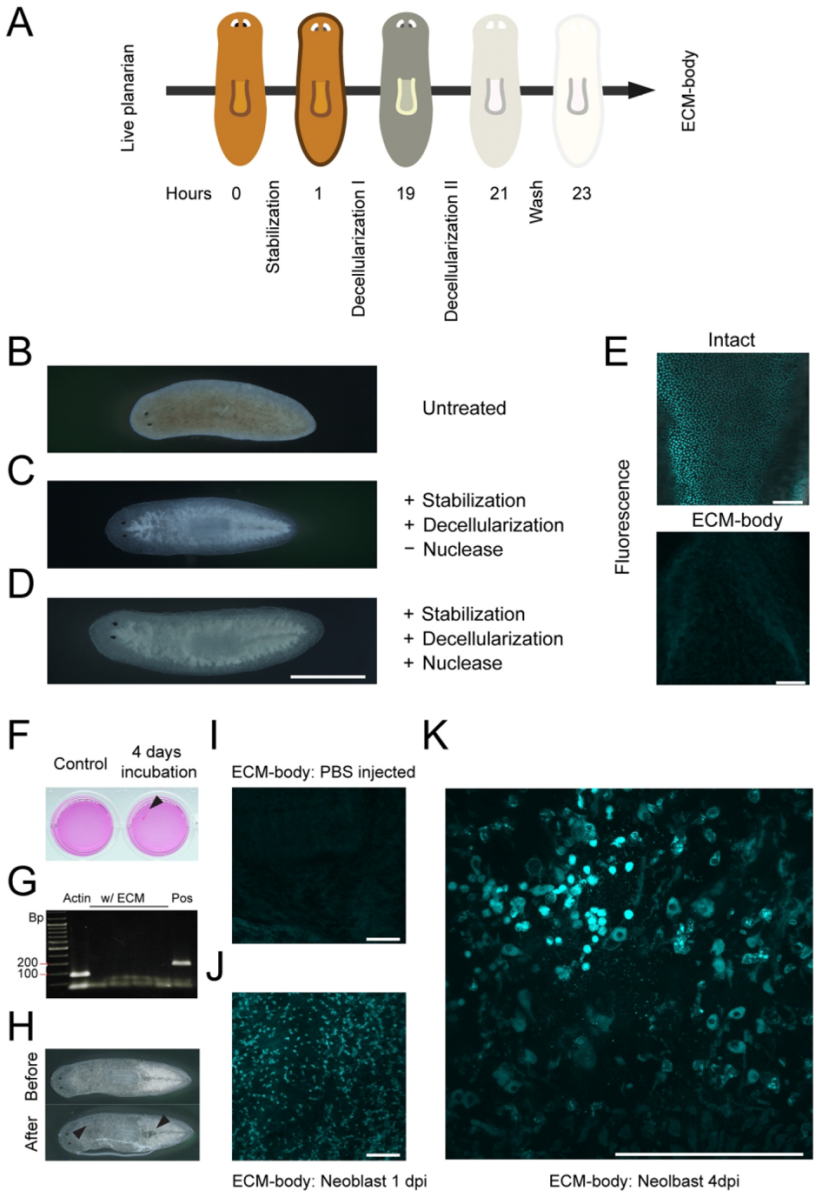

Fig 6 Decellularization and recellularization protocols for *D. japonica*. (A) Cartoon illustration demonstrating the steps required for decellularization of *D. japonica.* (B) Untreated *D. japonica* (C) isolated ECM body (D) Nuclease treated ECM body (E) Fluorescent nuclear staining revealed that the ECM-body isolated are acellular. (F-G) The incubation of decontaminated ECM body in enriched culture media and PCR based mycoplasma detection confirmed that there is no contaminating microbe in the ECM-body. (H) The delicate structure of ECM-body could be affected by the force introduced by microinjection (I-K) Recellularized neoblastic cells could remain in the ECM body for many days, presumably, supported by microenvironment provided by the ECM body.

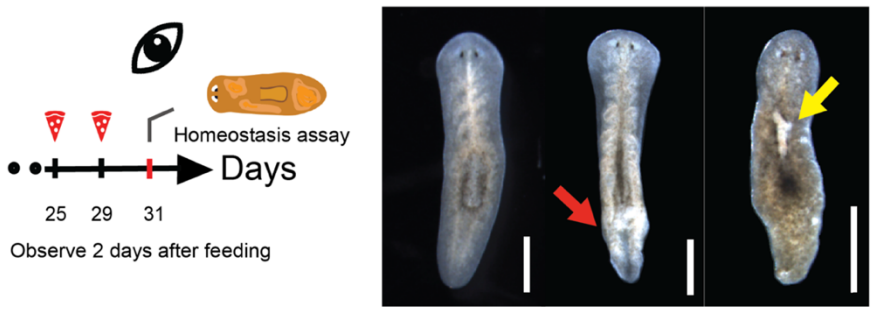

Gene number	*unc-22*	*tll*	*ky*
Alive	38/38	83/83	68/144
Defect phenotype	0/38	83/83	115/144

Fig 8 Observed defective phenotypes caused by RNAi in homeostasis assay.

The homeostasis defect phenotype of selected candidates from RNAi screening included tolloid-like protein 1(tll) and kyphoscoliosis peptidase (ky). Red arrow indicates tail curling with rough surface; yellow arrow indicates tissue lesion. Scale bars represent 500 μm.

Gene number	*unc-22*	*tll*	*ky*	*hspg*
Alive	24/24	4/40	9/30	40/60
Defect phenotype	3/24	4/4	8/9	35/40

Fig 9 Observed defective phenotypes caused by RNAi in regeneration assay.

The regeneration defect phenotypes of selected candidates from RNAi screening included tolloid-like protein 1 (tll), kyphoscoliosis peptidase (ky), and heparan sulfate proteoglycan core protein (hspg). Yellow arrow indicates rough surface and red arrow indicates the hump-like structure. Scale bars represent 500 μm.

same even after the radiation. Finally, *ky* was found to be expressed only in the planarian intestine. After a radiation, similar to the other two selected candidates, the expression pattern of the *ky* remained unaltered.

Gene expression during tissue regeneration

Further investigation using combination between series of planarian amputation and *in situ* hybridization were conducted to scrutinize whether the candidate genes of interest are involved in tissue regeneration processes (Figure 12). Briefly, planarians were amputated sagittally and collected at 1, 3, 5, 7 and 13 dpa for *in situ* hybridization. The results confirmed the dispersed expression of *hspg* throughout the planarian body. It was clear that the expression was markedly intensified at the pharynx of planarian at day 0. Interestingly, at day 1, the pharynx was discharged from the worm. We found increased expression of *hspg* gene at the base area where the original pharynx used to be. At day 3, global expression was reduced. The expression of *hspg* was found more prominently in the newly formed pharyngeal tissue and persistent throughout the regeneration process.

Similarly, at day 0, the expression of *tll* was found to spread throughout the body. Decrease in expression of *tll* was found at day 1. It should be noted that no signal of *tll* expression was detected on the wounded site. At day 3, global expression of *tll* surged. the signal reemerged at the newly regenerated blastema. The expression of *tll* was persistent particularly at the newly regenerated blastema from day 7 onward.

The expression of *ky* took slightly different pattern. It was accumulated in the newly regenerated blastema especially in the intestine region near the wounded area at day 1 and day 3. At day 7 and day 13, the expression was established at the newly regenerated blastema particularly in the area that formed the shape resembling regenerating intestine.

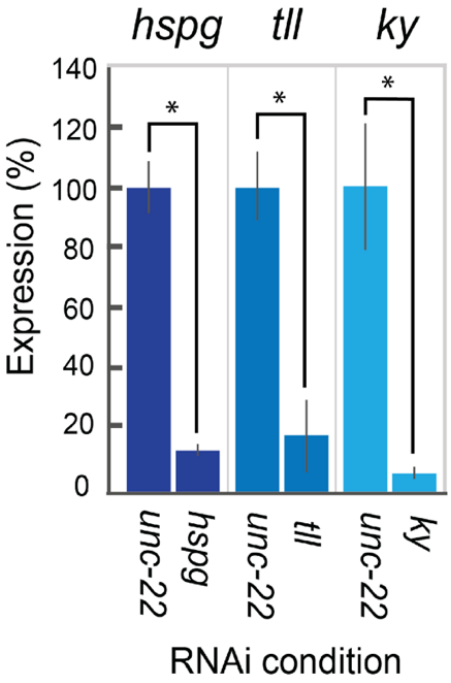

Fig 10 The RNAi knockdown efficiency. The evaluation of RNAi knockdown efficiency of unamputated planarians by qPCR. The feeding *unc-22* (RNAi) was a negative control for RNAi experiment. Tubulin gene was an internal control for qPCR. Error bars represent standard deviation. Stars indicate statistically differences. The data were calculated from 3 independent experiments, ANOVA, (* = $P<0.05$).

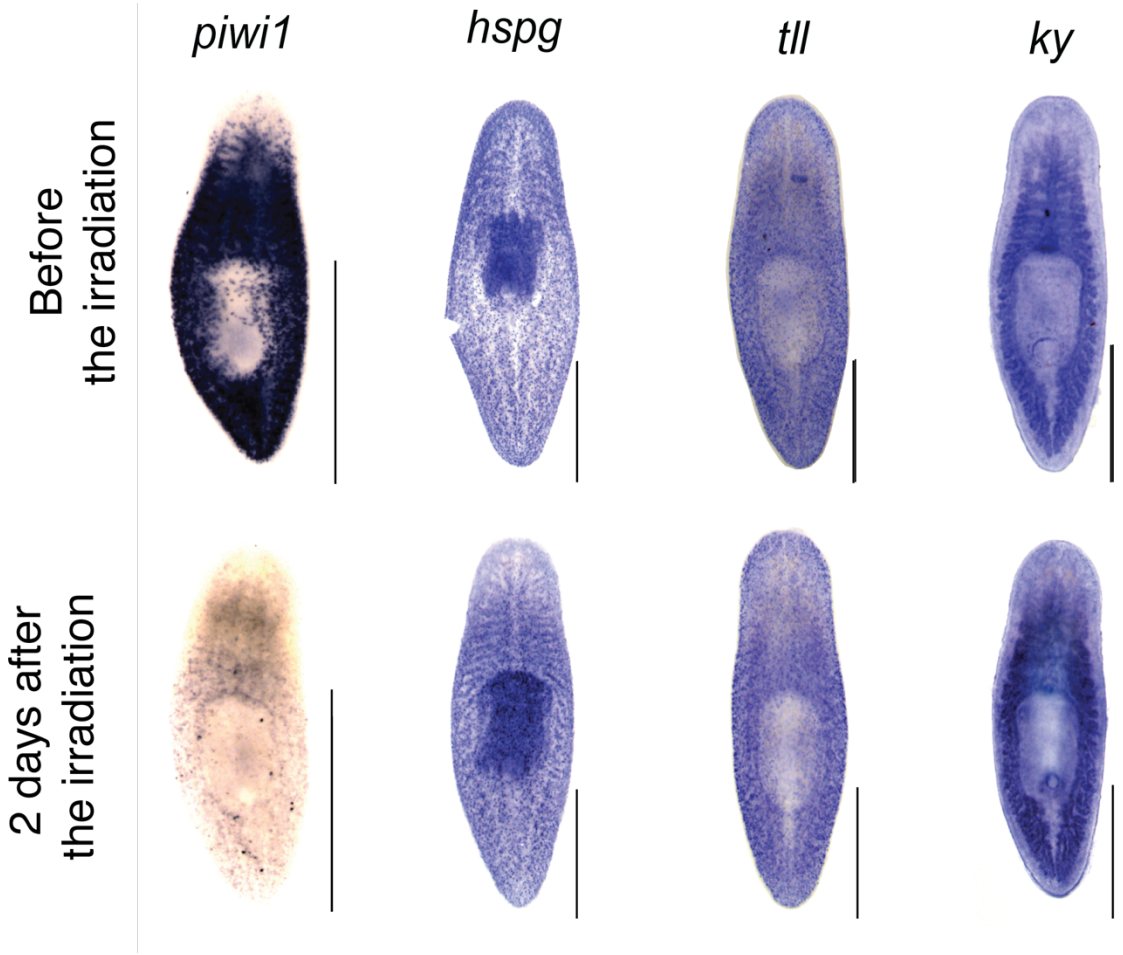

Fig 11 *In situ* hybridization of radiated and non-radiated planarians.

In situ hybridization of gene candidates on unamputated planarian before and 2 days after irradiation worm. Scale bars represent 500 μm.

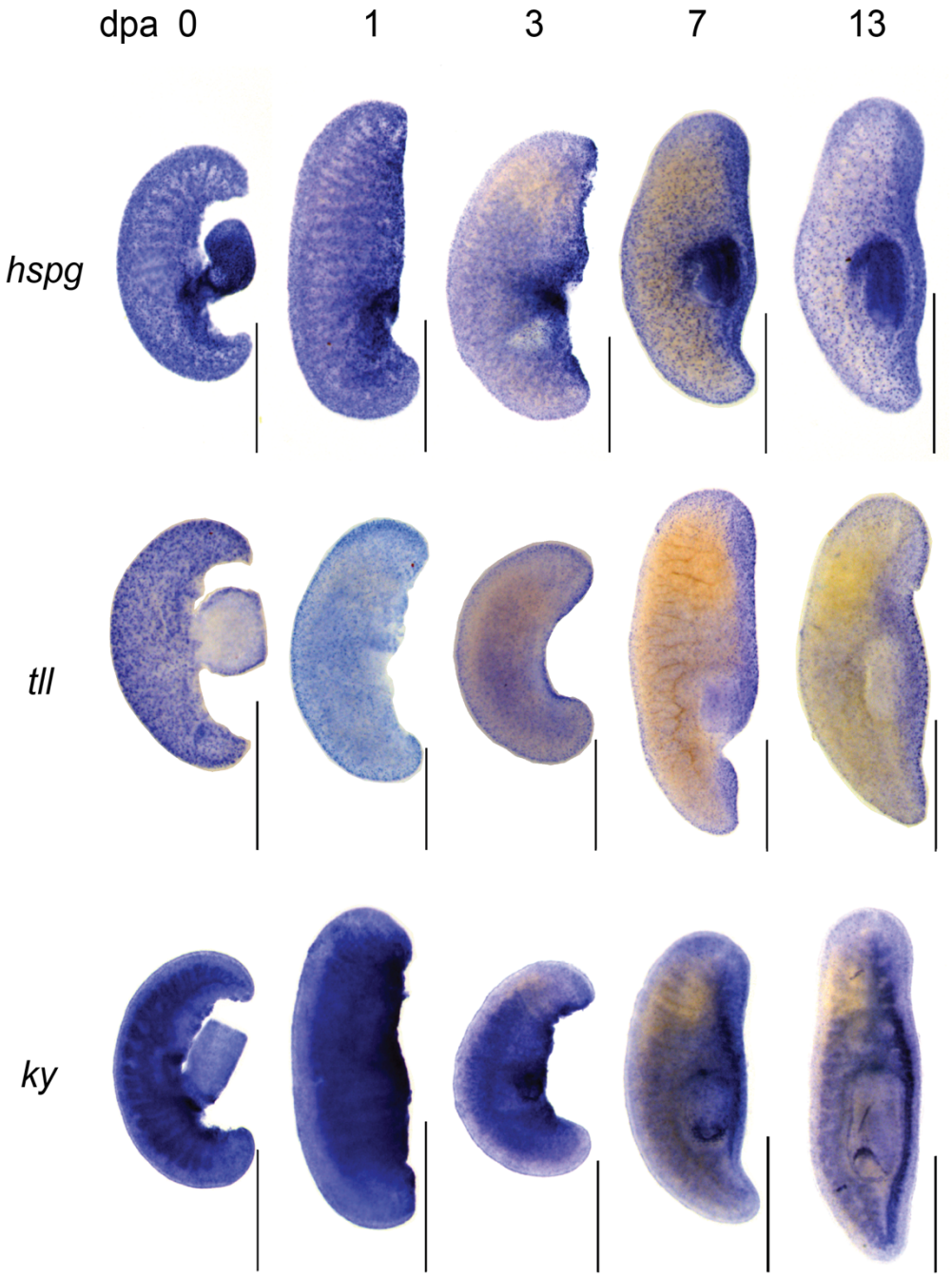

Fig 12 *In situ* hybridization of regenerating planarians.
In situ hybridization of gene candidates on sagittal amputated planarians regenerated for 1, 3, 7 and 13 days. Scale bars represent 500 µm.

Discussion

Project 1: Characterization of ciliary growth dynamics and 3D structure of ciliary distal tip complex

In this project, we have identified and characterized the development process of the motile ciliary tip region. The ciliary tip region of motile cilia undergoes a progressive development which involves an extension of the central pair microtubules followed by extension of the A-tubules of MTDs and eventually B-tubules on the scale of hours. The morphology of the developing motile cilia exhibits a characteristic progression. First cilia appear as a hemi-capsule of short length, and it is likely that the FTC might have not fully assembled at this point, which is consistent with plastic section studies on early regrowth of *Chlamydomonas* cilia (Rosenbaum et al., 1969). Then, developing cilia extend an FTC-capped tip of central pair microtubules. Our SEM study provides a low-detail view of the cilia when they are still on the cells, and this set the stage for further studies. Using negative staining electron microscopy, we further characterized this development based on diameter profiles and lengths of the ciliary tip region, and this gave insight into assembly characteristics. For the analysis, we developed and provide a set of programs that can easily be used by others to also measure tip region length. In the negatively stained micrographs, we can clearly see contrast from individual MTDs, but it is difficult to identify how many there are. The diameter profiles allow us to determine that these diameters may be as thin as 60 nm, which may only accommodate one MTD or the central pair. This raised the question of whether the central pair projects forward, or whether a MTD projects forward. This is answered by our cryo-EM study, which shows that the central pair leads cilium growth at the tip region.

Previous studies of motile ciliogenesis often measure the full length of cilia, and they generally considered cilia to be mature once they reach the slow elongation phase. Furthermore, after cilia reach full length, they continue to exhibit dynamic turnover (Marshall et al., 2005; Marshall and Rosenbaum, 2001). This balance is known to regulate ciliary length. However, our data suggest that cilia continue to develop several hours after they reach full length. Therefore, the slow elongation phase is not just a period of protein turnover and overall length maintenance, but it is also a period of continued development in the tip region. Furthermore, these investigations give insight into organelle size regulation because throughout the process of tip region development, the cilium maintains an essentially constant overall length.

Although the growing motile ciliary tip region is largely similar to the mature axoneme, our cryo-ET investigations reveal important distinctions in composition and structure between the two. It is well established that the motile ciliary tip region contains the FTC, which is composed of several proteins not found in the mature axoneme (Miller et al., 1990; Pedersen et al., 2003). The FTC-capped microtubule central pair leads the ciliary tip and reaches the full length first before others, and elongation of the A-tubules of MTDs do not extend beyond the central pair tip. This makes the FTC-capped microtubule central pair the defining factor or the controller of the maximum length of the cilia. In our studies, the central pair complexes of the Tetrahymena cilia display a left-handed twist, in agreement with previous reports that bend propagation during the ciliary beat

drives twisting of the central pair in *Chlamydomonas reinhardtii* and *Paramecium tetraurelia* (Mitchell and Nakatsugawa, 2004; Omoto and Kung, 1980). Our cryo-tomographic study of the membrane-intact, isolated Tetrahymena thermophila cilia, demonstrates that the central pair complex also exhibits left-handed twisting, and such twisting is also present in the tip regions where radial spokes are not mature. This result supports the conclusion that the twist does not depend on the interactions between radial spoke heads and the central pair(Mitchell and Nakatsugawa, 2004).

Our structural investigations from cryo-EM of splayed ciliary tip regions and cryo-ET of membrane-intact ciliary tip regions demonstrate that the ciliary tip region lacks the full complement of proteins found in the mature axoneme. These differences bear consequences on both ciliary assembly and IFT train turnaround. The immature ciliary tip region is composed of microtubule singlets, which are long extensions of the A-tubules from axonemal MTDs. Such structural features provide important insight into cilium assembly that is involved in IFT. It has been well established that IFT serves as the primary mechanism for protein transportation across the base and distal ends of the cilium during both cilium assembly and maintenance. In growing cilia, particularly in the fast growing stage (the first two hours in Figure 3), the central pair, capped by the FTC, can be more than a micrometer far away from the distal end of the doublet B-tubule. We know, anterograde IFT trains rely on kinesin motors walking along the B-tubule of the MTD (Stepanek and Pigino, 2016). This indicates that normal anterograde IFT may stop far away from the ciliary tip end. Meanwhile, the central pair and the A-tubules are tightly wrapped by ciliary membrane as shown in Fig 4b. This means there is limited room for a fast diffusion of large IFT complexes to the very tip of the growing cilium where the FTC caps the central pair microtubules. Therefore, it is unlikely that the FTC plays a major role in IFT reorganization and turnover, as previously hypothesized(Sloboda, 2005).

While anterograde IFT does not directly reach the growing tip ends where the extension happens for central pair microtubules and singlet A-tubules, diffusion may be required for precursor proteins to reach the growing tip end of developing central pair and the A-tubules of doublets. On the other hand, a small restricted space, due to tightly-wrapped ciliary membrane around the central pair, does not favor a free diffusion of precursor proteins. Therefore, it is unclear how precursor proteins reach the growing tips of the central pair complex and the A-tubules of the doublet microtubules.

At the growing tip regions, both the central pairs and the A-tubule are singlet microtubules with tubulin as the primary component protein. If their extension is simply limited by the available tubulins that reach the tip region, the singlet A-tubules and the central pair should be of a similar length. However, our data have demonstrated that central pair microtubules are always longest at the growing tip with a significant length difference from that of the A-tubules. This indicates the microtubule growth at the tip is not a simple extension limited by availability of tubulins. The FTC may play a role in promoting central pair microtubule extension. The time required for ciliary tip

region development is on the scale of hours, which also suggests that tip region development is not limited by microtubule-doublet polymerization kinetics (Binder et al., 1975). It is unclear at this moment what the limiting factor is for the maturation of the ciliary tip. Likely factors include post-translational modification of the microtubule complexes (Schneider et al., 2008; Sloboda, 2009), or the availability of MTD-specific intralumenal microtubule associated proteins(Amos, 2010; Downing and Sui, 2007; Nicastro et al., 2006; Sui and Downing, 2006)

In this study, we discovered that tip regions of growing motile cilia are subject to a process of development and maturation, which only completes long after a cilium reaches its full length. This new finding is not species specific, and therefore it is an important complementary knowledge to what we have known about cilia development. Using a customized program, we analyzed the morphologies of growing cilia tips at different growth time and clearly revealed the trend of ciliary tip development and maturation. The trend profiles and the structural information from our electron tomographic study provided important insight into ciliogenesis and maintenance, that involves FTC and IFT as summarized in Fig 12.

Project 2: Isolation and characterization of microenvironmental factors from planarians

In order to elucidate the influence of microenvironment in stem cell fate determination in highly regenerative animal that could be utilized as a model for advancing our understanding of organ regeneration, a detergent-based decellularization protocol to isolate intact 3D scaffold of ECM from planarians was established. We found that the addition of stabilization step to cross-link the structure and terminate the worm

Subsequently, a proteomic profile of planarian ECM was constructed using LC-MS/MS. Mass spectrometry revealed a complex landscape of planarians ECM including some common ECM proteins such as collagen, laminin, nidogen, and MMPs. The enrichment of ECM proteins in the samples was confirmed by volcano plot and gene ontology-enrichment (GO-enrichment) analyses. The results clearly indicated the enrichment of several ECM proteins including several types of collagen and many ECM proteins that have been proposed to be involved in tissue homeostasis and regeneration in planarians. From 73 candidate genes selected from the list for RNA screening, three genes including heparan sulfate proteoglycan core protein (*hspg*), tolloid-like protein 1 (*tll*) and kyphoscoliosis peptidase (*ky*), were found to be crucial for tissue regeneration since the blastema of amputated *tll* (RNAi) and *ky* (RNAi) animals were underdeveloped and an unusual hump appeared in *hspg* (RNAi) animals. Moreover, after sagittally amputating *hspg* (RNAi), *tll* (RNAi) and *ky* (RNAi), the survival rate of the regenerating fragments dramatically dropped.

The three selected genes were further characterized using whole mount *in situ* hybridization (WISH) and single-cell RNA sequencing. The results revealed localization of each three genes during homeostasis. The *hspg* was highly expressed at the pharynx region. While the *tll* gene was expressed throughout the body. *ky* was only expressed in the intestine.

Furthermore, a WISH time-course on sagittally amputated planarians showed that all three candidate genes responded to wounding. In addition, a density of H3P positive cells were augmented in *tll* (RNAi) and *ky* (RNAi) animal. This suggested that the balance between cell proliferation and cell death in tissue homeostasis was altered in RNAi animal.

Application

Some protocols developed in this research work has been utilized in the development of a novel pedagogical design for zoology laboratory classes for undergraduate students for a classroom with limited setting. In order to mitigate the problem of insufficient numbers of taxidermy specimen and permanent slides, we developed a time-restricted guided inquiry-based learning to increase the active engagement of students in the class despite limitation.

The outline of the organization of learning experience is shown in Fig 13.

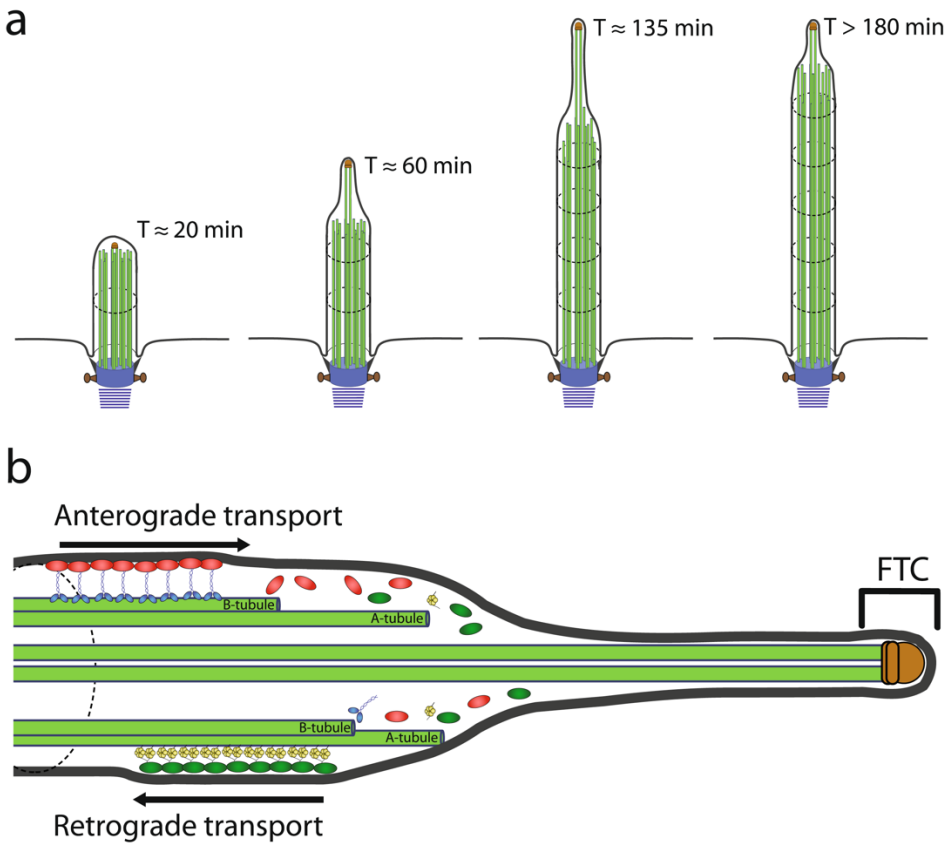

Fig 12 Decontamination of the planarian extracellular matrix. (A) 4 days cultivation of planarian ECM in culture media revealed no bacterial or fungal contamination (B) isolated ECM from a planarian

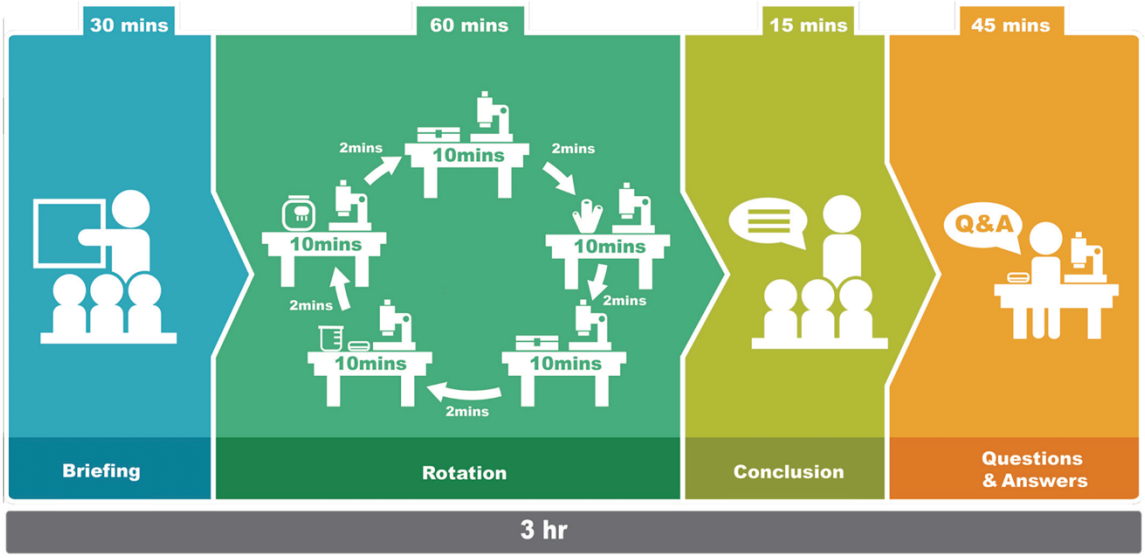

Fig 13 Time Restricted Guided Inquiry Based Learning. Strategic time management in the in-class activity

References

Amos, L.A. (2010). Articulated Tubes. Structure *18*, 892-894.

Auclair, W., and Siegel, B.W. (1966). Cilia regeneration in the sea urchin embryo: evidence for a pool of ciliary proteins. Science (New York, NY) *154*, 913-915.

Binder, L.I., Dentler, W.L., and Rosenbaum, J.L. (1975). Assembly of chick brain tubulin onto flagellar microtubules from Chlamydomonas and sea urchin sperm. Proceedings of the National Academy of Sciences of the United States of America *72*, 1122-1126.

Braun, D.A., and Hildebrandt, F. (2017). Ciliopathies. Cold Spring Harbor perspectives in biology *9*, 1-28.

Broekhuis, J.R., Leong, W.Y., and Jansen, G. (2013). Regulation of cilium length and intraflagellar transport. International review of cell and molecular biology *303*, 101-138.

Brown, J.M., and Witman, G.B. (2014). Cilia and diseases. BioScience *64*, 1126-1137.

Craige, B., Brown, J.M., and Witman, G.B. (2013). Isolation of chlamydomonas flagella. Current Protocols in Cell Biology *48*, 1-6.

Deane, J.A., Cole, D.G., Seeley, E.S., Diener, D.R., and Rosenbaum, J.L. (2001). Localization of intraflagellar transport protein IFT52 identifies basal body transitional fibers as the docking site for IFT particles. Current Biology *11*, 1586-1590.

Dentler, W.L. (1980). Structures linking the tips of ciliary and flagellar microtubules to the membrane. Journal of cell science *42*, 207-220.

Dentler, W.L., and Rosenbaum, J.L. (1977). Flagellar elongation and shortening in chlamydomonas. III. Structures attached to the tips of flagellar microtubules and their relationship to the directionality of flagellar microtubule assembly. Journal of Cell Biology *74*, 747-759.

Downing, K.H., and Sui, H. (2007). Structural insights into microtubule doublet interactions in axonemes. Current Opinion in Structural Biology *17*, 253-259.

Gaertig, J., Wloga, D., Vasudevan, K.K., Guha, M., and Dentler, W. (2013). Discovery and functional evaluation of ciliary proteins in tetrahymena thermophila. In Methods in Enzymology, pp. 265-284.

Hadley, G.a., and Williams, N.E. (1981). Control of initiation and elongation of cilia during ciliary regeneration in Tetrahymena. Molecular and cellular biology *1*, 865-870.

Hall, T.C. (2017). Cilia Regeneration in the Sea Urchin Embryo : Evidence for a Pool of Ciliary Proteins Author (s): Walter Auclair and Barry W . Siegel Published by : American Association for the Advancement of Science Stable URL : http://www.jstor.org/stable/1719466 REF. *154*, 913-915.

Iomini, C., Babaev-Khaimov, V., Sassaroli, M., and Piperno, G. (2001). Protein particles in Chlamydomonas flagella undergo a transport cycle consisting of four phases. Journal of Cell Biology *153*, 13-24.

Jarvik, J.W., and Rosenbaum, J.L. (1980). Oversized flagellar membrane protein in paralyzed mutants of Chlamydomonas reinhardrii. The Journal of cell biology *85*, 258-272.

Kishchenko, G.P., Danev, R., Fisher, R., He, J., Hsieh, C., Marko, M., and Sui, H. (2015). Effect of fringe-artifact correction on sub-tomogram averaging from Zernike phase-plate cryo-TEM. Journal of structural biology *191*, 299-305.

Kozminski, K.G., Johnson, K.A., Forscher, P., and Rosenbaum, J.L. (1993). A motility in the eukaryotic flagellum unrelated to flagellar beating. Proceedings of the National Academy of Sciences of the United States of America *90*, 5519-5523.

Lin, J., Heuser, T., Carbajal-Gonzalez, B.I., Song, K., and Nicastro, D. (2012). The structural heterogeneity of radial spokes in cilia and flagella is conserved. Cytoskeleton (Hoboken, NJ) *69*, 88-100.

Marshall, W.F., Qin, H., Rodrigo Brenni, M., and Rosenbaum, J.L. (2005). Flagellar Length Control System: Testing a Simple Model Based on Intraflagellar Transport and Turnover. Molecular biology of the cell *16*, 270-278.

Marshall, W.F., and Rosenbaum, J.L. (2001). Intraflagellar transport balances continuous turnover of outer doublet microtubules: implications for flagellar length control. The Journal of cell biology *155*, 405-414.

McVittie, A. (1972). Flagellum mutants of Chlamydomonas reinhardii. Journal of general microbiology *71*, 525-540.

Miller, J.M., Wang, W., Balczon, R., and Dentler, W.L. (1990). Ciliary microtubule capping structures contain a mammalian kinetochore antigen. Journal of Cell Biology *110*, 703-714.

Mitchell, D.R., and Nakatsugawa, M. (2004). Bend propagation drives central pair rotation in Chlamydomonas reinhardtii flagella. Journal of Cell Biology *166*, 709-715.

Nicastro, D., Schwartz, C., Pierson, J., Gaudette, R., Porter, M.E., and McIntosh, J.R. (2006). The molecular architecture of axonemes revealed by cryoelectron tomography. Science (New York, NY) *313*, 944-948.

Oda, T., Yanagisawa, H., Yagi, T., and Kikkawa, M. (2014). Mechanosignaling between central apparatus and radial spokes controls axonemal dynein activity. The Journal of cell biology *204*, 807-819.

Omoto, C.K., and Kung, C. (1980). Rotation and twist of the central-pair microtubules in the cilia of paramecium. Journal of Cell Biology *87*, 33-46.

Pazour, G.J., and Rosenbaum, J.L. (2002). Intraflagellar transport and cilia-dependent diseases. Trends in Cell Biology *12*, 551-555.

Pedersen, L.B., Geimer, S., Sloboda, R.D., and Rosenbaum, J.L. (2003). The Microtubule Plus End-Tracking Protein EB1 Is Localized to the Flagellar Tip and Basal Bodies in Chlamydomonas reinhardtii. Current Biology *13*, 1969-1974.

Pigino, G., Bui, K.H., Maheshwari, A., Lupetti, P., Diener, D., and Ishikawa, T. (2011). Cryoelectron tomography of radial spokes in cilia and flagella. The Journal of cell biology *195*, 673-687.

Pigino, G., Geimer, S., Lanzavecchia, S., Paccagnini, E., Cantele, F., Diener, D.R., Rosenbaum, J.L., and Lupetti, P. (2009). Electron-tomographic analysis of intraflagellar transport particle trains in situ. Journal of Cell Biology *187*, 135-148.

Qin, H., Diener, D.R., Geimer, S., Cole, D.G., and Rosenbaum, J.L. (2004). Intraflagellar transport (IFT) cargo: IFT transports flagellar precursors to the tip and turnover products to the cell body. Journal of Cell Biology *164*, 255-266.

Rannestad, J. (1974). The regeneration of cilia in partially deciliated Tetrahymena. Journal of Cell Biology *63*, 1009-1017.

Rosenbaum, J.L., and Carlson, K. (1969). Cilia regeneration in Tetrahymena and its inhibition by colchicine. Journal of Cell Biology *40*, 415-425.

Rosenbaum, J.L., Moulder, J.E., and Ringo, D.L. (1969). Flagellar elongation and shortening in Chlamydomonas. The use of cycloheximide and colchicine to study the synthesis and assembly of flagellar proteins. Journal of Cell Biology *41*, 600-619.

Sale, W.S., and Satir, P. (1976). Splayed Tetrahymena cilia. A system for analyzing sliding and axonemal spoke arrangements. Journal of Cell Biology *71*, 589-605.

Schneider, C.A., Rasband, W.S., and Eliceiri, K.W. (2012). NIH Image to ImageJ: 25 years of image analysis. Nature methods *9*, 671-675.

Schneider, M.J., Ulland, M., and Sloboda, R.D. (2008). A protein methylation pathway in Chlamydomonas flagella is active during flagellar resorption. Molecular biology of the cell *19*, 4319-4327.

Sloboda, R.D. (2005). Intraflagellar transport and the flagellar tip complex. Journal of Cellular Biochemistry *94*, 266-272.

Sloboda, R.D. (2009). Posttranslational protein modifications in cilia and flagella. Methods in cell biology *94*, 347-363.

Sloboda, R.D., and Rosenbaum, J.L. (2007). Making sense of cilia and flagella. Journal of Cell Biology *179*, 575-582.

Stepanek, L., and Pigino, G. (2016). Microtubule doublets are double-track railways for intraflagellar transport trains. Science (New York, NY) *352*, 721-724.

Sui, H., and Downing, K.H. (2006). Molecular architecture of axonemal microtubule doublets revealed by cryo-electron tomography. Nature *442*, 475-478.

Thompson, G.A., Jr., Baugh, L.C., and Walker, L.F. (1974). Nonlethal deciliation of Tetrahymena by a local anesthetic and its utility as a tool for studying cilia regeneration. The Journal of cell biology *61*, 253-257.

บทคัดย่อ

รหัสโครงการ : RSA5980078

ชื่อโครงการ : การศึกษาการขนส่งสารผ่านซิเลีย: การศึกษาโครงสร้างโดยรวมของ ciliary pore complex และ ciliary barrier ของ *Tetrahymena thermophila*

ชื่อนักวิจัย : ผศ. ดร. ป๋วย อุ่นใจ ภาควิชาชีววิทยา คณะวิทยาศาสตร์ มหาวิทยาลัยมหิดล

E-mail Address : puey.oun@mahidol.edu

(ระยะเวลาโครงการ)

การสื่อสารระดับเซลล์เป็นปัจจัยสำคัญที่ควบคุมชะตาชีวิตของเซลล์ การกระจายสัญญาณและการรับสัญญาณของเซลล์ยูคาริโอตจะเกี่ยวข้องกับออร์แกเนลล์ที่เรียกว่าซิเลีย ทว่ากลไกการควบคุมการสร้างซิเลียนั้นยังไม่เป็นที่ทราบแน่ชัด ในงานวิจัยนี้จึงใช้เทคนิคทางชีวฟิสิกส์เพื่อศึกษาพลศาสตร์ของกระบวนการการสร้างซิเลียในเซลล์ยูคาริโอต โดยใช้โปรโตซัว *T. thermophila* และสาหร่ายสีเขียว *Chlamydomonas reinhardtii* เป็นโมเดลในการศึกษา เราได้ค้นพบว่ากลไกการสร้างซิเลียนั้นจะประกอบไปด้วยสองระยะ นั่นคือจะมีการยืดยาวของโครงสร้างแอคโซนีม (axoneme) และการพัฒนาไปเป็นโครงสร้างสมบูรณ์ที่จะเกิดที่บริเวณส่วนปลายสุดของซิเลีย โครงสร้างสามมิติของปลายซิเลียช่วยให้เราเข้าใจกระบวนการเปิดและปิดการทำงานของจักรกลขนส่งภายในซิเลีย (Intraflagellar transport (IFT) machinery) ที่ทำหน้าที่ควบคุมการขนส่งโปรตีนเข้าและออกจากซิเลีย นอกจากนี้ เพื่อเป็นการต่อยอดองค์ความรู้ให้สามารถเข้าใจบทบาทของสิ่งแวดล้อมจุลภาคที่มีผลต่อการควบคุมชะตาชีวิตของเซลล์ได้ เราจึงได้พัฒนาวิธีการแยกสกัดสารเคลือบเซลล์ที่สมบูรณ์จากสิ่งมีชีวิตที่สามารถซ่อมแซมส่วนที่เสียหายไปได้อย่างรวดเร็วนั่นคือหนอนตัวแบน โครงร่างสารเคลือบเซลล์ที่แยกได้ไม่มีเซลล์และจุลินทรีย์ปนเปื้อน การทดลองฉีดเซลล์ต้นกำเนิดของหนอนตัวแบนกลับเข้าไปในโครงร่างเคลือบเซลล์พบว่ามันสามารถช่วยพยุงชีวิตของเซลล์ต้นกำเนิดได้ การศึกษาทางโปรติโอมและการน๊อคดาวน์ยีนช่วยบ่งชี้ถึงโปรตีนในสารเคลือบเซลล์ที่มีบทบาทสำคัญทั้งในการซ่อมแซมอวัยวะและการสร้างอวัยวะใหม่ งานวิจัยนี้จะช่วยวางรากฐานเพื่อความเข้าใจกระบวนการควบคุมชะตาชีวิตของเซลล์ต้นกำเนิดได้

คำหลัก: การสร้างซิเลีย ซิเลีย สิ่งแวดล้อมจุลภาค สารเคลือบเซลล์

Abstract

Project Code : RSA5980078

Project Title : Characterization of ciliary transport: assessment of overall structure of ciliary pore complex and ciliary barrier of T.thermophila

Investigator : Puey Ounjai, Department of Biology, Faculty of Science, Mahidol University

E-mail Address : puey.oun@mahidol.edu

Project Period :

Cellular communication is an important factor that control cell fate. The reception and distribution of signal in eukaryotic cell often involved a unique organelle called cilium. However, the control mechanism for cilia formation is still unclear. In this research, we thus exploited biochemical and biophysical approaches to characterize the dynamic nature of ciliogenesis in eukaryotic organism including T. thermophila and C. reinhardtii. We proposed a two-step model of ciliogenesis. (I) the growth of the axonemal structure and the maturation of the distal tip complex. The three dimensional structure of the ciliary distal tip provided unique insights on the site of protein complex that regulate the activity of IFT machinery, the transport complex responsible for protein trafficking in and out of ciliary compartment. Furthermore, in order to advance our understanding regarding the impact of microenvironment in the fate determination of stem cell, we established a protocol to isolate the intact extracellular matrix from highly regenerative animal, freshwater flatworm. Recellularization revealed that the ECM structure could support the survival of microinjected stem cells. Proteomic characterization and RNAi screening identified a few proteins of ECM that are important not only in tissue homeostasis but also organ regeneration. This work lays foundation for a better understanding of the mechanism of fate determination of stem cells.

Keywords: ciliogenesis, cilia, microenvironment, extracellular matrix

Output จากโครงการวิจัยที่ได้รับทุนจาก สกว.

1. ผลงานตีพิมพ์ในวารสารวิชาการนานาชาติ (ระบุชื่อผู้แต่ง ชื่อเรื่อง ชื่อวารสาร ปี เล่มที่ เลขที่ และหน้า)

Reynolds MJ, Phetruen T, Fisher RL, Chen K, Pentecost BT, Gomez G, Ounjai P, Sui H, 2018, The Developmental Process of the Growing Motile Ciliary Tip Region. Scientific Reports. 8(1):7977. doi: 10.1038/s41598-018-26111-2.

Sumranwanich T, Boonthaworn K, Singhakaew S, Ounjai P, 2019, Time-Restricted Inquiry-Based Learning Promotes Active Student Engagement in Undergraduate Zoology Laboratory. Journal of Microbiology and Biology Education, 26;20(1). pii: 20.1.2. doi: 10.1128/jmbe.v20i1.1571.

Sonpho E, Wootthichairangsan C, Ishida M, Inoue T, Agata K, Maleehuan A, Charngkaew K, Chomanee N, Moonsom S, Wongtrakoongate P, Chairoungdua A, Ounjai P. 2020, ECM-body: A cell-free 3D biomimetic scaffold derived from intact planarian body. Zoological Science, (in press).

2. การนำผลงานวิจัยไปใช้ประโยชน์
   - เชิงสาธารณะ (มีเครือข่ายความร่วมมือ/สร้างกระแสความสนใจในวงกว้าง)
     แนวคิดด้านการพัฒนาการเรียนการสอนแบบใหม่ที่ต่อยอดมาจากองค์ความรู้ที่ได้จากการทำงานวิจัยในโครงการนี้ได้มีสื่อเอกชนให้ความสนใจและมาสัมภาษณ์เพื่อขยายผลสู่วงกว้าง

   - เชิงวิชาการ (มีการพัฒนาการเรียนการสอน/สร้างนักวิจัยใหม่)
     องค์ความรู้และเทคนิคที่พัฒนาขึ้นมาจากงานนี้ได้ถูกนำไปพัฒนาการเรียนการสอนในห้องเรียนวิชาปฏิบัติการสัตววิทยา สำหรับนักศึกษาในระดับปริญญาตรี ปีที่ 2 ของภาควิชาชีววิทยา คณะวิทยาศาสตร์ มหาวิทยาลัยมหิดล

3. อื่นๆ (เช่น ผลงานตีพิมพ์ในวารสารวิชาการในประเทศ การเสนอผลงานในที่ประชุมวิชาการ หนังสือ การจดสิทธิบัตร)

   International conferences:

   Reynolds MJ, Phetruen T, Fisher R, Wu W, Pintercost B, Gomez G, Ounjai P, Sui H, 2018. The growing of motile cilium tip undergoes a time-dependent

developmental process, ASCB | EMBO 2018 meeting, Philadelphia, PA, USA, Dec 2-6, 2017

Ishida M, Sonpho E, Bagherzadeh R, Kayo H, Ounjai P, Agata K, 2018, The road to making planarian bodies from the isolated neoblasts by FACS, International Planarian Meeting, Morgridge Institute for Research, Madison, WI, July 16-20, 2018.

Sonpho E, Wootthichairangsan C, Charngkaew K, Chomanee N, Chairoungdua A, Ishida M, Inoue T, Agata K, Ounjai P, 2018, Extracellular matrix body: new approach for studying planarian microenvironment, International Planarian Meeting, Morgridge Institute for Research, Madison, WI, July 16-20, 2018.

Preprint:

Sonpho E, Wootthichairangsan C, Ishida M, Inoue T, Agata K, Maleehuan A, Charngkaew K, Chomanee N, Moonsom S, Wongtrakoongate P, Chairoungdua A, Ounjai P. 2019, ECM-body: A cell-free 3D biomimetic scaffold derived from intact planarian body. bioRxiv 763714; doi: https://doi.org/10.1101/763714

<u>แบบสรุปปิดโครงการวิจัย *(จัดทำแยกต่างหากจากรายงานฉบับสมบูรณ์)*</u>

สัญญาเลขที่ RSA5980078 ชื่อโครงการ การศึกษาการขนส่งสารผ่านซิเลีย: การศึกษาโครงสร้างโดยรวมของ ciliary pore complex และ ciliary barrier ของ *Tetrahymena thermophila*

หัวหน้าโครงการ ผศ. ดร. ป่วย อุ่นใจ **หน่วยงาน** ภาควิชาชีววิทยา คณะวิทยาศาสตร์ มหาวิทยาลัยมหิดล

โทรศัพท์ 022015478 **โทรสาร** 023547161 **อีเมล์** puey.oun@mahidol.edu

สถานะผลงาน ☐ **ปกปิด** √ **ไม่ปกปิด**

ความสำคัญ / ความเป็นมา

Cilia are important organelles that could govern the determination of cell fate through regulation of cellular communication and microenvironmental signaling. In the original proposal for this work, we aimed to determine the structure of ciliary pore complex from a model organism, *Tetrahymena thermophilia,* that would allow us to scrutinize the three-dimensional structure of the ciliary gatekeeper. The work will provide insights on the regulation of protein trafficking in and out of the cilia. The understanding of ciliary transport process could lead to a better understanding of how external signal could have vast effect on cellular behaviors which would be fundamentally important to understand cell fate determination.

วัตถุประสงค์ของโครงการ

1. To develop and optimize a method to purify the ciliary component from *T. thermophila* for structural analysis.
2. To characterize the dynamic process of ciliary transport through structural and biochemical approaches using *T. thermophila* and other model organisms.
3. To advance the understanding of how cell fate determination are influenced by different microenvironmental factors.

ผลการวิจัย *(สั้น ๆ ที่บ่งชี้ประเด็นข้อค้นพบ กระบวนการ ผลผลิต และการเรียนรู้)*

In the actual work we have to make some modification on the experiment to characterize ciliogenesis. The experiment was altered to match the facility and the time that we have to work on the project. For this work, we delineated in detail the dynamic process of ciliary regrowth and revealed for the first time that the distal tip region undergo maturation during the final stages of ciliogenesis. The 3D structure of the ciliary distal tip complex was derived using electron cryotomographic reconstruction. The structure also suggested the location of IFT remodeling complex that control the dynamic of ciliary regrowth at the tip of the cilia as well.

In order to pursue our goal, to gain a better understanding of how microenvironment impact cell fate in animal. We adopted the protocol that we established for purification of CPC and further optimized it for not only purifying ciliary component but also intact microenvironmental compartment so-called ECM body from different planarian models. Isolated ECM was then further characterized for their proteomic content. Despite the fact that the ECM body clearly displayed remarkable preservation on the gross structure of the important organs of the planarians, found that the ECM body was enriched in ECM proteins and components confirming the validity of the protocol. In addition, we also identified a few novel ECM proteins that are important for tissue homeostasis and regeneration of missing planarian tissues using RNAi screening assay. Preliminary experiment to microinject FACS sorted stem cell from planarian into the isolated ECM scaffold consolidated that the ECM body prepared with our method could be

used as a 3D scaffold for cell cultivation, and thus providing a unique ECM microenvironment for development of organoid system and application in tissue engineering.

คำสืบค้น (Keywords)

Ciliary transport, ciliogenesis, organellar biogenesis, regeneration, extracellular matrix, ECM-body

การนำผลงานวิจัยไปใช้ประโยชน์ *(ดูคำจำกัดความ และตัวอย่างด้านหลังแบบฟอร์ม)*

☐ **ด้านนโยบาย** **โดยใคร** *(กรุณาให้ข้อมูลเจาะจง)*.....

มีการนำไปใช้อย่างไร

.....

.....

√ **ด้านสาธารณะ** **โดยใคร** *(กรุณาให้ข้อมูลเจาะจง)* .....

มีการนำไปใช้อย่างไร

เนื่องจากมีการเพาะเลี้ยงสิ่งมีชีวิตตัวอย่างหลายชนิด ทางผู้วิจัยจึงได้เล็งเห็นประโยชน์จากการนำการทดลองบางส่วนที่มาจากงานวิจัยนี้ไปประยุกต์เพื่อพัฒนาปรับปรุงแนวคิดนวัตกรรมการเรียนการสอนในห้องเรียนปฏิบัติการสัตววิทยา สำหรับนักศึกษาวิทยาศาสตร์ ในระดับปริญญาตรี พบว่าได้ผลดีมาก ช่วยแก้ปัญหาการขาดแคลนตัวอย่างสัตว์ทดลอง และสร้างบรรยากาศการเรียนรู้แบบ team based learning ที่มุ่งเน้นผู้เรียนเป็นหลักและเป็น active learning ทางผู้วิจัยดีตีพิมพ์ผลงานวิจัยนี้ ใน Journal of Microbiology and Biology Education ซึ่งเป็นหนึ่งในวารสารการศึกษาของสมาคมจุลชีววิทยาของประเทศสหรัฐอเมริกา (American Society for Microbiology, ASM) สามารถสืบค้นได้จากฐานข้อมูล Pubmed และฐานข้อมูลสากลอื่นๆ

แนวคิดเกี่ยวกับการจัดการเรียนการสอนจากงานวิจัยนี้ได้ผ่านการเผยแพร่ต่อสาธารณะชนผ่านสื่อมวลชนด้านการศึกษา เช่น เว็บไซต์และช่อง Youtube ของ starfish labz และมีการถ่ายทอดแนวทางการนำไปประยุกต์ใช้ผ่านการบรรยายในสถาบันอุดมศึกษาหลายแห่ง

☐ **ด้านชุมชนและพื้นที่** **โดยใคร** *(กรุณาให้ข้อมูลเจาะจง)* .....

มีการนำไปใช้อย่างไร

.....

.....

☐ **ด้านพาณิชย์** **โดยใคร** *(กรุณาให้ข้อมูลเจาะจง)* .....

มีการนำไปใช้อย่างไร

.....

.....

☐ **ด้านวิชาการ** **โดยใคร** *(กรุณาให้ข้อมูลเจาะจง)*

มีการนำไปใช้อย่างไร *(กรุณาให้ข้อมูลเจาะจง)*

.....

.....

☐ **ยังไม่มีการนำไปใช้** (โปรดกรอกในกรอบถัดไป)

(กรณีที่ยังไม่มีการใช้ประโยชน์) **ผลงานวิจัยมีศักยภาพในการนำไปใช้ประโยชน์**

☐ **ด้านนโยบาย** ☐ **ด้านสาธารณะ** ☐ **ด้านชุมชนและพื้นที่** ☐ **ด้านพาณิชย์** √ **ด้านวิชาการ**

ข้อเสนอแนะเพื่อให้ผลงานถูกนำไปใช้ประโยชน์

องค์ความรู้จากผลงานวิจัยเกี่ยวกับกลไกการสร้างซิเลียนี้ ถือเป็นองค์ความรู้ใหม่ที่สำคัญในทางชีววิทยาของเซลล์ สามารถนำไปใช้เป็นตัวอย่างในการเรียนการสอนทั้งในระดับมัธยม ปริญญาตรี ไปจนถึงระดับบัณฑิตศึกษา ผลงานวิจัยในด้าน ECM เป็นข้อมูลตั้งต้นที่สำคัญในการนำไปศึกษากลไกการสร้างอวัยวะใหม่ที่อาจจะนำไปวิจัยต่อยอดเพื่อการผลิตและสกัดสารเคลือบเซลล์จากหนอนตัวแบนเพื่อนำไปสร้างระบบออร์แกนอยด์ของอวัยวะต่างๆ ที่จะเป็นประโยชน์ในการทดสอบยา และการนำไปใช้ในด้านวิศวกรรมเนื้อเยื่อ

การเผยแพร่/ประชาสัมพันธ์ *(กรุณาให้รายละเอียด พร้อมแนบหลักฐาน)*

1. สิ่งพิมพ์ หรือสื่อทั่วไป

   ☐ **หนังสือพิมพ์** ☐ **วารสาร** ☐ **โทรทัศน์** ☐ **วิทยุ** √ **เว็บไซต์** ☐ **คู่มือ/แผ่นพับ** ☐ **จัดประชุม/อบรม** ☐ **อื่น ๆ**

   Youtube channel ของ Starfish labz ซึ่งเป็นเว็บไซต์ที่เน้นให้ข้อมูลทางด้านนวัตกรรมการศึกษา

2. สิ่งพิมพ์ทางวิชาการ *(วารสาร, การประชุม ให้ระบุรายละเอียดแบบการเขียนเอกสารอ้างอิง เพื่อการค้นหาซึ่งควรประกอบด้วย ชื่อผู้แต่ง ชื่อเรื่อง แหล่งพิมพ์ ปี พ.ศ. (ค.ศ.) ฉบับที่ หน้า)*

   International conferences:

   Reynolds MJ, Phetruen T, Fisher R, Wu W, Pintercost B, Gomez G, Ounjai P, Sui H, 2018. The growing of motile cilium tip undergoes a time-dependent developmental process, ASCB | EMBO 2018 meeting, Philadelphia, PA, USA, Dec 2-6, 2017

   Ishida M, Sonpho E, Bagherzadeh R, Kayo H, Ounjai P, Agata K, 2018, The road to making planarian bodies from the isolated neoblasts by FACS, International Planarian Meeting, Morgridge Institute for Research, Madison, WI, July 16-20, 2018.

   Sonpho E, Wootthichairangsan C, Charngkaew K, Chomanee N, Chairoungdua A, Ishida M, Inoue T, Agata K, Ounjai P, 2018, Extracellular matrix body: new approach for studying planarian microenvironment, International Planarian Meeting, Morgridge Institute for Research, Madison, WI, July 16-20, 2018.

   Preprint:

   Sonpho E, Wootthichairangsan C, Ishida M, Inoue T, Agata K, Maleehuan A, Charngkaew K, Chomanee N, Moonsom S, Wongtrakoongate P, Chairoungdua A, Ounjai P. 2019, ECM-body: A cell-free 3D biomimetic scaffold derived from intact planarian body. bioRxiv 763714; doi: https://doi.org/10.1101/763714

   Publication:

   Reynolds MJ, Phetruen T, Fisher RL, Chen K, Pentecost BT, Gomez G, Ounjai P, Sui H, 2018, The Developmental Process of the Growing Motile Ciliary Tip Region. Scientific Reports. 8(1):7977. doi: 10.1038/s41598-018-26111-2.

   Sumranwanich T, Boonthaworn K, Singhakaew S, Ounjai P, 2019, Time-Restricted Inquiry-Based Learning Promotes Active Student Engagement in Undergraduate Zoology Laboratory. Journal of Microbiology and Biology Education, 26;20(1). pii: 20.1.2. doi: 10.1128/jmbe.v20i1.1571.

   Sonpho E, Wootthichairangsan C, Ishida M, Inoue T, Agata K, Maleehuan A, Charngkaew K, Chomanee N, Moonsom S, Wongtrakoongate P, Chairoungdua A, Ounjai P. 2020, ECM-body: A cell-free 3D biomimetic scaffold derived from intact planarian body. Zoological Science, (accepted).

SCIENTIFIC REPORTS

OPEN

The Developmental Process of the Growing Motile Ciliary Tip Region

Matthew J. Reynolds[1,2], Tanaporn Phetruen[1,3], Rebecca L. Fisher[1], Ke Chen[1], Brian T. Pentecost[1], George Gomez[2], Puey Ounjai[3] & Haixin Sui[1,4]

Received: 19 January 2018
Accepted: 1 May 2018
Published online: 22 May 2018

Eukaryotic motile cilia/flagella play vital roles in various physiological processes in mammals and some protists. Defects in cilia formation underlie multiple human disorders, known as ciliopathies. The detailed processes of cilia growth and development are still far from clear despite extensive studies. In this study, we characterized the process of cilium formation (ciliogenesis) by investigating the newly developed motile cilia of deciliated protists using complementary techniques in electron microscopy and image analysis. Our results demonstrated that the distal tip region of motile cilia exhibit progressive morphological changes as cilia develop. This developmental process is time-dependent and continues after growing cilia reach their full lengths. The structural analysis of growing ciliary tips revealed that B-tubules of axonemal microtubule doublets terminate far away from the tip end, which is led by the flagellar tip complex (FTC), demonstrating that the FTC might not directly mediate the fast turnover of intraflagellar transport (IFT).

Eukaryotic motile cilia/flagella are microtubule-based structures responsible for cellular locomotion and movement of extracellular fluids. In mammals, motile cilia are present in ciliated epithelial tissue of the airway, oviduct, or brain ependyma, and they serve as the tails of sperm cells. Defects in the cilium developmental process (or so-called ciliogenesis) are associated with medical disorders and dysfunction of related tissues, organs, and gametes[1–3]. Motile ciliogenesis has been studied for a half a century, primarily through investigations of cilium length and/or motility as cilia regrow following a deciliation event[4–7]. During development of the ciliary axoneme, microtubule bundles exhibit plus-end directed elongation at the ciliary tip region. The mechanism behind transportation of axonemal precursors to the ciliary tip was unclear until the discovery of intraflagellar transport (IFT)[8]. The current model for motile ciliogenesis involves a complex coordination of protein trafficking, protein production, and axonemal assembly[9,10]. Ciliated cells possess a pool of axonemal precursors localized beneath the cilium base[11]. These precursors can pass through the flagellar pore, and then be transported to the distal end of the cilium via anterograde IFT, which ensures a continuous growth event at the ciliary tip. Retrograde IFT is responsible for turnover of proteins at the distal ends of axonemal microtubule doublets (MTDs)[12,13]. Even after cilia reach full length, the IFT process and protein turnover continue at the ciliary tip. A dynamic balancing of the relative rates of anterograde and retrograde transport controls ciliary length[14,15]. A recent study determined that bi-directional transport on the same microtubule doublet is possible because motor proteins that transport IFT particles move in trains along different MTD sub-fibers; kinesin motors walk along the B-tubule, and dynein motors walk along the A-tubule[16]. It remains unknown whether this dynamic activity causes structural remodeling of the ciliary tip region during ciliogenesis and maintenance.

Although the processes by which axonemal precursors are transported to and from the ciliary tip region have been elucidated, the events of ciliary tip assembly and the transition from anterograde to retrograde IFT at the tip region remain unclear. The motile cilium tip has been studied, and its structure was diagrammed, based on results from negative staining and conventional electron microscopy (EM)[17]. There is an amalgamation of proteins at the tip of growing cilia known as the flagellar tip complex (FTC). The FTC remains enigmatic partially because few proteins within it have been identified. The proteins that have been identified include the microtubule end-binding protein EB1 and a 97-kDa protein otherwise found exclusively in kinetochores[18,19]. The FTC is proposed to play a role not only in regulation of ciliary beating but also in the transition between anterograde and the retrograde IFT[20]. There is evidence to suggest that IFT particles remodel at the cilium tip[13,21]. However, no

[1]Wadsworth Center, New York State Department of Health, Albany, NY, 12201, USA. [2]Biology Department, University of Scranton, Scranton, PA, 18510, USA. [3]Department of Biology, Faculty of Science, Mahidol University, Bangkok, 10400, Thailand. [4]Department of Biomedical Sciences, School of Public Health, University at Albany, Albany, NY, 12201, USA. Correspondence and requests for materials should be addressed to H.S. (email: haixin.sui@health.ny.gov)

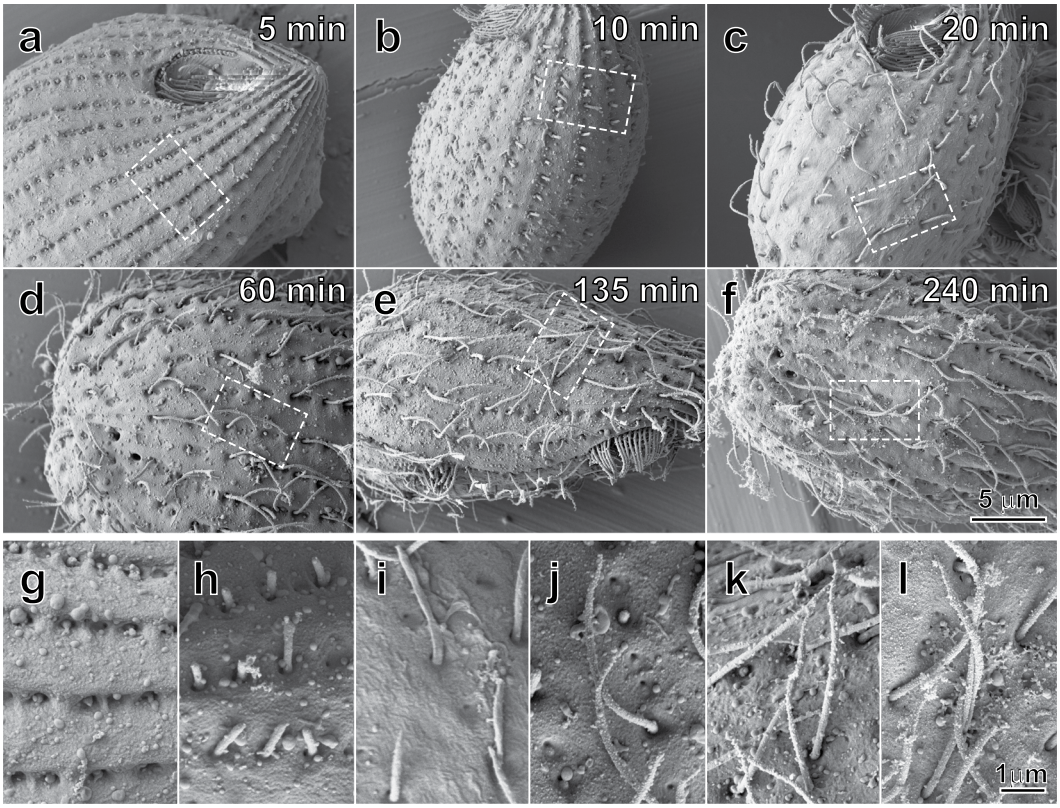

Figure 1. Scanning electron microscopy of re-growing motile cilia on deciliated *Tetrahymena* cells after different regrowth periods. Deciliated *Tetrahymena* cells after (**a**) 5 minutes, (**b**) 10 minutes, (**c**) 20 minutes, (**d**) 60 minutes, (**e**) 135 minutes, and (**f**) 240 minutes, respectively. The re-growing motile cilia in the local areas of (**a**–**f**), marked by the rectangles, have been enlarged and displayed in 5 minutes (**g**), 10 minutes (**h**), 20 minutes (**i**), 60 minutes (**j**), 135 minutes (**k**), and 240 minutes (**l**), respectively. The tip regions of these re-growing cilia display morphologies from relatively blunt (**g** and **h**), to beginning to protrude an extension (**i** and **j**), and reach a maximum at 135 minutes (**k**). Eventually, the lengths of the tip regions shorten and stabilize.

evidence has been provided to support a direct interaction between the FTC and IFT trains, so whether IFT trains and the FTC interact to regulate IFT transition remains an open question.

In our pilot studies on cilia isolated from wild-type *Tetrahymena thermophila*, we noticed that isolated cilia displayed at least two distinct morphologies under negative staining EM. It motivated us to hypothesize that the morphological differences are related to various re-growth stages of the isolated cilia. In the work reported in this paper, we investigated the re-growing motile cilia from *Tetrahymena* using scanning electron microscopy and confirmed that the ciliary tip regions are subjected to morphological changes during ciliogenesis. We isolated re-growing motile cilia from deciliated *Tetrahymena* and *Chlamydomonas* at different time points, and studied their tip morphology by negative staining EM and a customized set of diameter profile analysis programs. Our results demonstrate that motile cilia tips display a dynamic, time-dependent morphology during re-growth. Cryo-electron tomography (cryo-ET) confirmed that these progressive differences are associated with the length difference between the central-pair microtubules and the growing ends of the MTDs.

Results

Tips of growing cilia display a morphological progression during cilia development. To investigate ciliary formation and development, *Tetrahymena* were deciliated using the dibucaine-HCl method, and cells recovering their cilia were examined at different time points using scanning electron microscopy. *Tetrahymena* cilia exhibited several distinct morphological features as they developed. During the initial phase of ciliary regrowth, cilia were typically less than two microns in length, and they had a hemi-capsule morphology as they emerged from the ciliary pocket (Fig. 1(a–c,g–i)). In agreement with previous studies[4], somatic cilia regrew uniformly along rows following a complete deciliation event. There was also a period of rapid growth between 10 and 135 minutes.

As early as 20 minutes after deciliation, the distal ciliary region began to extend a pointed tip (Fig. 1c,i). This ciliary tip region extension coincided with elongation of the whole cilium (Fig. 1(d,e,j,k)). At later time points, ciliary tip regions exhibited shorter lengths (Fig. 1f,l). Proximal to this tip region, the cilia appeared to be of constant diameter. Taken together, these observations suggest that the tip region undergoes a consistent remodeling process as the cilium grows. However, resolution limits and variations in three-dimensional orientations of the cilia made it difficult to characterize this dynamic morphology systematically using scanning electron micrographs.

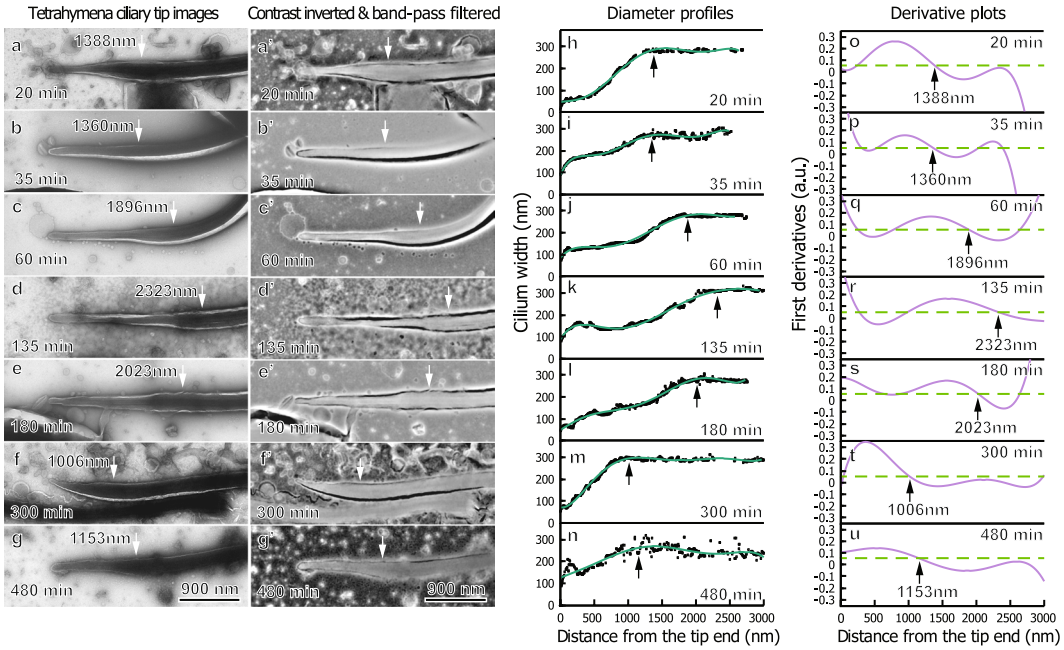

Figure 2. *Tetrahymena* ciliary tip regions remodel during cilia development. Negatively stained, re-growing cilia isolated from *Tetrahymena* at specified times are shown above. Electron micrographs of cilia isolated at various re-growth time before (**a**–**g**) and after (**a'**–**g'**) contrast inversion and band-pass filtering. The arrows indicate the end of a cilium's tip region. (**h**–**n**) show the corresponding width profiles for each cilium and an interpolating best-fit curve. (**o**–**u**) show the first derivative plots of these curves. The tip region length is defined using the best-fit curve's derivative and a cutoff slope at 0.052, corresponding to a 1.5° angle on both sides. The growing *Tetrahymena* ciliary tip region initially increases in length, until it reaches a maximum, then it decreases in length. Typically, cilia with longer tip regions had thinner diameters at the thinnest points.

We next expanded these studies using negative-staining transmission electron microscopy to view developing ciliary ultrastructure in greater detail.

The ciliary tip diameter profile progressively transitions during cilium development. We used negative-staining EM on re-growing cilia isolated from *Tetrahymena* (Fig. 2) to validate and further characterize this time-dependent morphological transition. The micrographs provided sufficient morphological detail for a quantitative description of ciliary ultrastructural features. Typical morphological features of the growing cilium include a thin diameter at the distal end, followed by a region of increasing diameter, until the cilium reaches full-width (Fig. 2a–g). It appears that the ciliary region intermediate to the absolute tip and the point of full width is an immature zone lacking the full complement of axonemal components. Portions distal to the mature regions are considered part of the ciliary tip region in our analysis.

We designed a systematic method to define the transition point between the immature zone and the mature regions objectively. This was accomplished using a set of customized Java programs as a plug-in package for ImageJ[22], as briefly described in the method section. Using this method, the length of the ciliary tip region can be defined and the progress of the tip growth can be described based on the length of this region. An explanation of the theory and implementation of this method is summarized in the supplemental text.

Figure 2 shows representative isolated cilia (Fig. 2a–g), along with their processed images (Fig. 2a'–g'), diameter profiles (Fig. 2h–n), and derivative plots (Fig. 2o–u). The arrows in panels indicate the end of the ciliary tip region, as defined above. This quantitative measure clearly showed that the length of the ciliary tip region changes over the 8 h regrowth period. In the beginning of cilia growth, the length of the ciliary tip region elongated and reached its maximum length after around 135 minutes of regrowth (Fig. 2d). After this maximum length was reached, the ciliary tip region slowly decreased in length until the cilia exhibit short-tipped morphologies (Fig. 2f,g). This growth process took place over the course of several hours, with the stable, short-tipped morphologies being present around 5 hours after the initial deciliation.

From these profiles, trends in tip diameter and length could be ascertained. In general, cilia with the longest tips (such as those shown at 60, 135, and 180 minutes) had very thin extensions (Fig. 2c–e); oftentimes cilia with tip regions around two microns had diameters as narrow as 75 nm. In ciliary tip regions with these very narrow extensions, a bulging of the very distal portion was occasionally visible, apparently due to the FTC. Meanwhile, cilia with shorter tip regions (such as those shown at 35 and 300 minutes) typically displayed wider, though still less than full-width, tip regions. In agreement with typical ciliary diameters, all cilia had full diameters between 200 nm and 300 nm, suggesting that negative staining produced minimal artifacts affecting ciliary diameter. In all of the isolated cilia, the FTC was clearly seen, indicating that the flagellar tip complex assembles at the distal ciliary tip region within 20 minutes of ciliary re-growth, and that the FTC persists throughout the cilium's lifetime.

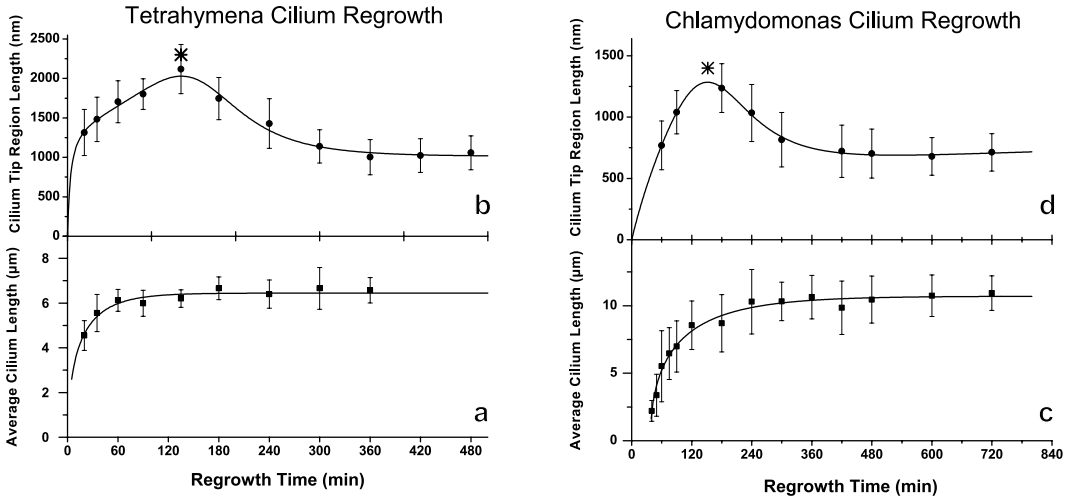

Figure 3. Maturation of the ciliary tip region continues after whole cilia reach full length. Plots (**a** and **c**) display the mean full lengths of growing cilia, with error bars representing standard deviation, which extend rapidly during the first phase of growth, reaching a maximum length of approximately 6.5 microns for *Tetrahymena* (after about two hours) and 10.7 microns for *Chlamydomonas* (after about four hours), respectively. Plots (**b** and **d**) show the mean tip region lengths, with error bars representing standard deviation, of growing cilia measured using our objective method. In both species, the ciliary tip region initially increases in length, with a maximum of 2020 nm at 135 minutes in *Tetrahymena* and 1280 nm at 150 minutes in *Chlamydomonas* (as denoted with an asterisk) before decreasing in length. The tip region length asymptotically decreases to 1070 nm for *Tetrahymena* and 680 nm for *Chlamydomonas*. Figure S2 displays the ratio of ciliary tip region length to whole cilium length, which demonstrates that the length percentile of the ciliary region reaches a peak at a growth time of about 135 min in both *Tetrahymena* and *Chlamydomonas*. Notably, the maturation of the ciliary tip region continues for over five hours following deciliation, whereas the whole cilium reaches full-length around two hours after deciliation.

Lastly, many ciliary diameter profiles exhibited a stepped appearance, which may be due to uneven termination of axonemal MTDs in the tip region.

In order to determine whether these observed morphological characteristics of regenerating *Tetrahymena* cilia are conserved among protists, isolation and width profile determination experiments were replicated using re-growing cilia from *Chlamydomonas reinhardtii*, as shown in (Fig. S1). Overall, *Chlamydomonas* exhibited a similar trend of the ciliary tip region growing in length before decreasing in length. However, *Chlamydomonas* cilia did not typically exhibit diameters below 100 nm, and the tip regions were typically less than 20% of the total ciliary length. Therefore, *Chlamydomonas* cilia exhibit a similar, though less dramatic, tip region re-growth trend.

Development of the ciliary tip region continues after the cilium reaches full length. Previous investigations into ciliogenesis primarily studied length of the entire cilium during the elongation phase and/or cell motility[4,6,23–25]. In order to consider tip region development in the context of the growing cilium's length, we determined both the average ciliary tip length and the average length of the entire cilium at different times of regrowth.

The method described above was used to measure the average length of the ciliary tip region from at least 27 cilia isolated at different time points for each cell type. As shown in Fig. 3, the ciliary tip regions of both *Tetrahymena* and *Chlamydomonas* initially extended outwards reaching a maximum length of over 2 microns at 135 minutes for *Tetrahymena* (Fig. 3a) and a maximum length of 1.3 microns at 150 minutes for *Chlamydomonas* (Fig. 3c). After the tip region reached its maximum length, it decreased in length until it asymptotically approaches 1070 nm in *Tetrahymena* and 680 nm in *Chlamydomonas*. Based on the rate of change, in both species, it took approximately six hours to reach full, mature tip length. The results of these flagellar regeneration kinetics experiments on the full length of both *Tetrahymena* and *Chlamydomonas* cilia closely followed previously reported trends[6,23]. Based on their respective trend profiles, *Tetrahymena* cilia reached a full length of 6.5 microns, while *Chlamydomonas* cilia reached a full length of 10.7 microns.

Comparing the length profiles for the full length of the whole re-growing cilia (Fig. 3b,d) to that of the tip region (Fig. 3a,c), the whole cilia display a fast extension phase initially, followed by a plateau growth phase with minimum elongation of the full length. In contrast, the tip region development and maturation continued long after the cilia had reached full length. It took approximately six hours for the ciliary tip region to establish a stable length. During the initial, fast extension phase, the ciliary tip region made up approximately one third of the total cilium length (Fig. S2). This proportion decreased non-monotonically until stabilizing at a species-dependent proportion. The time scale of this process was much longer than polymerization rates of tubulin on MTDs[26].

Structural features of the growing cilium tip. Conventional EM has revealed the tip structure of mature *Tetrahymena* cilia[17,27,28], in which the longest portion is the central pair microtubule singlets capped by a

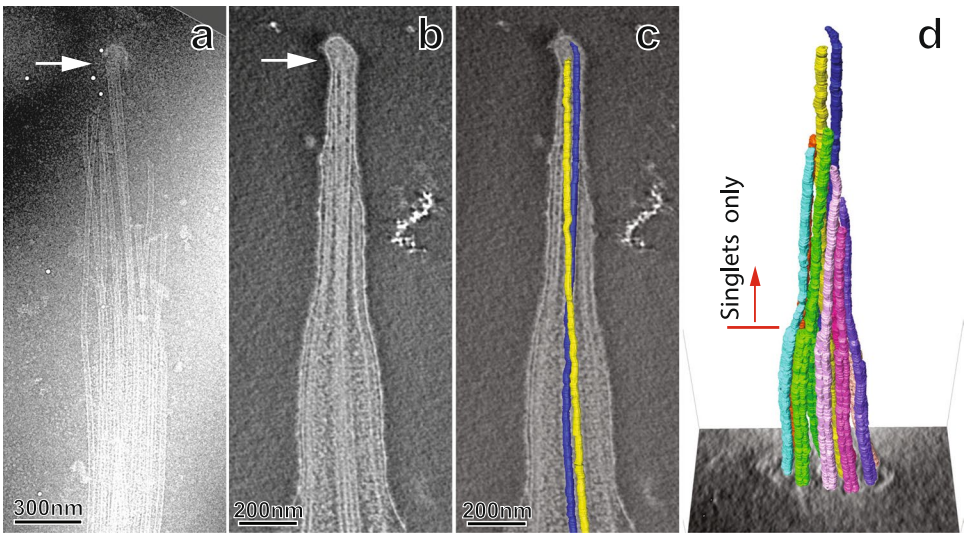

Figure 4. The cryo-electron microscopy of growing ciliary tip region after re-growth for 180 minutes. A micrograph of a splayed ciliary tip region, shown in (**a**), suggests that the distal axoneme lacks standard axonemal components. Tomograms of the ciliary tip region, shown in (**b**) (a central slice) and (**c**) (with added model of the central pair), confirm that the FTC sits on the central pair, and the central pair is physically constrained by membrane. The central pair twists, is outlined by the model microtubules in blue and yellow in (**c**). The MTD A-tubules extend into the ciliary tip region at least 400 nm farther than the B-tubules do. The distal tip therefore composes only microtubule singlets as marked by the red arrow in (**d**). These extended A-tubules are not decorated with axonemal spacer proteins.

ball-shaped FTC resembling a post-light, and the central pair complex is surrounded by 9 microtubule doublets forming a cylindrical configuration. At the distal ends of the microtubule doublets, the complete A-tubule extends farther and is stabilized by a globular protein complex that links to the ciliary membrane by fibrous proteins known as distal filaments. We performed a cryo-EM study on the cilium tips of re-growing cilia to better understand the tip structure in the regrowth phase. Our EM study demonstrates that the overall structure of the growing tip is largely similar to the architecture of the mature cilium tip; however, the more proximal portion of the ciliary tip region differs from the mature cilium. The growing axoneme's most distal components are two microtubule singlets of the central pair complex and a FTC that caps the central pair microtubule singlets together.

Previous studies have used splayed cilia as indications of axonemal composition in the tip region[29], and during specimen preparation, isolated cilia occasionally displayed membrane damage localized to the tip region. This resulted in a splaying of the tip region's contents, while the remainder of the cilium remained intact. These frayed tip regions allowed for easier visualization of the ciliary tip region's components. Figure 4a shows that the zone approximately 50 to 400 nm proximal to the FTC is occupied by the central pair microtubules and extended singlet A-tubules. Notably, the A-tubules extended into the ciliary tip region appear undecorated, whereas axonemal spacer proteins (radial spokes and outer dynein arms) are usually visible under cryo-EM[30–33]. This observation, along with the absence of B-tubules suggests that the growing ciliary tip region lacks a full complement of axonemal proteins.

While splayed ciliary tip regions provide clear visualization of the ciliary tip region's contents, it is possible that these features could be artifacts caused by membrane disruption. A more detailed, native state of the growing ciliary tip region was achieved via cryo-ET. Tomograms of growing cilia allowed us to verify that the immature ciliary tip region lacks well-organized spacer proteins like those of the mature axoneme, and the FTC is positioned in the most distal region of the cilium, as marked by the arrow in the longitudinal central section of a cryo-tomogram of a 3 h-regrowth cilium tip (Fig. 4b). At the tip of the growing cilium, the FTC-capped central pair is surrounded by a set of long microtubule singlets, not the standard nine doublet microtubules. These singlets are extensions of the MTD's A-tubule. These microtubule singlets are visible in the tomogram (Fig. 4b), and they are clearly shown in the frayed tip (Fig. 4a). In the tomogram of Fig. 4b, the B-tubules are separated from the tip end, where the FTC is located, by over half a micrometer (ranging from 511 nm to 1,029 nm). In addition, we observed that the central pair has a left-handed twist as shown in the model maps in Fig. 4c.

Discussion

In this study, we identified and characterized the growth process of the motile ciliary tip. Mechanistic similarities in the growth process of the ciliary tip were found in both *T. thermophila* and *C. reinhardtii*, indicating that this process is not species specific. Although the regeneration kinetics of ciliary growth calculated using the full-length of isolated cilia from both *Tetrahymena* and *Chlamydomonas* are consistent with previously modelled regeneration kinetics[15], in our observation, ciliogenesis contains two main steps: an initial step where the length of the full cilia undergoes rapid extension, followed by a step of plateau phase growth, in which cilium length remains almost constant but the tip region continues to develop and mature. Interestingly, the morphology of

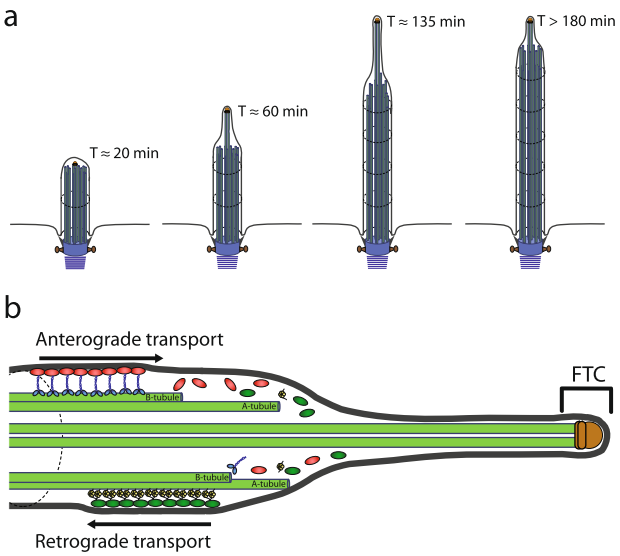

Figure 5. Schematic summary of cilium re-growth following amputation. The previously unidentified morphological transition of re-growing cilia is diagrammed in (**a**) (with Adobe Illustrator). First, the re-growing cilium extends from the ciliary pit with a round-tipped morphology (T ∼ 20 min), and the MTDs and central pair microtubule singlets are all approximately the same length. Then, when the cilium rapidly grows, the central pair microtubule singlets, capped by the FTC extend farther than the neighboring MTDs (T ∼ 60 min and 135 min). After the cilium reaches full length at T ∼ 135 min, the ciliary tip region continues to remodel as the distal axoneme assembles. The proposed molecular mechanism of distal axoneme assembly is shown in (**b**). In this model, anterograde IFT trains dissociate at the MTD B-tubule terminus several hundred nanometers proximal to the FTC and retrograde IFT train assembly occurs on the MTD A-tubules.

the tip region of growing motile cilia exhibits a characteristic progression. During the rapid growth, cilia appear as hemi-capsules of short length, which is consistent with previous studies on the early regrowth of *C. reinhardtii* cilia[6]. It is likely that the FTC might have not fully assembled at this point. The tip region of motile cilia then undergoes a progressive structural modification, which involves an extension of the central pair microtubules followed by extension of the A-tubules of MTDs and eventually the B-tubules, on the scale of hours. To gain a better understanding of the assembly characteristics, we developed a set of user-friendly programs to measure the length of the tip region from negative stained images of growing cilia. Diameter profiles and lengths of each ciliary tip region were determined. In the negatively stained micrographs, we can clearly see contrast from individual MTDs, but it is difficult to identify how many there are. The diameter profiles allow us to determine that these cilia tip regions may be as narrow as 60 nm: an enclosed space that can accommodate either only one MTD or just the central pair. This raised the question of whether the central pair or a MTD projects forward. This question is answered by our cryo-EM study, which showed that indeed the central pair, not a MTD, leads cilium growth at the tip region.

Although cilia continue to exhibit dynamic turnover after they have already reached full length, previous investigations of motile ciliogenesis often measured the full length of cilia, and they generally considered cilia mature once they reach the slow elongation phase[14,15]. Our data, however, suggest that the cilia continue to mature several hours after they reach full length. Therefore, the slow elongation phase is not just a period of protein turnover and overall length maintenance, but it is also a period of continued maturation process in the tip region. The overall morphologic changes and the underlying changes in ciliary architecture are diagrammed in Fig. 5a. These investigations give insights into organelle size regulation and maturation, because throughout the process of tip region development, the overall length of a cilium is very well maintained at an essentially constant length.

Although the architecture of the growing motile ciliary tip region is largely similar to the mature axoneme, our cryo-ET investigations revealed important distinctions in composition and structure. It is well established that the motile ciliary tip region contains the FTC, which is composed of several proteins not found in the mature axoneme[18,19]. The FTC-capped central pair microtubules appear to push the membrane at the tip of the regenerating cilium. The capped central pair reaches the full length before other axonemal microtubules. It is also clear that the elongated A-tubules of MTDs do not extend beyond the central pair tip. This makes the FTC-capped central pair microtubule the defining factor or the controller of the maximum length of cilia. In our studies, the central pair complexes of the *Tetrahymena* cilia display a left-handed twist, in agreement with previous reports that bend propagation during the ciliary beat drives twisting of the central pair in *Chlamydomonas reinhardtii* and *Paramecium tetraurelia*[34,35]. Furthermore, our cryo-tomographic study of the membrane-intact, isolated *Tetrahymena thermophila* cilia, demonstrates that central pair complex twisting is also present in the tip regions where radial spokes are not mature. This result supports the conclusion that the twist does not depend on the interactions between radial spoke heads and the central pair[35].

Our structural investigations from cryo-EM of splayed ciliary tip regions and cryo-ET of membrane-intact ciliary tip regions of regenerating cilia demonstrated that the growing ciliary tip region lacks the full complement of proteins

found in the mature axoneme. These differences have consequences for both ciliary assembly and IFT train turnaround. The immature ciliary tip region is composed of microtubule singlets, which are long extensions of the A-tubules from axonemal MTDs. Such structural features provide important insights into cilium assembly that involves IFT system. It has been well established that IFT serves as the primary mechanism for protein transportation across the base and distal ends of the cilium during both cilium assembly and maintenance. In growing cilia, particularly in the fast-growing stage (the first two hours in Fig. 3), the central pair, capped by the FTC, can be over a micrometer from the distal end of the B-tubules of MTDs. We know that anterograde IFT trains rely on kinesin motors walking along the B-tubule of the MTD[16]. Our data indicate that in the growing cilium, the normal anterograde IFT may stop at where the B-tubules terminates (marked by red arrow in Fig. 4d), far away from the ciliary tip end. Meanwhile, the central pair and the A-tubules are tightly wrapped by ciliary membrane as shown in Fig. 4b. This means there is limited room for a fast diffusion of large IFT complexes to the very tip of the growing cilium where the FTC caps the central pair microtubules. Therefore, it is unlikely that the FTC would play major roles in IFT reorganization and turnover, in contrast to a previously suggested model[20]. The proposed molecular mechanisms of distal axonemal assembly that are most plausible in the context of our tomographic studies are diagrammed in Fig. 5b.

Diffusion may be required for precursor proteins to reach the growing tip end of the extending central pair and the A-tubules of MTDs because anterograde IFT does not directly reach the growing tip ends where the extension happens for central pair microtubules and singlet A-tubules (Fig. 4d). However, the small, restricted space available, due to the tightly wrapped ciliary membrane around the central pair, does not favor a free fast diffusion of precursor proteins. Therefore, it is unclear how precursor proteins reach the growing tips of the central pair complex and the A-tubules of the doublet microtubules.

At the growing tip regions, both the central pairs and the A-tubule are singlet microtubules with tubulin as the primary component protein. If their extension is simply limited by the available tubulins that reach the tip region, the singlet A-tubules and the central pair should be of a similar length. However, our data have demonstrated that central pair microtubules are always longest at the growing ciliary tip with a significant length difference from that of the A-tubules. It could also be possible that the FTC plays a role in promoting central pair microtubule extension. However, the microtubule growth at the tip is not a simple extension limited by availability of tubulins. The time required for ciliary tip region maturation is on the scale of hours, which also suggests that tip region maturation is not limited by microtubule-doublet polymerization kinetics[26]. The nature of factors limiting the ciliary tip maturation process is unclear. Likely factors include post-translational modification of the microtubule complexes[36,37], and/or the availability of MTD-specific intralumenal microtubule associated proteins[38–41].

In this study, we discovered that tip regions of growing motile cilia are subject to a process of structural remodelling and maturation, which completes long after a cilium reaches its mature length. This new finding is not species specific, and therefore it is an important complementary knowledge to what we have known about cilia generation and maturation. Using a customized set of programs, we analyzed the morphologies of growing cilia tips at different growth times and clearly revealed the trend of ciliary tip growth and maturation. Cryo-electron tomographic studies of the growing ciliary tips determined that the growing ends of MTD B-tubules are significantly far away from the tip end led by the FTC. The trend profiles and the structural information from our electron tomographic study provided important insights into the relationship between IFT and FTC in ciliogenesis and the maintenance of cilia length.

Materials and Methods

Cell culture. Standard *Tetrahymena* and *Chlamydomonas* cell culture conditions were followed to maintain cell lines and to prepare cells for deciliation. Room-temperature stock cultures of the non-exocytozing *Tetrahymena thermophila* strain SB711, a gift from Prof. Eduardo Orias, were grown in modified Neff's media. To prepare cells for cilia isolation, stock culture cells were inoculated in SSP media and allowed to grow for 24 h at 30 °C, with shaking. The volume of SSP media was then increased eight-fold and cells were cultured for another 24 h under these conditions. Cells were then spun down at 700x*g* and then transferred to an equal volume of starvation media (10 mM Tris-HCl, pH = 7.5) and cultured for 18 to 20 h before deciliation.

Chlamydomonas reinhardtii algae, strain CC-137+, a gift from Prof. George Witman, were cultured in TAP media at room temperature. A light/dark cycle of 18/6 h was used. Cells were grown to approximately 1×10^6 cells/ml, and approximately 150 ml of cells were used for each deciliation.

Tetrahymena cilia isolation. To ensure that cilia from the same sample were at the same stage of growth, an initial deciliation was performed. It was determined through pilot studies that cells deciliate most completely using a modified version of the dibucaine method[42]. Briefly, cells were spun down at 600x*g* for 7 minutes and re-suspended in half of their growth volume of starvation media, and dibucaine-HCl was added to a concentration of 300 µM for a 5-minute incubation. Then, fresh starvation media was added to double the volume immediately before pelleting cells at 1200x*g* for 5 minutes. The deciliated cells were suspended in the original volume of fresh starvation media for the regrowth period. After allowing the cilia to regrow for a specified time between 35 minutes and 6 h, the second deciliation was performed. The second deciliation was identical to the first deciliation, except the dibucaine concentration was 450 µM. After the 5-minute dibucaine-HCl incubation, glutaraldehyde was added to 0.025% and EGTA was added to 0.5 mM for a 30 s incubation. Then, an equal volume of 4% sucrose in ice-cold starvation media was added to dilute the dibucaine, and all subsequent steps were performed at 4 °C. The sample was centrifuged at 1550x*g* for 7 minutes to pellet cell bodies. The supernatant was recovered and centrifuged at 1550x*g* for 7 minutes again. The supernatant was recovered and centrifuged at 17,000x*g* for 40 minutes to pellet cilia. The final pellet containing isolated cilia was suspended in a minimal volume of starvation media for plunge-freezing.

Chlamydomonas flagella isolation. *Chlamydomonas* cultures could not survive the dibucaine deciliation method, so the pH-shock method was employed for the first deciliation[43]. Briefly, cells were centrifuged at 600x*g* for 5 minutes and re-suspended in one-tenth their growth volume in fresh TAP media, and acetic acid was used to rapidly drop the pH from neutral to 4.5 for 60 s. Then, the media's pH was rapidly neutralized with aqueous KOH. Fresh TAP media was added to double the volume, and cells were pelleted before resuspension in fresh TAP media. After allowing the cilia to regrow for a specified time between 35 minutes and 3 h, the second deciliation was performed using the dibucaine method, with the following modifications. The cells were concentrated to one-eighth the original volume in modified HMES buffer (10 mM HEPES, 5 mM $MgSO_4$, 0.5 mM EGTA, and 2% sucrose, pH = 7.4), plus 0.025% glutaraldehyde, and 625 µM dibucaine was used for deciliation. The cilia were isolated in the same manner as the *Tetrahymena*, except the final centrifugation was at 31,000x*g* for 30 minutes.

Negative staining. Preparation of isolated cilia for negative staining TEM observation was carried out using 400-mesh copper grids with a thick, continuous carbon coating that had been glow-discharged for 60 s immediately before sample deposition. A 3.0 µl aliquot of specimen was applied to the grid for 90 s. The specimen was blotted, and 1% uranyl acetate was applied to the grid for 90 s. The grid was then blotted and allowed to dry for at least 1 h before transferring into a JEOL-JEM1400 electron microscope operating at 100 keV. For each of the areas of interest, the z-height was adjusted to eucentric position before taking images to ensure magnification accuracy. Micrographs were taken at 8000X magnification and were analyzed using ImageJ.

Analysis of ciliary tip region diameter. The analysis of the tip region of isolated cilia in negatively stained micrographs was performed using a set of custom-written Java programs. A detailed description is provided in the supplementary material. Briefly, micrographs were contrast-inverted and then bandpass-filtered to enhance the cilium's edge contrast. Then, a polyline was drawn along the central axis of each cilium, starting from the absolute tip, and a width-determination program generated a diameter profile. An interpolating polynomial curve of degree six was fit to the diameter profile, and the location where the slope decreased below 0.0532 (equivalent to a 1.5° incline on each side) is used to define the position separating the mature full diameter region with the cilium tip region of an increasing diameter (shown as the arrows in Fig. 2). Then potential lengths were reported. From these potential lengths, the cilium's tip region length was measured by determining which potential length agreed with the original micrograph. Parameters for the best-fit curves were determined using the nonlinear least-squares Marquardt-Levenberg algorithm implemented in Gnuplot. With the above strategy, a set of Java programs were written as a plug-in package for ImageJ[22] and used for this analysis of approximately 900 electron micrographs of cilia. The diagrams of the tip architecture changes during cilium growth, shown in Fig. 5, were prepared using Adobe Illustrator (Adobe Systems In., San Jose, CA).

Characterization of growing cilia and ciliary tip regions. In order to characterize ciliary development using the length of the entire cilium and the length of the tip region, average lengths of these features were plotted as functions of time. The ciliary tip region measurements appeared to exhibit the following characteristics: the ciliary tip region started at length zero, and it then sequentially reached a local maximum, an inflection point, and asymptotically approached a final length. Based on these conditions, a curve of best fit was determined using a quotient of two trinomials of the form $(ax^3 + bx^2 + cx)/(dx^3 + ex^2 + fx + g)$. From these curves, the local maxima and horizontal asymptotes were determined. In order to characterize the length of the entire cilium as a function of time, we fit our data to the solution to the differential equation described in[15].

Cryo-EM sample preparation. Preparation of isolated cilia for cryo-EM observation was carried out using 300-mesh copper grids with a thin, continuous carbon coating that had been glow-discharged for 30 s immediately before sample preparation. A 2.5 µl aliquot of 0.1% poly-L-lysine (w/v in water) was applied to the grid for 1 minute. The grid was blotted, and subsequently washed twice in water. Then, water was applied to the grid a third time, and the grid was loaded into the Gatan CryoPlunger3. The grid was blotted, and a 2.5 µl aliquot of cilia specimen that had been mixed 3:1 with 15 nm gold particles was applied to it for 20 s. Then, single-side blotting was used to blot the grid for 6.0 s before plunging into liquid ethane at −174 °C. The frozen grids were stored in liquid nitrogen until loaded into a JEOL-JEM3200FSC/PP electron microscope. Data were acquired using either a CCD camera or a Gatan K2 Summit direct-electron detector.

Cryo-ET data collection and processing. All electron tomographic tilt series data sets were collected using SerialEM[44] with a tilt increment of 2 or 3 degrees. The JEM-3200FSC was operated at 300 keV with zero-loss energy filtering, slit width 24 eV. The pixel size on the specimen was 0.36 nm and the total electron dose was about 70 e^-/A^2. Images were recorded at a target underfocus between 4 and 8 µm on a K2 Summit direct-electron-detection camera (Gatan, Pleasanton, CA) with 5 to 8 frames per second during an exposure time of 1 to 1.5 sec. Frame alignment was carried out with the "Unblur & Summovie" package[45–47]. Tomographic reconstruction were carried out using Etomo/IMOD[48]. Bilateral filtering was applied to denoise the reconstructed tomograms with functions provided in EMAN2 package[49,50].

Scanning electron microscopy. Tetrahymena samples collected from different time points of regrowth after deciliation were fixed by 1% glutaraldehyde and placed in pre-processed aluminum carriers from the M. Wohlwend GmbH, Engineering office. Before adding *Tetrahymena* cells, the carriers were carbon coated and glow discharged (two minutes) followed by treatment of poly-L-lysine coating to increase cell attachment. The *Tetrahymena* cells in the carriers were subjected to a six-step gradient dehydration of ethyl alcohol (10%, 20%, 40%, 70%, 90%, and 100%) followed by critical-point drying using Samdri-795 with a 15 minutes purging process. Afterwards, the samples in the carrier were fixed on conductive stubs with silver glue and gold-coated for

45 seconds using a CRESSINGTON Sputter Coater. SEM images were captured at 2 kx, 5 kx, and 10 kx magnifications using Secondary Electrons Secondary Ions detector of a ZEISS NEON 40EsB High Resolution Dual Beam Scanning Electron Microscope.

References

1. Pazour, G. J. & Rosenbaum, J. L. Intraflagellar transport and cilia-dependent diseases. *Trends Cell Biol.* **12**, 551–555 (2002).
2. Brown, J. M. & Witman, G. B. Cilia and diseases. *BioScience* **64**, 1126–1137 (2014).
3. Braun, D. A. & Hildebrandt, F. Ciliopathies. Cold Spring Harb. Perspect. Biol. **9**, a028191 (2017).
4. Rannestad, J. The regeneration of cilia in partially deciliated Tetrahymena. *J. Cell Biol.* **63**, 1009–1017 (1974).
5. Rosenbaum, J. L. & Carlson, K. Cilia regeneration in Tetrahymena and its inhibition by colchicine. *J. Cell Biol.* **40**, 415–425 (1969).
6. Rosenbaum, J. L., Moulder, J. E. & Ringo, D. L. Flagellar elongation and shortening in Chlamydomonas. The use of cycloheximide and colchicine to study the synthesis and assembly of flagellar proteins. *J. Cell Biol.* **41**, 600–619 (1969).
7. Auclair, W. & Siegel, B. W. Cilia regeneration in the sea urchin embryo: evidence for a pool of ciliary proteins. *Science (New York, N.Y.)* **154**, 913–915 (1966).
8. Kozminski, K. G., Johnson, K. A., Forscher, P. & Rosenbaum, J. L. A motility in the eukaryotic flagellum unrelated to flagellar beating. *Proc. Natl. Acad. Sci. U. S. A.* **90**, 5519–5523 (1993).
9. Sloboda, R. D. & Rosenbaum, J. L. Making sense of cilia and flagella. *J. Cell Biol.* **179**, 575–582 (2007).
10. Broekhuis, J. R., Leong, W. Y. & Jansen, G. In *International Review of Cell and Molecular Biology* Vol. Volume 303 (ed. W. Jeon Kwang), 101–138 (Academic Press, 2013).
11. Deane, J. A., Cole, D. G., Seeley, E. S., Diener, D. R. & Rosenbaum, J. L. Localization of intraflagellar transport protein IFT52 identifies basal body transitional fibers as the docking site for IFT particles. *Curr. Biol.* **11**, 1586–1590 (2001).
12. Qin, H., Diener, D. R., Geimer, S., Cole, D. G. & Rosenbaum, J. L. Intraflagellar transport (IFT) cargo: IFT transports flagellar precursors to the tip and turnover products to the cell body. *J. Cell Biol.* **164**, 255–266 (2004).
13. Pigino, G. *et al*. Electron-tomographic analysis of intraflagellar transport particle trains *in situ*. *J. Cell Biol.* **187**, 135–148 (2009).
14. Marshall, W. F., Qin, H., Rodrigo Brenni, M. & Rosenbaum, J. L. Flagellar Length Control System: Testing a Simple Model Based on Intraflagellar Transport and Turnover. *Mol. Biol. Cell* **16**, 270–278 (2005).
15. Marshall, W. F. & Rosenbaum, J. L. Intraflagellar transport balances continuous turnover of outer doublet microtubules: implications for flagellar length control. *J. Cell Biol.* **155**, 405–414 (2001).
16. Stepanek, L. & Pigino, G. Microtubule doublets are double-track railways for intraflagellar transport trains. *Science (New York, N.Y.)* **352**, 721–724 (2016).
17. Dentler, W. L. Structures linking the tips of ciliary and flagellar microtubules to the membrane. *J. Cell Sci.* **42**, 207–220 (1980).
18. Miller, J. M., Wang, W., Balczon, R. & Dentler, W. L. Ciliary microtubule capping structures contain a mammalian kinetochore antigen. *J. Cell Biol.* **110**, 703–714 (1990).
19. Pedersen, L. B., Geimer, S., Sloboda, R. D. & Rosenbaum, J. L. The Microtubule Plus End-Tracking Protein EB1 Is Localized to the Flagellar Tip and Basal Bodies in Chlamydomonas reinhardtii. *Curr. Biol.* **13**, 1969–1974 (2003).
20. Sloboda, R. D. Intraflagellar transport and the flagellar tip complex. *J. Cell. Biochem.* **94**, 266–272 (2005).
21. Iomini, C., Babaev-Khaimov, V., Sassaroli, M. & Piperno, G. Protein particles in Chlamydomonas flagella undergo a transport cycle consisting of four phases. *J. Cell Biol.* **153**, 13–24 (2001).
22. Schneider, C. A., Rasband, W. S. & Eliceiri, K. W. NIH Image to ImageJ: 25 years of image analysis. *Nat. Methods* **9**, 671–675 (2012).
23. Hadley, G. A. & Williams, N. E. Control of initiation and elongation of cilia during ciliary regeneration in Tetrahymena. *Mol. Biol. Cell* **1**, 865–870 (1981).
24. Jarvik, J. W. & Rosenbaum, J. L. Oversized flagellar membrane protein in paralyzed mutants of Chlamydomonas reinhardrii. *J. Cell Biol.* **85**, 258–272 (1980).
25. McVittie, A. Flagellum mutants of Chlamydomonas reinhardii. *J. Gen. Microbiol.* **71**, 525–540 (1972).
26. Binder, L. I., Dentler, W. L. & Rosenbaum, J. L. Assembly of chick brain tubulin onto flagellar microtubules from Chlamydomonas and sea urchin sperm. *Proc. Natl. Acad. Sci. U. S. A.* **72**, 1122–1126 (1975).
27. Dentler, W. L. & Rosenbaum, J. L. Flagellar elongation and shortening in chlamydomonas. III. *Structures attached to the tips of flagellar microtubules and their relationship to the directionality of flagellar microtubule assembly. J. Cell Biol.* **74**, 747–759 (1977).
28. Gaertig, J., Wloga, D., Vasudevan, K. K., Guha, M. & Dentler, W. In *Methods in Enzymology* Vol. 525, 265–284 (2013).
29. Sale, W. S. & Satir, P. Splayed Tetrahymena cilia. A system for analyzing sliding and axonemal spoke arrangements. *J. Cell Biol.* **71**, 589–605 (1976).
30. Oda, T., Yanagisawa, H., Yagi, T. & Kikkawa, M. Mechanosignaling between central apparatus and radial spokes controls axonemal dynein activity. *J. Cell Biol.* **204**, 807–819 (2014).
31. Pigino, G. *et al*. Cryoelectron tomography of radial spokes in cilia and flagella. *J. Cell Biol.* **195**, 673–687 (2011).
32. Lin, J., Heuser, T., Carbajal-Gonzalez, B. I., Song, K. & Nicastro, D. The structural heterogeneity of radial spokes in cilia and flagella is conserved. *Cytoskeleton (Hoboken, N.J.)* **69**, 88–100 (2012).
33. Kishchenko, G. P. *et al*. Effect of fringe-artifact correction on sub-tomogram averaging from Zernike phase-plate cryo-TEM. *J. Struct. Biol.* **191**, 299–305 (2015).
34. Omoto, C. K. & Kung, C. Rotation and twist of the central-pair microtubules in the cilia of paramecium. *J. Cell Biol.* **87**, 33–46 (1980).
35. Mitchell, D. R. & Nakatsugawa, M. Bend propagation drives central pair rotation in Chlamydomonas reinhardtii flagella. *J. Cell Biol.* **166**, 709–715 (2004).
36. Sloboda, R. D. Posttranslational protein modifications in cilia and flagella. *Methods Cell Biol.* **94**, 347–363 (2009).
37. Schneider, M. J., Ulland, M. & Sloboda, R. D. A protein methylation pathway in Chlamydomonas flagella is active during flagellar resorption. *Mol. Biol. Cell* **19**, 4319–4327 (2008).
38. Nicastro, D. *et al*. The molecular architecture of axonemes revealed by cryoelectron tomography. *Science (New York, N.Y.)* **313**, 944–948 (2006).
39. Sui, H. & Downing, K. H. Molecular architecture of axonemal microtubule doublets revealed by cryo-electron tomography. *Nature* **442**, 475–478 (2006).
40. Downing, K. H. & Sui, H. Structural insights into microtubule doublet interactions in axonemes. *Curr. Opin. Struct. Biol.* **17**, 253–259 (2007).
41. Amos, L. A. Articulated Tubes. *Structure* **18**, 892–894 (2010).
42. Thompson, G. A. Jr., Baugh, L. C. & Walker, L. F. Nonlethal deciliation of Tetrahymena by a local anesthetic and its utility as a tool for studying cilia regeneration. *J. Cell Biol.* **61**, 253–257 (1974).
43. Craige, B., Brown, J. M. & Witman, G. B. Isolation of chlamydomonas flagella. *Curr. Protoc. Cell Biol.* **48**, 1–6 (2013).
44. Mastronarde, D. N. Automated electron microscope tomography using robust prediction of specimen movements. *J. Struct. Biol.* **152**, 36–51 (2005).
45. Grant, T. & Grigorieff, N. Measuring the optimal exposure for single particle cryo-EM using a 2.6 A reconstruction of rotavirus VP6. *Elife* **4**, e06980 (2015).

46. Campbell, M. G. *et al*. Movies of ice-embedded particles enhance resolution in electron cryo-microscopy. *Structure* **20**, 1823–1828 (2012).
47. Brilot, A. F. *et al*. Beam-induced motion of vitrified specimen on holey carbon film. *J. Struct. Biol.* **177**, 630–637 (2012).
48. Kremer, J. R., Mastronarde, D. N. & McIntosh, J. R. Computer visualization of three-dimensional image data using IMOD. *J. Struct. Biol.* **116**, 71–76 (1996).
49. Tang, G. *et al*. EMAN2: An extensible image processing suite for electron microscopy. *J. Struct. Biol.* **157**, 38–46 (2007).
50. Jiang, W., Baker, M. L., Wu, Q., Bajaj, C. & Chiu, W. Applications of a bilateral denoising filter in biological electron microscopy. *J. Struct. Biol.* **144**, 114–122 (2003).

Acknowledgements

We thank Prof. Eduardo Orias at UC Santa Barbara for the gift of *Tetrahymona* strain SB711, and Prof. George Witman at University of Massachusetts Medical School for the gift of *Chlamydomaonas* strain CC-137+. We are also in debt to Drs. Jie He and Yongping Wu for discussion on cryo-EM specimen preparation, to Chyongere Hsieh for assistance and suggestion on SEM operation, and to Mr. Shufeng Sun for advice and help on SEM specimen preparation. This work is supported by the National Institutes of Health grants GM101026 and GM097010 to H.S. In addition, M.J.R. was partially supported with National Science Foundation funding in the Wadsworth Center's Research Experience for Undergraduates (REU) program (grant DBI1062963). P.O. is supported by Thailand Research Funds (RSA5980078). T.P. worked on this project under the support of the undergraduate oversea-training fellowship from the Faculty of Science, Mahidol University.

Author Contributions

P.O. and H.S. initialized the project. T.P., under the assistance from R.L.F. on TEM, discovered the morphological difference at the tip region of isolated *Tetrahymena* cilia. H.S. and P.O. discussed and hypothesized that the difference may be related to different regrowth times. T.P. performed initial experimental work and confirmed that the morphology of the ciliary tip region changes with re-growth time. M.J.R. optimized deciliation and regrowth conditions, isolated cilia, prepared EM specimens (negatively staining and vitreously frozen), collected negatively staining EM images, and worked with H.S. together for cryo-electron tomographic data collection, reconstruction and analysis. M.J.R. and H.S. designed the method of image processing and the algorithm for analyzing ciliary tip morphology. M.J.R. composed the Java modules as plug-ins for ImageJ, and carried out the analysis for the ciliary tip morphology under the supervision of G.G. and H.S.; Under the supervision of B.T.P. and H.S., R.L.F. contributed to cell culture, cilia specimen preparation, data collection of negatively staining EM, specimen preparation for SEM, and determination of cilium full-length at various time points. K.C. optimized SEM specimen preparation, performed SEM data collection and analysis, and contributed to negatively staining EM data collection, cilia full length profile determination, and performed segmentation of tomograms. M.J.R., G.G. and H.S. prepared the original manuscript. B.T.P., and P.O. participated in manuscript writing with critical review and editing. All authors have reviewed and approved the manuscript.

Additional Information

Supplementary information accompanies this paper at https://doi.org/10.1038/s41598-018-26111-2.

Competing Interests: The authors declare no competing interests.

Publisher's note: Springer Nature remains neutral with regard to jurisdictional claims in published maps and institutional affiliations.

International Education
DOI: https://doi.org/10.1128/jmbe.v20i1.1571

JMBE Journal of Microbiology & Biology Education

Time-Restricted Inquiry-Based Learning Promotes Active Student Engagement in Undergraduate Zoology Laboratory †

Thitinun Sumranwanich[1], Kanpong Boonthaworn[1,2], Sombat Singhakaew[1]*, and Puey Ounjai[1,2]*
[1]*Department of Biology, Faculty of Science, Mahidol University, Bangkok, Thailand 10400,*
[2]*Center of Excellence on Environmental Health and Toxicology, Office of Higher Education Commission, Ministry of Education, Bangkok, Thailand 10400*

Organizing a zoology laboratory for an undergraduate course is often a challenge, particularly in a limited-resource setting, due to the vast variety of topics to cover and the limited numbers of preserved specimens and permanent slides. In zoology, the class structure generally takes the form of a lecture demonstration followed by sample exhibition stations. This setting often fails to actively engage the majority of students in exploring the specimens. Here we propose an alternative organization of a zoology class lab format comprised of short guided-inquiry, time-restricted lab stations, and a freely structured follow-up project intended to increase attention and conceptual understanding of the lab topic. The lab is designed in two parts: a 10-minute in-class rotation portion, where small groups of students take turns investigating specimens following an instructor demonstration, and an after-class group assignment. We implemented the strategy for two years, and it is clear that our approach significantly increased students' active engagement in the class. The time-restricted scheme ensures all students participate despite limited resources, while the guided instructions keep the students focused on the topic. Furthermore, the team assignment portion, in particular the media creation aspect, promoted teamwork among group members.

การจัดประสบการณ์การเรียนรู้ในวิชาปฏิบัติการสัตววิทยาสำหรับนักศึกษาในหลักสูตรระดับปริญญาตรีนั้นมักจะเป็นสิ่งที่ท้าทาย ทั้งนี้ เนื่องจากทรัพยากรที่จำกัดทั้งในด้านตัวอย่างและสไลด์ถาวร ด้วยเหตุนี้ การเรียนในห้องปฏิบัติการสัตววิทยาจึงมักถูกจัดในรูปแบบของการสาธิตและการจัดแสดงนิทรรศการเป็นฐานกิจกรรมย่อย แม้ว่าการจัดประสบการณ์การเรียนรู้แบบนี้อาจจะใช้ได้ดีกับนักเรียนที่มีผลสัมฤทธิ์สูงที่มีความสนใจในการศึกษาตัวอย่างและนิทรรศการที่จัดไว้ด้วยตนเอง แต่มักจะไม่สามารถกระตุ้นให้นักเรียนส่วนใหญ่สนใจศึกษาตัวอย่างได้ ในการนี้ ผู้วิจัยได้เสนอแนวทางในการจัดประสบการณ์การเรียนรู้ในวิชาปฏิบัติการสัตววิทยาแบบใหม่ซึ่งอาศัยการจัดกิจกรรมเพื่อการสืบเสาะหาความรู้แบบชี้แนะแนวทาง (guided inquiry) แบบสั้นๆ เพื่อเพิ่มความสนใจนักศึกษาในชั้นเรียน การจัดปฏิบัติการในแต่ละฐานนั้นจะมุ่งเน้นเพื่อพัฒนากรอบแนวคิดในหัวข้อเฉพาะ การจัดปฏิบัติการในงานวิจัยนี้ถูกออกแบบให้มี 2 ส่วนหลัก ส่วนแรกคือกิจกรรมในห้องเรียน ซึ่งแบ่งเป็นกิจกรรมในฐานต่างๆ (rotation station) โดยแต่ละกิจกรรม นักเรียนกลุ่มเล็ก ๆ จะเวียนกันทำกิจกรรมในสถานีย่อยตามการชี้นำในเอกสารประกอบ เป็นเวลาฐานละ 10 นาที และกิจกรรมกลุ่มนอกเวลาเพื่อทำงานตามที่ได้รับมอบหมายให้สำเร็จ หลังจากทดลองประยุกต์ใช้กลยุทธ์ในการจัดปฏิบัติการเช่นนี้เป็นเวลา 2 ปี พบว่ากลวิธีนี้สามารถเพิ่มการมีส่วนร่วมของนักเรียนในชั้นเรียนได้อย่างเห็นได้ชัด การให้เวลาที่จำกัดจะช่วยกระตุ้นให้นักศึกษาเร่งรัดและใส่ใจที่จะทำการทดลองแม้จะมีทรัพยากรที่จำกัด ส่วนคำแนะนำในการทำกิจกรรมตามเอกสารประกอบนั้นจะช่วยให้นักศึกษาสามารถทำงานไปตามหัวข้อที่กำหนดได้ นอกจากนี้ยังพบว่าการมอบหมายงานกลุ่มนั้นยังช่วยให้ทุกคนมีส่วนร่วมในงานของกลุ่ม โดยเฉพาะอย่างยิ่ง การสร้างสื่อแบบต่างๆ ยังมีส่วนช่วยในการส่งเสริมการทำงานเป็นหมู่คณะของสมาชิกภายในกลุ่มอีกด้วย

*Corresponding author. Mailing address: Department of Biology, Faculty of Science, Mahidol University, 272 Rama VI Rd., Ratchathewi, Bangkok, Thailand 10400. Phone: +6622015478.
E-mail: Sombat.Sin@mahidol.ac.th, Puey.Oun@mahidol.edu.
Received: 4 January 2018, Accepted: 23 April 2018, Published: 26 April 2019.
†Supplemental materials available at http://asmscience.org/jmbe

INTRODUCTION

Zoology courses cover a broad range of topics, including knowledge of animal taxonomy, life cycle, biodiversity, and the role of evolution in shaping the form and function of different animals. As a result, zoology courses must incorporate large numbers of specimens to introduce students to different types of animals at various points of

their life cycle. However, some regions, including Thailand, have limited resources and access to only limited numbers of preserved specimens, permanent slides, and microscopes. Undergraduate zoology laboratory courses in Thailand are often arranged as a lecture with exhibition stations to cope with the lack of available learning materials.

In this traditional setting, student instructions are often provided in the form of a laboratory manual and a laboratory briefing prior to starting the lab class. After a short briefing, students are expected to explore the different stations and complete a lab assignment worksheet, on which they report individually. Frequently, other activities, such as a lab quiz, are implemented at the end of class to motivate students to rigorously explore all the stations. Although this setting has been widely used in the classroom for decades, it often fails to engage the majority of students. It was found that despite the rigorous prelaboratory briefing, students still lacked conceptual and procedural understanding of the topic (1, 2). Some students were able to develop a conceptual understanding of how biodiversity, evolution, and taxonomic classification are interconnected, but this understanding was largely dependent on the quality of class teaching assistants (TAs) and instructors (2). These higher-achieving students often gathered around stations where the TA was present and active, while other students were at other stations working on their own. Often, students relied on images of a specimen captured using a phone or tablet to complete drawing or sketching assignments rather than studying the actual specimen at the station. Sometimes, they used images from the Internet. This negated the purpose of the zoological lab class, reducing students' conceptual understanding of the course material. Moreover, students also struggled in labs with complex experiments, becoming mired in procedural details about the experiment rather than developing a conceptual understanding of the subject being studied. Finally, when a group project was assigned, a few members of the team tended to complete the report while the rest of the team remained unengaged in the course content and lab activities.

To address this lack of engagement, we added an inquiry-based aspect to the lab class. It has been widely shown that an inquiry-based strategy can help improve student engagement and increase student performance in different classroom settings (3–7). The guided inquiry process allows students to develop their own ideas from different sources of information, with only a simple guided instruction from the lab instructor or TA. After each individual develops an understanding of the topic, ideas and resources are shared and developed among peers in small groups to promote student engagement in the activity (8–10). Finally, groups present their results in various creative ways, such as small science projects or group presentations (8–10). Despite some advocacy from the government, the implementation of inquiry-based learning in science education in Thailand is still largely limited, even in schools and institutions where resources are abundant (11). Most inquiry-based approaches implemented in schools in Thailand are structure-based (11). Guided and open inquiries are sometime arranged for senior undergraduate students in large universities or for gifted students in well-funded schools. One of the major concerns in incorporating inquiry-based learning in the classroom is the lack of supporting facilities (12). Moreover, this type of learning often takes longer to implement. Our approach was developed to help maximize the use of limited resources to increase student engagement using task-based

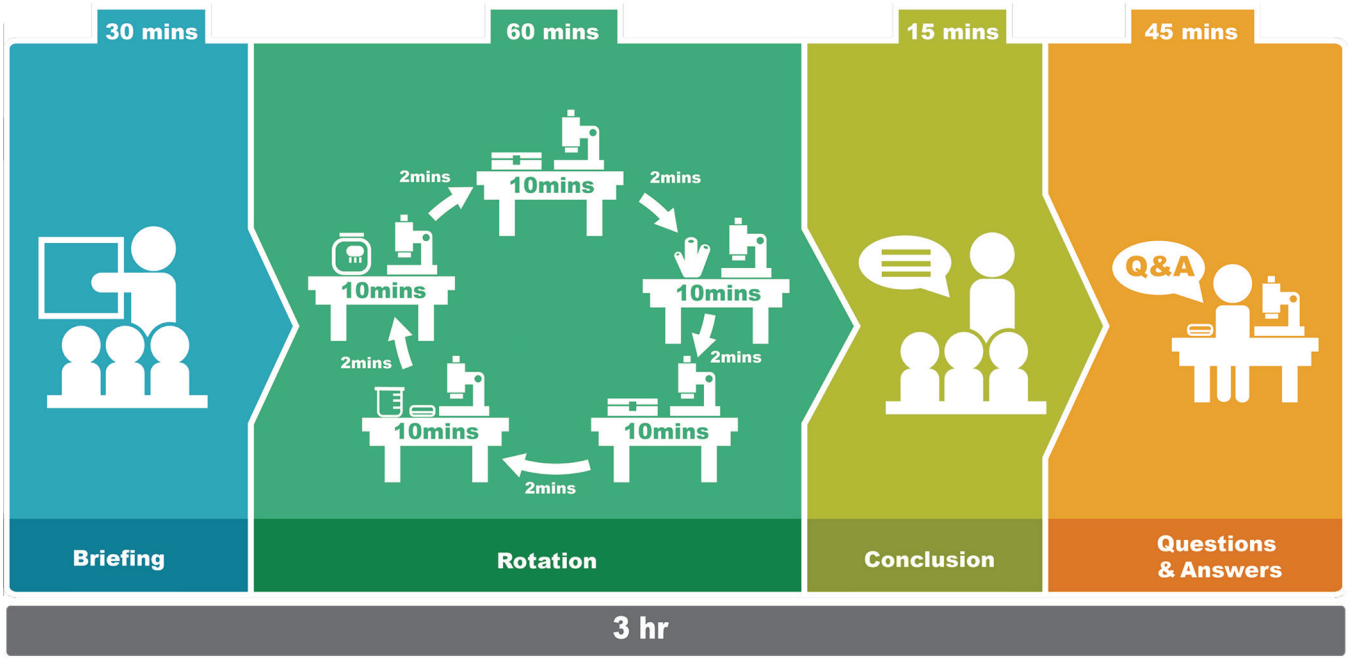

FIGURE 1. Strategic time management for the in-class activities.

assignments and a time-restricted guided-inquiry learning protocol. The tasks were designed to incorporate different levels of inquiry-based learning from structured to guided to simple open inquiries. From our observations, the time restriction significantly helps encourage students to focus their attention on specimens and class materials and participate in the team effort. Our approach appears to not only help actively engage students with the lab activities but also promote peer-to-peer communication and team work. With some modifications, our laboratory design can be beneficial to similarly sample-limited regions in which zoological courses are taught.

PROCEDURE

The strategy was implemented in an undergraduate zoology class of 50 students. Students were in their sophomore year, ranging from 18 to 20 years old. Each lab class correlated with a preceding instructor lecture in corresponding topics. Students were divided into 10 groups of five students. Five lab stations were set up to accommodate two groups (10 students) at each station. A guided inquiry–based laboratory assignment was designed to require both in-class activities and after-class activities. Both parts of the assignment were completed in groups based on the notion that cooperative learning helps increase the learning performance of students (13, 14). Students worked collaboratively to collect data and complete the in-class activity, and the group discussed and developed a presentation idea during the after-class activity. Often, the presentation incorporated media such as movies and infographics. Group assignments were due within two weeks of the lab class.

In-class activities: Time-restricted lab rotation

The guided inquiry–based practical task is designed based on the key conceptual idea for each topic and includes a variety of activities to ensure the task is both interesting and challenging for students (15). The guided instruction for in-class activities was planned to train both cognitive and psychomotor skills. As the average attention span of students has been reported to be around 10 to 15 minutes, all the tasks for in-class activities were designed to be completed within 10 minutes (16). In each task, students were allowed to collect data using provided specimens at the station table. An alarm signal was used to remind students to move to the next station, forcing students in the group to participate in activities at each station and encouraging active contribution among the team members. To foster respect for others and for the materials, students used two minutes after the alarm signal to clean up and reset their current station before rotating to the next station. A question-and-answer session at the end of class enabled students to discuss, collect more data, and implement critical thinking on the more challenging aspects of the task. Sample lab stations are shown in Appendix 1.

After-class assignment: Collaborative learning

To foster a group active-learning experience, after-class assignments challenged the students to scrutinize the problem and find a way to effectively communicate their ideas to their peers (8, 14). The in-class team activities were designed to be different at every station, ranging from drawing to comparing animal structures and forms to capturing images for their assignments and answering questions related to the topics. The after-class assignments combined the in-class stations with student creativity. Free tools such as "Facebook live" and "Piktochart" (17) were used to make movies or infographics to be published online. The format of the presentation was left open so individual groups could decide how to present the assignment. Impressively, the students in the study produced high-quality movies presented in different styles, including conventional voice-narrated shows, animation, and stop motion. Samples of these movies are available upon request.

CONCLUSION

After two years of implementation, our lab strategy has been found to promote active student engagement in zoology classes. Students not only learned about the topic, but were also able to organize themselves to work as a team. We found that students successfully collaborated and distributed tasks among themselves within minutes during the in-class time-restricted challenge. The time-restriction was essential to encourage contribution from all team members. Diverse tasks, such as drawing, experiments, and collecting data for presentations, were used during the in-class assignments to accommodate the attention span of the students. Students quickly leveraged online social tools, including Facebook groups, Line, Google Drive, and Dropbox, to share resources among the team to complete the after-class project. The collaborative nature of the assignments helped promote team-building skills within the groups of students. Our approach clearly demonstrated that the time-restricted guided inquiry could be effectively implemented in undergraduate zoology laboratory classes to actively engage students in class activities.

SUPPLEMENTAL MATERIALS

Appendix 1: Lab instruction for class about sponges and *Cnidaria* (for TAs & instructors)

ACKNOWLEDGMENTS

Work in Ounjai lab is supported by Thailand Research Funds Grant RSA5980078 to P.O. K.B. is a Sri Trang Thong Scholar. Support for P.O. from the Department of Biology, Faculty of Science, Mahidol University, is also gratefully acknowledged. We would further like to express our gratitude to Shilpika Chowdhury and Edward Makoto Johns for their

help in editing and proofreading of the manuscript. We thank Assoc. Prof. Sompoad Srikosamatara, Prof. Miriam Segura-Totten, and the panel of reviewers for valuable suggestions. The authors have no conflicts of interest to declare.

REFERENCES

1. Rollnick M, Zwane S, Staskun M, Lotz S, Green G. 2001. Improving pre-laboratory preparation of first year university chemistry students. Int J Sci Educ 23(10):1053–1071.
2. Pogacnik L, Cigic B. 2006. How to motivate students to study before they enter the lab. J Chem Educ 83(7):1094–1098.
3. Adams DJ. 2015. Current trends in laboratory class teaching in university bioscience programmes. Bioscience Educ 13(1):1–14.
4. Burrowes PA. 2007. How to make a field trip a hands-on investigative laboratory: learning about marine invertebrates. Am Biol Teach 69(4):54–58.
5. Martineau C, Traphagen S, Sparkes TC. 2013. A guided inquiry methodology to achieve authentic science in a large undergraduate biology course. J Biol Educ 47(4):240–245.
6. Timmerman BE, Strickland DC, Carstensen SM. 2008. Curricular reform and inquiry teaching in biology: where are our efforts most fruitfully invested? Integr Comp Biol 48(2):226–240.
7. Kuhlthau CC, Maniotes LK, Caspari AK. 2007. Guided inquiry: learning in the 21st century. Libraries Unlimited, Santa Barbara, CA.
8. Tornee N, Bunterm T, Tang KN. 2017. The impacts of inquiry-based learning model on teaching science subject: a case study in Thailand. Turk Online J Educ Tech Spec Iss INTE 395–402.
9. Kuhlthau CC, Maniotes LK, Caspari AK. 2012. *Guided inquiry design: a framework for inquiry in your school.* Libraries Unlimited, Santa Barbara, CA.
10. Bonwell C, Eison J. 1991. Active learning: creating excitement in the classroom. AEHE-ERIC Higher Education Report No. 1. Jossey-Bass, Washington, DC.
11. Bunterm T, Lee K, Ng Lan Kong J, Srikoon S, Vangpoomyai P, Rattanavongsa J, Rachahoon G. 2014. Do different levels of inquiry lead to different learning outcomes? A comparison between guided and structured inquiry. Int J Sci Educ 36(12):1937–1959.
12. Zion M, Mendelovici R. 2012. Moving from structured to open inquiry: challenges and limits. Sci Educ Int 23(4):383–399.
13. Eberlein T, Kampmeier J, Minderhout V, Eberlein T, Kampmeier J, Minderhout V, Moog RS, Platt T, Varma-Nelson P, White HB. 2008. Pedagogies of engagement in science: a comparison of PBL, POGIL, and PLTL. Biochem Mol Biol Educ 36(4):262–273.
14. Bowen CW. 2000. A quantitative literature review of cooperative learning effects on high school and college chemistry achievement. J Chem Educ 77:116.
15. Bruck LB, Towns MH. 2009. Preparing students to benefit from inquiry-based activities in the chemistry laboratory: guidelines and suggestions. J Chem Educ 86(7):820–822.
16. Wilson K, Korn JH. 2007. Attention during lectures: beyond ten minutes. Teach Psychol 34:85–89.
17. Bellei M, Welch P, Pryor S, Ketheesan N. 2016. A cost-effective approach to producing animated infographics for immunology teaching. J Microbiol Biol Educ 17(3):477–479.

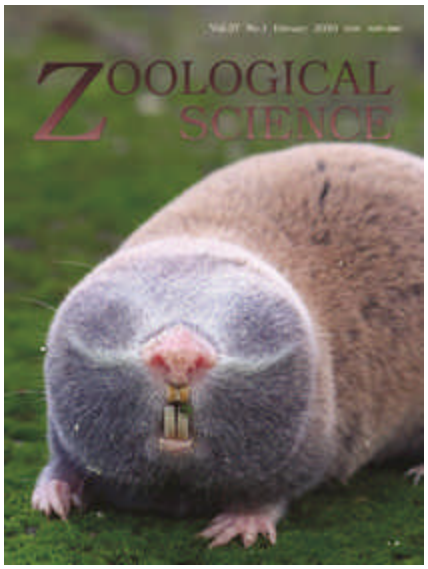

ECM-body: A cell-free 3D biomimetic scaffold derived from intact planarian body

Journal:	*Zoological Science*
Manuscript ID	ZS-O-2019-0135
Manuscript Type:	Original Article
Date Submitted by the Author:	11-Nov-2019
Complete List of Authors:	Sonpho, Ekasit; Mahidol University Faculty of Science, Biology Wootthichairangsan, Chanida; Mahidol University Faculty of Science Ishida, Miyuki ; Gakushuin Daigaku, Department of Life Science Inoue, Takeshi; Gakushuin Daigaku Rigakubu Daigakuin Shizen Kagaku Kenkyuka, Department of Life Science Agata, Kiyokazu; Gakushuin Daigaku, Department of Life Science Maleehuan, Anchuleerat; Mahidol University Faculty of Science Charngkaew, Komgrid; Mahidol University Faculty of Medicine Siriraj Hospital Chomanee, Nusara; Mahidol University Faculty of Medicine Siriraj Hospital Moonsom, Saengduen ; Mahidol University Faculty of Tropical Medicine Wongtrakoongate, Patompon; Mahidol University Faculty of Science Chairoungdua, Arthit; Mahidol University Faculty of Science Ounjai, Puey; Mahidol University Faculty of Science,
Keywords:	extracellular matrix, planarian, regeneration., decellularization, 3D cell culture, Tissue engineering

ECM-body: A cell-free 3D biomimetic scaffold derived from intact planarian body

Running head: Decellularization of Planarian Body

Ekasit Sonpho[1,2], Chanida Wootthichairangsan[1], Miyuki Ishida[3], Takeshi Inoue[3], Kiyokazu Agata[3], Anchuleerat Maleehuan[1], Komgrid Charngkaew[4], Nusara Chomanee[4], Saengduen Moonsom[5], Patompon Wongtrakoongate[6], Arthit Chairoungdua[7], and Puey Ounjai[1,2]*

[1]Department of Biology, Faculty of Science, Mahidol University, Thailand 10400.

[2]Center of Excellence on Environmental Health and Toxicology (EHT), Office of Higher Education Commission, Ministry of Education, Thailand, 10400.

[3]Department of Life Science, Faculty of Science, Gakushuin University, Tokyo, Japan 171-8588

[4]Department of Pathology, Faculty of Medicine Siriraj Hospital, Mahidol University, Thailand 10700.

[5]Department of Protozoology, Faculty of Tropical Medicine, Mahidol University, Thailand 10400.

[6]Department of Biochemistry, Faculty of Science, Mahidol University, Thailand 10400.

[7]Department of Physiology, Faculty of Science, Mahidol University, Thailand 10400.

*Author for correspondence: Puey.Oun@mahidol.edu (P.O.)

Suggested Disciplines: Developmental Biology

Abstract

Extracellular matrix (ECM) plays key roles in shaping fates of stem cells, not only by providing suitable niche but also by mediating physical and biochemical cues. Despite intensive investigations on regeneration, the roles of ECM on fate determination of stem cells in animal with great regenerative potency, such as planarian, remained unclear. Here, we developed a method to decellularizing and isolating extracellular matrix from planarians. Although the isolated scaffold appears translucent, it contains all the internal features, resembling the structure of intact planarian, and which we thus called "ECM-body". Nuclear staining demonstrated that ECM-body contains very little or no cell remained. Histological sections displayed a well-preserved morphological integrity of the specimen. Scanning electron microscope showed porous surface on ECM-body, potentially suitable for housing cells. Furthermore, our preliminary experiment suggested that ECM-body can be utilized as biomimetic scaffold for cell culture as it may support survival of injected neoblasts.

Keywords:

Extracellular matrix, Planarian, Decellularization, Scaffold, Tissue engineering, ECM-body

Introduction

Planarians have been widely utilized for studying regeneration as they are able to regenerate their body parts within weeks (Agata and Watanabe, 1999; Reddien and Alvarado, 2004; Umesono et al., 2013). Using planarians as models, various processes responsible for regeneration and development have been thoroughly elucidated (Cebrià et al., 2002; Reddien, 2018; Rink, 2013; Umesono et al., 2013). Furthermore, the detailed characterization of stem cell types as well as genes involved in tissues homeostasis and organ formation in planarians have also been established (Fincher et al., 2018; Plass et al., 2018; Zeng et al., 2018). It has been shown that the stemness of adult stem cells require physical interactions between the cells

and the ECM (Guilak et al., 2009). ECM plays key roles in modulating the dynamic microenvironment by providing suitable physical habitat for the resident cells, allowing the cell to develop and differentiate into specialized cells and governing cell to cell communications through controlled distribution of chemicals and biochemical signals (Frantz et al., 2010). Therefore, various attempts have been made to create suitable biomimetic 3D scaffold in order to simulate the microenvironment of ECM, especially for understanding the complex interaction between the ECM and the stem cells (Gilbert et al., 2006). Indeed, a method of choice to prepare cell-free ECM is so-called decellularization due to the fact that the ECM obtained from this method could potentially provide suitable microenvironment for the cells, offering not only mechanical and physical cues but also some cryptic biochemical signals that are involved in regulating growth and developmental processes (Schultz and Wysocki, 2009). To date, various protocols have been developed for decellularizing various mammalian tissue systems (Goh et al., 2013; Mazza et al., 2015; Ott et al., 2008). However, there was only limited information regarding isolation of ECM of invertebrates (Gambini et al., 2012; Shimizu et al., 2008). To our knowledge, there is currently no decellularization protocol developed for planarian tissues.

Here, we established a protocol for preparing intact decellularized ECM, which we called ECM-body, from freshwater planarians, *Dugesia* sp. (Thai isolate) and *Dugesia japonica* and preliminarily explored the possibility to utilize ECM-body as biomimetic scaffold for 3D cultivation of planarian neoblasts. Our work offered broad application in investigating the role of ECM components not only in regeneration but also in stem cell biology.

Materials and Methods

Animals

Freshwater planarian, *D. japonica,* were maintained in artificial spring water at room temperature (24℃) and were fed twice a week with chicken liver. Animals were starved for at least 1 week before experiment.

Isolation of planarian ECM-body

Planarians were terminated and stabilized in stabilization solution composed of 1% Nitric acid, 50 μM $MgSO_4$ and 0.8% Formaldehyde. After that, the animals were decellularized in decellularization solution I composed of 0.08% SDS, EDTA pH 8.0 5 mM, PMSF 1mM, and Tris-HCl pH 7.6 10 mM for 18 hours. Next, the solution was replaced with decellularization solution II composed of 0.04% SDS, EDTA pH 8.0 5 mM, PMSF 1 mM, and Tris-HCl pH 7.6 10 mM and incubated for at least 2 hours. Isolated ECM was then washed in wash solution composed of EDTA pH 8.0 5 mM, PMSF 1 mM, and Tris-HCl pH 7.6 10 mM for at least three times. ECM was finally stored at 4℃ in a freshly prepared washing solution. For the ECM aimed for cell culture, an additional nuclease treatment was added to remove potential contamination of small nucleic acid fragments. Afterward, samples were intensively washed with sterile PBS. Then, samples were cleaned with culture medium supplemented with antibiotics. Isolated ECMs were kept by submerging them in sterile PBS at 4℃ prior to use in the experiment. Detailed protocol is provided in supplementary file S1 online. The components of all solutions were indicated in supplementary table S1 online.

Characterization of decellularization efficiency using DAPI staining

DAPI staining was conducted to determine the presence of cells in the ECM- body. At first, the mucus layer of the worm was removed to enhance the accessibility of the solution. Both ECM-body and the worm were then fixed in formaldehyde solution. Afterward, the samples were incubated in permeabilizing solution. After that, the samples were incubated in DAPI

solution for an hour in the dark. Stained samples were washed to remove the excess amount of DAPI and submerged in glycerol solution to increase the clarity of the sample. Mounted samples were observed under fluorescent microscope. Detailed protocol is provided in supplementary file S1 online.

Histological Characterization

Masson's trichrome histological staining was conducted to evaluate the internal structure and general tissue architecture. Detailed protocol is provided in supplementary file S1 online.

Scanning Electron Microscopy

For ultrastructural investigation, both of samples were fixed with Glutaraldehyde and Osmium tetroxide. Planarians was dehydrated in ethanol whereas ECM-body was dehydrated in acetone. Subsequently, the samples were proceeded to critical point drying, platinum coating and mounted on SEM stub. The samples were visualized under scanning electron microscope. Detailed protocol is provided in supplementary file S1 online.

Fluorometric quantification of DNA and RNA in ECM

The amount of DNA and RNA in the ECM-body were evaluated by nanophotometer and fluorometer respectively. Detailed protocol is provided in supplementary file S1 online.

Planarian cell dissociation and neoblast microinjection into ECM-body

The preparation of single-cells for fluorescence-activated cell sorting analysis was conducted as described in Hayashi et al., 2006. X-ray sensitive neoblast cells (X1 population) were centrifuged and proceeded to injection. Aggregated cells were equally injected into posterior and anterior of pharynx and incubated in the culture medium at 24°C in CO2 incubator. After

1 and 3 days post injection, the ECM-body was stained with Hoechst 33342 or DAPI to visualize in injected cell and observed under confocal microscope (FV1000, Olympus). Detailed protocols of neoblast sorting and cell injection are stated in supplementary file S1 online.

Results and discussion

Optimization of Decellularization Procedure for Freshwater Planarians – Decellularization is a technique to prepare three-dimensional biomimetic scaffold for tissue engineering and microenvironmental studies (Goh et al., 2013; Mazza et al., 2015; Ott et al., 2008; Schultz and Wysocki, 2009). The goal of successful decellularization is to completely get rid of all the cellular components while faithfully preserving the intact architecture of ECM as well as other potential microenvironmental factors.

While the application of decellularization have been tremendously fruitful for tissue engineering and regenerative research, the decellularization method has not been established in planarians (Hussey et al., 2018; Kim et al., 2012). It should be noted that current widely utilized method for investigation of gene function in planarians are only RNA interference and *in situ* hybridization (Rouhana et al., 2013). Additionally, proteomics characterization of planarian ECM has not been experimentally unravelled (Cote et al., 2019). Therefore, establishment of a protocol for isolating planarian ECM are absolutely essential for the advancement of regenerative biology research.

To date, various methods have been established for decellularizing mammalian organs (Gilbert et al., 2006), the decellularization of freshwater planarians was obviously quite challenging because their bodies are often quickly disintegrated upon the death of animal. Due to the rapid growth and the ease of cultivation of the animal, we chose to initially optimized a protocol for whole-body decellularization of planarian using the *Dugesia* sp. (Thailand isolate).

Sodium dodecyl sulfate (SDS) has been utilized as an effective agent for removing nuclei from decellularized tissues (Mecham, 2012), we therefore selected SDS as the first line of decellularizing agent. Although the resulting ECM-body prepared in this condition appeared to largely resemble the shape of planarians (Fig. 1A and B), the internal organization of ECM-body prepared using this method appeared to be less defined. To better preserve the internal and external 3D organization of planarian, we decided to include a step to stabilize the planarian body using cross-linking agents such as formaldehyde prior to the decellularization process. The ECM-body prepared by this improved procedure appeared translucent with well-preserved internal organ systems of the intact planarians i.e. digestive tract, eye spots and pharynx (Fig. 1A and C). However, it was of our concern as well that fixation need to be applied prior to the decellularization as structure of decellularized hydra could be maintained to a certain extent using no fixation (Shimizu et al., 2008). We hypothesized that tissue disintegration may be due to sensitivity of the live planarians to the treatment with SDS (Hagstrom et al., 2015). Rapid termination of the worms by chemical fixative may thus minimize the detrimental effect caused by SDS-induced response and aid preservation of intact ECM.

Albeit fixative treatment stabilize planarian body and aid structural preservation of ECM, the stabilization process could potentially cause negative impact on the efficiency of cellular removal, we therefore rescreened the panel of detergents, consisting of Triton X-100, Tween-20 and SDS, to seek for the most effective decellularizing agent for removing the cell from stabilized planarian bodies. Although all the selected decellularizing agents were able to successfully dissolve cellular content from the stabilized worms, cellular removal capability of SDS-based extraction was still superior in comparison with the other two selected detergents (Fig. 1D). It should be noted that the internal structure of digestive tract of the worm within 1 hour after treatment with low concentration of SDS (Fig. 1D). Translucent ECM-body containing clear intact internal structures was achieved within 4 hours (Fig. 1D). To verify the

cellular removal efficacy of different detergents, the amount of residual DNA in the sample was determined at various time points during the treatment (Fig. 1E). The results confirmed that the decrease of residual DNA 0.08% SDS was significant faster than the other two detergents tested (Fig. 1E). Therefore, SDS was chosen as a detergent of choice for subsequent decellularization experiment. Choice of detergent is critical for decellularization since it has been reported that different type of detergent could affect cellular removal efficiency as well as microstructure of ECM scaffold (Nakayama et al., 2010; Crapo et al., 2011, Vavken et al., 2009). In any case, the residue of SDS has been reported to often found deposited inside the decellularized ECM after the preparation process (White et al., 2017). Intensive washing was implemented after SDS treatment to minimize possible remaining of chemical fixative and detergent.

Characterization of Acellular Planarian ECM-body - As one of the minimal criteria for acceptable decellularization is the lacking of visible nuclear material, the ECM-body was stained with 4',6-diamidino-2- phenylindole (DAPI) (Kapuscinski, 1995). The results demonstrated that there was no nucleus remained in the isolated ECM (Fig. 1F). However, weak signals of DAPI can still be observed in the background perhaps from the residual nucleic acid fragment remained attached to the scaffold. However, agarose gel electrophoresis revealed no band of remaining genomic DNA (Fig. 1G). Further fluorometric quantification of RNA also displayed marked decrease in the RNA content in the ECM body (Fig. 1H). Although nucleic acid left in the structure may be only of negligible amount. It did not escape our attention that the trace amount of residual nucleic acid may have negative effect on replanted cells (Nagata et al., 2010).

To verify the integrity of the ECM architecture, ECM body was stained with Masson's trichrome dyes (Goldner, 1938). Histological cross sections at the pharyngeal plane elucidated

intact organization of fibrous ECM structures similar to that of the untreated worm (Fig. 2 A and B). Notably, little or no cell were found remained in the scaffold. Using scanning electron microscopy (SEM), the surface topography of intact worm and isolated ECM-body were characterized. The results displayed that the dorsal and ventral sides of the planarian body were easily distinguishable as the former are covered with mucus layer while the latter contains tremendous ciliature on the surface (Fig. 2C and D). On the contrary, both dorsal and ventral surfaces of the ECM body displayed similar porous structure. This is in great agreement with the corresponding three-dimensional fibrous network observed in the histological staining (Fig. 2E). It should be noted that the ECM-body visualized using SEM appeared flattened. This effect was likely caused by the dehydration during SEM sample preparation. The flattening of the ECM-body may also suggest that ECM body comprised soft and airy 3D scaffold. Notably, the observed microstructure was consistent with isolated ECM from jelly fish, suggesting similarity of the invertebrate tissue microstructures (Gambini et al., 2012). Taken together, this thus confirmed that our developed protocol did not only effectively remove residential cells from the worms but also provide faithful preservation of intact internal architecture of cell free matrix. Our optimized decellularization protocol is summarized in Fig. 3A.

Preliminary Utilization of ECM-body as Three-Dimensional Scaffold – To explore the potential of utilizing the ECM body as a biological 3D scaffold for replanting of the neoblasts, we shifted our attention to a well-established helminth model, *Dugesia japonica* due to the availability of genomic information and an established protocol for FACS sorting of neoblast (Kawakatsu et al., 1995). Without any modification, the intact ECM-body from *D. japonica* can be similarly prepared using our established procedure (Fig. 3B-C, E). To further reduce the possible influence from nucleic acid remnants on the behaviour of the replanted cells (Nagata et al., 2010), the ECM body was further subjected to DNase and RNase treatment. We observed

that the additional nuclease treatment did not affect overall morphology of the ECM-body (Fig. 3C-D). Although the use of formaldehyde in stabilization solution should kill all the potential contaminating microbes (Chen et al., 2016), we ensured the suitability of exploitation of ECM-body as a 3D scaffold in cell culture, the ECM-body was further assayed for bacterial and fungal contamination by incubating in mammalian cell culture media. As a result, based on the colour and clarity of the media, no sign of microbial growth was observed after 4 days of incubation (Fig. 3F). We further tested for mycoplasmas as they have been used as the indicator for media contamination (Young et al., 2010). PCR based mycoplasma detection assay validated that the ECM-body prepared with our method was mycoplasma free (Fig. 3G) (Masters et al., 2000). Finally, in order to set stage for future utilization of the ECM-body in advancing the study of interaction between planarian stem cell and niche, we performed ex vivo recellularization of the FACS isolated X1 fraction (FACS sorted S or G2/M phase neoblasts) from planarians into sterile ECM-body both at the anterior and posterior using microinjection (Hayashi et al., 2006). Upon injection, some swelling effects were observed at the sites of microinjection, possibly due to the pressure build up during the microinjection (Fig. 3H). After incubation at 24℃, the microinjected ECM-body were taken out at 1 and 4 post-injection (dpi) for evaluating the cell retention. Of interest, the Hoechst stain revealed random distribution of cell and cell clusters in the ECM, suggesting that ECM-body was unlikely to contain residual fixatives and SDS and was not toxic to the replanted stem cells.

In fact, the ECM-body might be able to support the settlement of neoblast as it could provide the site for cell attachment (Fig. 3I-K). It should be noted that the viability of the seeded the X1 neoblasts in ECM-body was maintained until the last day of experiment (4 dpi). In any case, we observed no sign of nuclear fragmentation in the replanted cell, implying that there was little or no apoptotic event (Fig. 3K) (Toné at al., 2007).

Because the objective of this work was to develop a protocol for isolating intact ECM from planarians, we did not characterize neither the proliferation rate nor the apoptotic event of the recellularized neoblasts. It would be of great interest to determine whether the neoblast could proliferate and inside the three-dimensional microenvironment of the ECM-body. Further work should also further be conducted to monitoring the alteration in behaviour of repopulating cell. Optimization of the culture condition to promote other cellular processes such as migration, differentiation, stem cell renewal and eventually immortalization of the neoblast cells in the ECM-body would be greatly beneficial for the planarian community.

Acknowledgement

We thank S. Singhakaew for experimental assistance, S. Leetacheewa and K. Boonthaworn for helpful discussion. The work was supported by the Center of Excellence on Environmental Health and Toxicology, Office of Higher Education Commission, Ministry of Education, Thailand and Thailand Research Funds (RSA5980078 to PO). We also thank financial support from Faculty of Science, Mahidol University. Oversea exchange scholarship from Gakushuin University and Mahidol University to ES is gratefully acknowledged.

Competing Interests

There are no competing interests by any authors listed in this manuscript

Author Contributions

PO and AC conceived the idea and designed the experiment. KA and TI further improved experimental design. ES, CW, MI and AM performed the experiments. SM and PW helped with characterization of decellularized ECM. KC and NC helped with SEM data collection.

PO, TI and KA supervised the project. ES and PO wrote the original manuscript. All authors have reviewed and approved the manuscript.

References

Agata K, and Watanabe K (1999) Molecular and cellular aspects of planarian regeneration. Sem Cell Dev Biol 10: 377–383

Cebrià F, Kobayashi C, Umesono Y, Nakazawa M, Mineta K, Ikeo K, Gojobori T, Itoh M, Taira M, Sánchez Alvarado A, Agata K (2002) FGFR-related gene nou-darake restricts brain tissues to the head region of planarians. Nature 419: 620–624

Chen NH, Djoko KY, Veyrier FJ, McEwan AG (2016) Formaldehyde stress responses in bacterial pathogens. Front Microbiol 7: 1–17

Cote LE, Simental E, Reddien PW (2019) Muscle functions as a connective tissue and source of extracellular matrix in planarians. Nat Commun 10: 1592

Crapo PM, Gilbert TW, Badylak SF (2011) An overview of tissue and whole organ decellularization processes. Biomaterials 32: 3233–3243

Fincher C, Wurtzel O, de Hoog T, Kravarik KM, Reddien PW (2018) Cell type transcriptome atlas for the planarian Schmidtea mediterranea. Science 1736: 1–20

Frantz C, Stewart KM, Weaver VM (2010) The extracellular matrix at a glance. J Cell Sci 123: 4195–4200

Gambini C, Abou B, Ponton A, Cornelissen AJM (2012) Micro- and macrorheology of jellyfish extracellular matrix. Biophys J 102: 1–9

Gilbert TW, Sellaro TL, and Badylak SF (2006) Decellularization of tissues and organs. Biomaterials 27: 3675–3683

Goh SK, Bertera S, Olsen P, Candiello JE, Halfter W, Uechi G, Balasubramani M, Johnson SA, Sicari BM, Kollar E, Badylak SF, Banerjee I (2013) Perfusion-decellularized pancreas as a natural 3D scaffold for pancreatic tissue and whole organ engineering. Biomaterials 34: 6760–6772

Goldner J (1938) A modification of the masson trichrome technique for routine laboratory purposes. Am J Pathol 14: 237–243

Guilak F, Cohen DM, Estes BT, Gimble JM, Liedtke W, Chen CS (2009) Control of stem cell fate by physical interactions with the extracellular matrix. Cell Stem Cell 5: 17–26

Hagstrom D, Cochet-Escartin O, Zhang S, Khuu C, Collins EMS (2015) Freshwater planarians as an alternative animal model for neurotoxicology. Toxicol Sci 147: 270–285

Hayashi T, Asami M, Higuchi S, Shibata N, Agata K (2006) Isolation of planarian X-ray-sensitive stem cells by fluorescence-activated cell sorting. Dev Growth Differ 48: 371–380

Hussey GS, Dziki JL, Badylak SF (2018) Extracellular matrix-based materials for regenerative medicine. Nat Rev Mater 3: 159–173

Kapuscinski J (1995) DAPI: A DMA-Specific fluorescent probe. Biotech Histochem 70: 220–233

Kawakatsu M, Oki I, Tamura S (1995) Taxonomy and geographical distribution of *Dugesia japonica* and *D. ryukyuensis* in the Far East. Hydrobiologia 305: 55–61

Kim TG, Shin H, Lim DW (2012) Biomimetic scaffolds for tissue engineering. Adv Funct Mater 22: 2446-2468

Masters JRW, Twentyman P, Arlett C, Daley R, Davis J, Doyle A, Dyer S, Freshney I, Galpine A, Harrison M, Hurst H, Kelland L, Stacey G, Stratford I, Ward TH (2000) UKCCCR

guidelines for the use of cell lines in cancer research. Br J Cancer 82: 1495–1509

Mazza G, Rombouts K, Rennie Hall A, Urbani L, Vinh Luong T, Al-Akkad W, Longato L, Brown D, Maghsoudlou P, Dhillon AP, Fuller B, Davidson B, Moore K, Dhar D, De Coppi P, Malago M, Pinzani M (2015) Decellularized human liver as a natural 3D-scaffold for liver bioengineering and transplantation. Sci Rep 5: 1–15

Mecham RP (2012) Overview of extracellular matrix. Curr Protoc Cell Biol 57: 1–14

Nagata S, Hanayama R, Kawane K (2010) Autoimmunity and the clearance of dead cells. Cell 140: 619–630

Nakayama KH, Batchelder CA, Lee CI, Tarantal AF (2010) Decellularized rhesus monkey kidney as a three-dimensional scaffold for renal tissue engineering. Tissue Eng Part A: 16 2207– 2216.

Ott HC, Matthiesen TS, Goh SK, Black LD, Kren SM, Netoff TI, Taylor DA (2008) Perfusion-decellularized matrix: Using nature's platform to engineer a bioartificial heart. Nat Med 14: 213–221

Plass M, Solana J, Alexander Wolf F, Ayoub S, Misios A, Glažar P, Obermayer B, Theis FJ, Kocks C, Rajewsky N (2018) Cell type atlas and lineage tree of a whole complex animal by single-cell transcriptomics. Science 360: 1723

Reddien PW (2018) The cellular and molecular basis for planarian regeneration. Cell 175: 327–345.

Reddien PW, Sánchez Alvarado A (2004) Fundamentals of planarian regeneration. Annu Rev Cell Dev Biol 20: 725–757

Rink JC (2013) Stem cell systems and regeneration in planaria. Dev Genes Evol 223: 67–84

Rouhana L, Weiss JA, Forsthoefel DJ, Lee H, King RS, Inoue T, Shibata N, Agata K, Newmark PA (2013) RNA interference by feeding in vitro-synthesized double-stranded RNA to planarians: Methodology and dynamics. Dev Dyn 242: 718–730

Schultz GS, Wysocki A (2009) Interactions between extracellular matrix and growth factors in wound healing. Wound Repair Regen 17: 153–162

Shimizu H, Aufschnaiter R, Li L, Sarras MP, Borza DB, Abrahamson DR, Sado Y, Zhang X (2008) The extracellular matrix of hydra is a porous sheet and contains type IV collagen. Zoology 111: 410–418

Toné S, Sugimoto K, Tanda K, Suda T, Uehira K, Kanouchi H, Samejima K, Minatogawa Y, Earnshaw WC (2007) Three distinct stages of apoptotic nuclear condensation revealed by time-lapse imaging, biochemical and electron microscopy analysis of cell-free apoptosis. Exp Cell Res 313: 3635–3644

Umesono Y, Tasaki J, Nishimura Y, Hrouda M, Kawaguchi E, Yazawa S, Nishimura O, Hosoda K, Inoue T, Agata K (2013) The molecular logic for planarian regeneration along the anterior-posterior axis. Nature 500: 73–76

Vavken P, Joshi S, Murray MM (2009) TRITON-X is most effective among three decellularization agents for ACL tissue engineering. J Orthop Res 27: 1612–1618

White LJ, Taylor AJ, Faulk DM, Keane TJ, Saldin LT, Reing JE, Swinehart IT, Turner NJ, Ratner BD, Badylak SF (2017) The impact of detergents on the tissue decellularization process: A ToF-SIMS study. Acta Biomater 50: 207–219

Young L, Sung J, Masters JR (2010) Detection of mycoplasma in cell cultures. Nat Protoc 5: 929–934

Zeng A, Li H, Guo L, Gao X, McKinney S, Wang Y, Yu Z, Park J, Semerad C, Ross E, Cheng

LC, Davies E, Lei K, Wang W, Perera A, Hall K, Peak A, Box A, Sánchez Alvarado A (2018) Prospectively isolated tetraspanin + neoblasts are adult pluripotent stem cells underlying planaria regeneration. Cell 173: 1593-1608

Figure Legends and Table Captions

Fig. 1. Optimization of planarian ECM-body Isolation. (A) The morphology of untreated planarians, (B) decellularization without and (C) with stabilization, scale bar = 1 mm (D) Effect of different detergents on decellularization, scale bar = 1 mm (E) Comparison of the DNA removing rate of different detergents during the course of decellularization, error bar indicated standard deviation from 2 independent experiments with 10 planarians per experiment, ANOVA, ($P<0.05$). (F) DAPI stained planarian and ECM-body, scale bar = 50 μm (G) Gel electrophoresis for gDNA (H) Significant reduction in the amount of RNA was detected in the ECM-body, data were calculated from 3 independent experiments, 10 planarians per experiment, ANOVA, ($P<0.05$).

Fig. 2. Integrity of the isolated ECM-body

Masson's trichrome histological cross sections at the pharyngeal plane of intact planarian (A) and ECM-body (B), scale bars = 50 μm. Scanning electron microscopy revealed the surface morphology of intact planarian, dorsal side (C), ventral side (D) and isolated ECM body (E), scale bars = 10 μm. The overall shapes of each specimen were shown in the insets, scale bars in the insets = 500 μm

Fig. 3. Preliminary recellularization of isolated *Dugesia japonica* ECM body

(A) A diagram showed overview of the optimized protocol for decellularization of freshwater planarian. The protocol was optimized using Thai planarian. To further test if our protocol can be applied to other freshwater flatworms, the decellularization based on this protocol were conducted on *D. japonica* (B) *D. japonica*, (C) *D. japonica* ECM body isolated using this protocol (D) Nuclease treated ECM body of *D. japonica* for cell cultivation. scale bar = 1 mm (E) DAPI stained planarian and ECM-body revealed little or no nucleus remained in the structure. scale bars = 100 μm. (F) The clarity of cell culture media after 4 days of incubation with ECM-body confirmed decontamination efficiency, arrowhead indicated the position of added ECM-body (G) Mycoplasma detection using PCR revealed no contamination in co-culture of ECM-body and NTERA2 cell line. (H) The appearance of ECM-body before and after microinjection, arrowheads indicated the site of cell injection. (I) DAPI staining of the PBS injected inside ECM-body. scale bar = 100 μm. (J) DAPI staining of the replanted cells inside ECM-body after 1 day incubation. scale bar = 100 μm. (K) Hoechst 33342 staining of the microinjected cells cultured inside ECM-body at 4 days post infection. scale bar = 100 μm.

Supplementary Table

Table S1: Buffer Recipes used in Planarian Decellularization

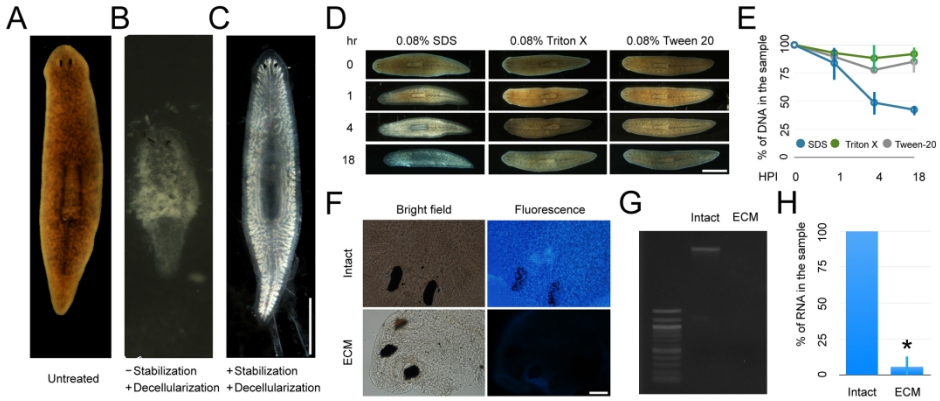

Fig. 1. Optimization of planarian ECM-body Isolation. (A) The morphology of untreated planarians, (B) decellularization without and (C) with stabilization, scale bar = 1 mm (D) Effect of different detergents on decellularization, scale bar = 1 mm (E) Comparison of the DNA removing rate of different detergents during the course of decellularization, error bar indicated standard deviation from 2 independent experiments with 10 planarians per experiment, ANOVA, ($P<0.05$). (F) DAPI stained planarian and ECM-body, scale bar = 50 μm (G) Gel electrophoresis for gDNA (H) Significant reduction in the amount of RNA was detected in the ECM-body, data were calculated from 3 independent experiments, 10 planarians per experiment, ANOVA, ($P<0.05$).

1058x429mm (72 x 72 DPI)

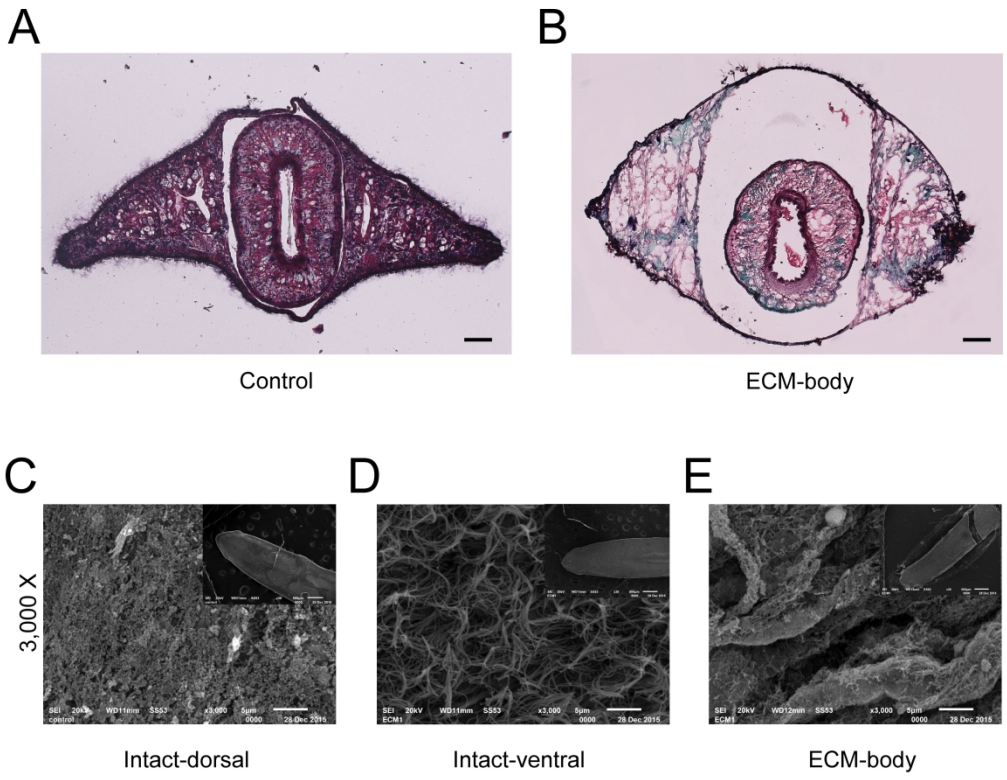

Fig. 2. Integrity of the isolated ECM-body
Masson's trichrome histological cross sections at the pharyngeal plane of intact planarian (A) and ECM-body (B), scale bars = 50 μm. Scanning electron microscopy revealed the surface morphology of intact planarian, dorsal side (C), ventral side (D) and isolated ECM body (E), scale bars = 10 μm. The overall shapes of each specimen were shown in the insets, scale bars in the insets = 500 μm

1220x941mm (72 x 72 DPI)

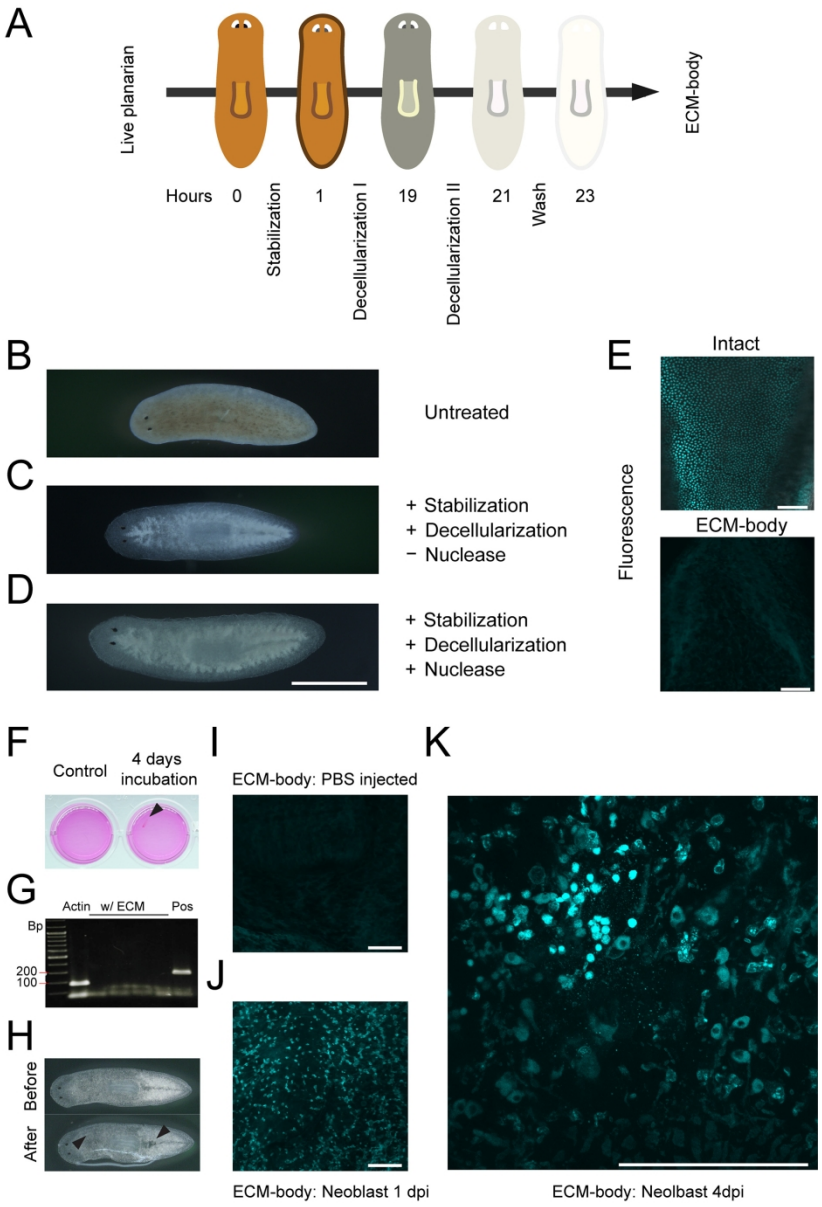

Fig. 3. Preliminary recellularization of isolated Dugesia japonica ECM body
(A) A diagram showed overview of the optimized protocol for decellularization of freshwater planarian. The protocol was optimized using Thai planarian. To further test if our protocol can be applied to other freshwater flatworms, the decellularization based on this protocol were conducted on D. japonica (B) D. japonica, (C) D. japonica ECM body isolated using this protocol (D) Nuclease treated ECM body of D. japonica for cell cultivation. scale bar = 1 mm (E) DAPI stained planarian and ECM-body revealed little or no nucleus remained in the structure. scale bars = 100 μm. (F) The clarity of cell culture media after 4 days of incubation with ECM-body confirmed decontamination efficiency, arrowhead indicated the position of added ECM-body (G) Mycoplasma detection using PCR revealed no contamination in co-culture of ECM-body and NTERA2 cell line. (H) The appearance of ECM-body before and after microinjection, arrowheads indicated the site of cell injection. (I) DAPI staining of the PBS injected inside ECM-body. scale bar = 100 μm. (J) DAPI staining of the replanted cells inside ECM-body after 1 day incubation. scale bar = 100 μm. (K) Hoechst 33342 staining of the microinjected cells cultured inside ECM-body at 4 days post infection. scale bar = 100 μm.

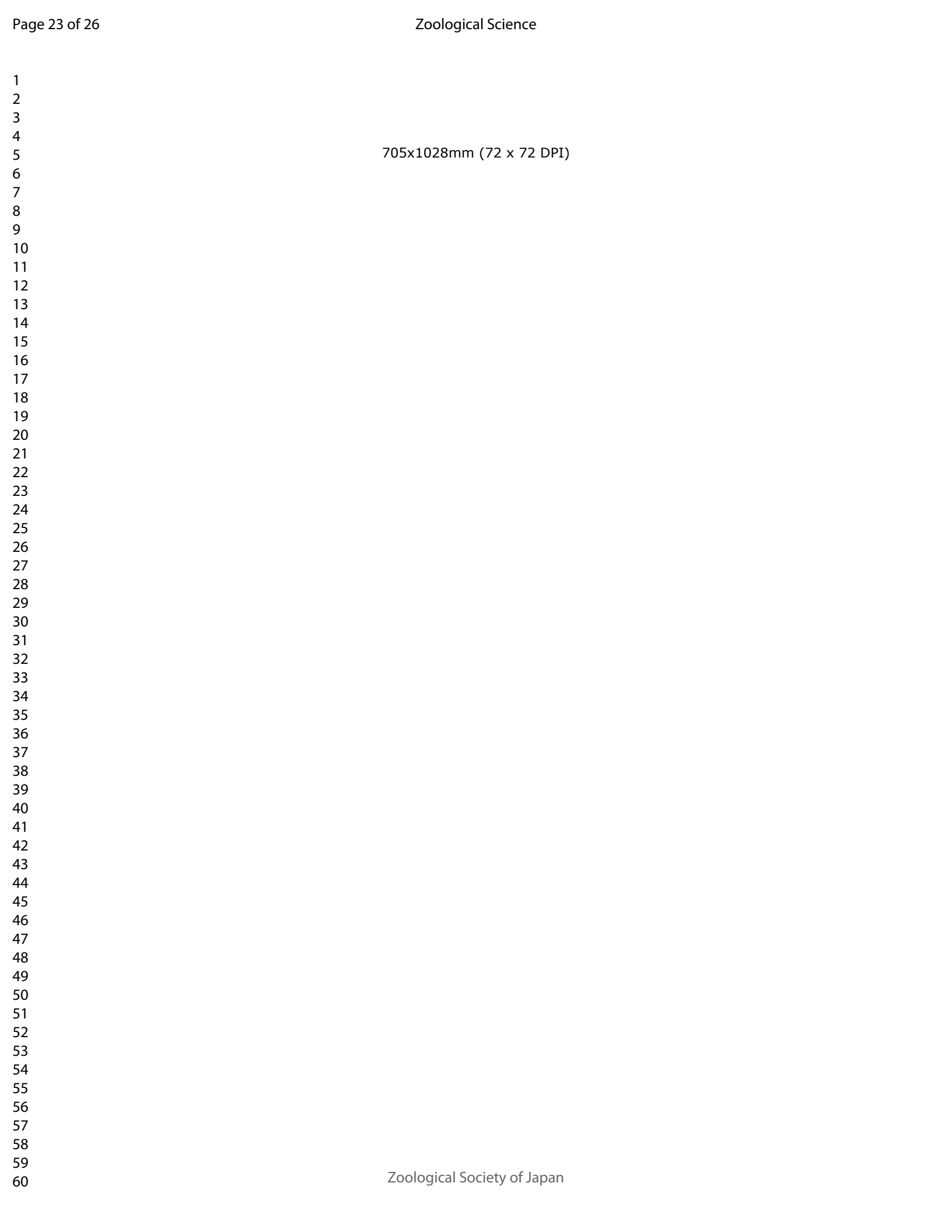
705x1028mm (72 x 72 DPI)

Supplementary Materials and Methods.

Isolation of Planarian Extracellular Matrix (ECM-body)

Seven-day starved planarians were collected from the tank. This protocol was designed for 40 planarians. Planarian was terminated and stabilized once at a time by replacing solution with stabilization solution (Ingredients of different solutions used for isolating planarians were listed in supplementary Table S1 online) and incubated at 4℃ for 1 hour without shaking. After the stabilization, the solution was replaced with 40 ml of decellularization solution I for 16-18 hours at 4℃. However, incubation time could be varied depending on the size and species of planarians. Subsequently, we replaced the solution with 40 ml decellularization solution II for 2 hours at 4℃. After that, the solution was gently replaced with wash solution for 20 minutes 3 times in 4℃ on a seesaw rocker. After this incubation step, the prepared ECM-body are ready for characterization using various visualization techniques. In case of ECM-body aimed to prepare as a biomimetic scaffold for 3D cell culture, additional nuclease treatment step was added to remove residual nucleic acid fragments contaminated in the sample. The treatment was incubated for 1 hours at 37℃ without shaking. The isolated ECM-body was subjected to extensive washing in sterile 1X at 4℃ PBS for 5 times, 10 minutes each. The sample was agitated gently on a seesaw rocker. The solution was washed with LCDM and EPSCM (Yang et al., 2017) supplemented with antibiotic for at least 3 times for 10 minutes each and incubated at 24℃ on a seesaw rocker. Isolated ECM- body were maintained in sterile PBS at 4C° prior to use in the experiment.

Nucleus Staining by DAPI and Hoechst 33342

Isolated extracellular matrix as well as intact animals were transferred into 24- well plate. A coverslip was added at the bottom of each well. The worm was treated with 5% N-

Acetylcysteine for 10 minutes at room temperature to terminate the worm and wash away all the excess mucus. The samples were fixed in 0.8% formaldehyde (Sigma) for 1 hour at 4℃. The samples were rinsed twice with PBSTx, or PBS supplemented with 0.3% Triton X-100 (Sigma). Samples were then incubated for 2 hours in a permeabilizing solution composed of 1X PBS and 0.5% Triton X-100 at 4℃, and then rinsed thrice with PBSTx prior to stain with 1:400 DAPI solution (Invitrogen). The samples were then incubated in PBSTx in dark condition for 1 hour at room temperature. Stained specimen was then washed 5 times in PBSTx, for 5 minutes each. The samples were then subjected to incubating in 80% glycerol for 30 minutes at 4℃. Finally, samples were transferred and mounted using 80% glycerol on a clean glass slide. DAPI stained sample was visualized under Olympus BX53 fluorescent microscope (Olympus, Singapore). For the samples stained with Hoechst 33342, samples were fixed with 4% paraformaldehyde, 5% methanol, PBS for 20 minutes, followed by double washing in PBSTx, for 10 minutes each. Subsequently, the solution was replaced with 1:2000 Hoechst 33342 in 1×PBS and incubated for 10 minutes. The samples were observed under Fluoview FV3000 confocal laser scanning microscope (Olympus).

Masson's trichrome staining

Specimen was fixed in 1% Nitric acid, 50 µM MgSO4 and 0.8% formaldehyde overnight. Then, the ECM was dehydrated in the serial dilution of acetone (Fisher Scientific) while the dehydration of planarian was done in dilution series of ethanol. Dehydrated samples were further incubated in 1, 4-Dioxane (Fisher Scientific) for 30 minutes. The samples were embedded in the paraffin thrice for 20 minutes each. The paraffin block was trimmed at a thickness of 5 µm using ultramicrotome (Leica Biosystems). The sections were proceeded by a routine protocol for trichrome staining, which is good for staining muscle fiber, collagen, cytoplasm and nucleus staining.

Ultrastructure of planarian extracellular matrix

To prepare sample for observation under scanning electron microscope, ECM of planarian were collected and fixed with 2.5% glutaraldehyde in 0.1 M sodium cacodylate pH 7.2 at 4℃ and washed with 0.1 M sodium cacodylate buffer pH 7.2 at 4℃. Next, ECM were fixed with 1% osmium tetroxide in 0.1 M sodium cacodylate buffer for 1 hour at 4℃. After that, the samples were washed with 0.1 M sodium cacodylate buffer pH 7.0 at 4℃. Worms were dehydrated by soaking in series of concentration of ethyl alcohol which were 30%, 50%, 70% 80%, 90% and 95% for 15 minutes each, at 4℃. After the samples are in 95% ethyl alcohol, absolute ethyl alcohol was used to replace the solution at 4℃. The residual ethyl alcohol was removed using critical point drying (CPD). The samples were mounted on stubs with double-coated conductive carbon tape. Specimen was coated with Pt-Pd for 4 minutes using ion sputter before observing under JSM- 6510 Series Scanning Electron Microscope (JEOL).

Fluorometric Quantification of DNA and RNA in Extracellular Matrix

Nucleic acid material remained in extracellular matrix were quantified using fluorometric method. Commercial kit (Bio Basic Canada Inc.) was utilized to extract DNA from the ECM sample in comparison with the intact planarian. The concentration of DNA was determined by nanophotometer (Implen, Germany). For RNA detection, RNA was extracted all ECM and intact planarian using Trizol reagent (Invitrogen). After extraction, the RNA was resuspended in mild base water. The concentration of RNA was determined by QFX Fluorometer (DeNovix).

Planarian Cell Dissociation and Neoblast Microinjection

Planarian was cut into 3-4 fragments by clean scalpel. The fragments were then soaked in Holtfreter's solution diluted in distilled water. The fragments were further subjected to physical mincing and treatment with 0.25% trypsin for several minutes at 20℃. The cells were dissociated by gentle pipetting up and down several times. The dissociated cells were orderly filtered through a 35 μm pore size cell strainer and 20 μm nylon net filter to remove tissue fragments. Single-cells suspension was stained with Dye Cycle (Invitrogen) for 30 minutes at room temperature. Flow cytometric analysis was performed using a BD FACS Melody Cell Sorter (Becton-Dickinson). X-ray-sensitive neoblast cell or X1 fraction were isolated and utilized in the microinjection. 1×10^5 X1 cells could be successfully temporarily maintained in 24-well plate in 1 ml culture medium on a rotary shaker at 20℃ in CO_2 incubator. The cells were collected by centrifuge at 300 g for 7 minutes. 10 μl of aggregated cells were drawn into capillary glass of the injector. ECM-body was placed firmly on the black sterile filter paper for the injection. The cells were then injected into the posterior and anterior parts of the pharynx. After the injection, ECM-body was transferred gently into culture medium and cultivate at 24℃ in a CO_2 incubator.

Supplementary Table

Table S1: Buffer Recipes used in Planarian Decellularization

Solution	Final concentration
Stabilization solution I	
Nitric acid (Merck)	1%
MgSO4 (Merck)	50 µM
Formaldehyde (Sigma-Aldrich)	0.80%
Decellularization solution I	
Sodium dodecyl sulfate, SDS (Sigma)	0.08%
EDTA pH 8.0 (Vivantis)	5 mM
PMSF (Calbiochem)	1 mM
Tris-HCl pH 7.6 (Biorad)	10 mM
Decellularization solution II	
Sodium dodecyl sulfate	0.04%
EDTA pH 8.0	5 mM
PMSF	1 mM
Tris-HCl pH 7.6	10 mM
Wash solution	
EDTA pH 8.0	5 mM
PMSF	1 mM
Tris-HCl pH 7.6	10 mM
Nuclease solution	
1000 U DNase I (Promega)	24 ul
DNase I buffer (Promega)	60 ul
100,000U/ml RNase T (Thermo Scientific)	10 ul
Up to 6 ml by Milli-Q water	